



CRITICAL REVIEWS

Cardiovascular fluid dynamics: a journey through our circulation

Karthik Menon^{1,2} , Zinan Hu³ and Alison L. Marsden^{1,2,3,4,*} 

¹Department of Pediatrics (Cardiology), Stanford University School of Medicine, Stanford, CA 94305, USA

²Institute for Computational and Mathematical Engineering, Stanford University, Stanford, CA 94305, USA

³Department of Mechanical Engineering, Stanford University, Stanford, CA 94305, USA

⁴Department of Bioengineering, Stanford University, Stanford, CA 94305, USA

*Corresponding author. E-mail: amarsden@stanford.edu

Received: 7 October 2023; **Revised:** 22 February 2024; **Accepted:** 23 March 2024

Keywords: Cardiovascular flows; Computational modelling; Biological flows

Abstract

This article presents a broad overview of the fluid mechanics of the human cardiovascular system. Beginning in the heart, we travel through the main features of our circulation to highlight important functions and diseases where fluid mechanics plays a central role. Of particular focus is the role of computational modelling in uncovering the dynamic flow phenomenon throughout our body, its association with cardiovascular disease mechanisms and progression and its importance in clinical treatment planning. We also emphasize the multiscale nature of the cardiovascular system, and associated challenges. The main aim of this review is to highlight progress and ongoing challenges in our understanding of cardiovascular haemodynamics, as well as the future outlook for translating the current state-of-the-art to widespread clinical application and improved patient outcomes.

Impact Statement

Cardiovascular disease is the leading cause of death worldwide. Fluid dynamics plays a central role in the functioning of the human cardiovascular system, as well in the progression and treatment of its associated diseases. This review highlights advances in our understanding of cardiovascular fluid dynamics, and ongoing challenges in translating engineering insights into clinical treatments for cardiovascular disease.

1. Introduction

The significance of the human cardiovascular system has intrigued philosophers and scientists for at least 3500 years. This is evidenced by the description of the *metou* system of vessels driven by central pulsations in the ancient Egyptian *Ebers Papyrus*, which is the earliest known documentation of humans' knowledge of their circulation, dated 1550 BC (Ritner 2006). Writings on the cardiovascular system are also present in various other ancient schools of thought, including by Greek physicians of the *Hippocratic Corpus*, the book *Nei Jing* in ancient Chinese medicine and the *Charaka Samhita* from ancient Indian *Ayurvedic* medicine (Fung 1984; Patwardhan 2012; Lemonnier *et al.* 2017).

We now know that the adult human circulation system consists of billions of blood vessels spanning approximately 100 000 km in length, through which blood is driven by the pumping of the heart



Table 1. Approximate values of the Reynolds number and Womersley number in different anatomical regions. Womersley numbers were estimated based on a pulsatile flow frequency of 1 Hz. Reported Reynolds numbers are the mean and peak values within cardiac cycles, based on the following references: Aortic flows – Ku (1997), Stein & Sabbah (1976), Stalder et al. (2011), Poelma, Watton & Ventikos (2015) and Ha et al. (2018). Coronary arteries – Kajiya et al. (1987), Perktold, Nerem & Peter (1991), He & Ku (1996) and Zhang et al. (2015). Carotid arteries – LoGerfo et al. (1981), Ku & Giddens (1983) and Lee et al. (2008). Pulmonary arteries – Sloth et al. (1994). Inferior vena cava – Joseph, Voit & Frahm (2020). Arterioles and capillaries – Secomb (2017).

Anatomical region	Mean Reynolds number	Peak Reynolds number	Womersley number
Ascending aorta	1000	4000–9000	19
Abdominal aorta	600	2500–4500	13
Coronary arteries	250	600–800	3
Carotid arteries	450	900–1200	4
Main pulmonary artery	1600	3000–4500	16
Arterioles	1	1	0.06
Capillaries	10^{-3}	10^{-3}	0.003
Inferior Vena Cava	400	1500–2500	13

(Jones 1969). The heart pumps roughly once every second, or approximately 2 billion times over the average lifespan, through blood vessels with diameters ranging from roughly 3 cm to 5 μm (Secomb 2017; United Nations 2022). The dynamics of blood flow within vessels, which occurs on the scale of seconds, has implications for cardiovascular health on the scale of years (Beere, Glagov & Zarins 1984; Giddens, Zarins & Glagov 1993). This wide range of values underscores the highly multi-scale nature of this interconnected system, which, from the fluid dynamics perspective, features phenomena that simultaneously occur at Reynolds numbers of $O(10^3)$ in the aorta and $O(10^{-3})$ in capillary networks (see table 1).

In the last few decades, fluid dynamics and its effect on surrounding tissues and micro-scale biological responses have emerged as key factors in our understanding of cardiovascular function, its associated diseases and their treatments (Ku 1997). For example, diseases related to atherosclerosis, which cause the narrowing of certain arteries and are the leading cause of death globally, have been significantly correlated with regions of low and oscillatory shear stress as well as the direction and topology of the shear stress field exerted on vessel walls (Giddens et al. 1993; Arzani & Shadden 2018; Kok et al. 2019; Morbiducci et al. 2020; Hoogendoorn et al. 2021; Mazzi et al. 2021). Complex flow features, such as vortices, jets and helical flow, have been reported in blood vessels throughout our bodies and are crucial determinants of heart, valve and vascular function, as well as the development of life-threatening blood clots, tears and other diseases in vessel walls (Sforza, Putman & Cebra 2009; Morbiducci et al. 2011; Seo et al. 2014; Liu et al. 2015; Sotiropoulos, Le & Gilmanov 2016; De Nisco et al. 2019). While these interactions between blood flow and cardiovascular health are predominantly analysed in the context of Newtonian fluid dynamics, blood ceases to behave as a continuum as we progress from these inertial flows in large vessels to Stokesian flows in the microcirculation. At these scales, the dynamics of suspended cells and other constituents plays several important roles – for example, in deadly diseases such as sickle cell disease and malaria, as well as in the formation of blood clots, which can be beneficial in preventing bleeding but also dangerous when they impede flow within blood vessels (Freund 2014; Secomb 2017).

In many of these scenarios, flow-induced forces play an important role in mechanobiological sensing at the cellular level, which elicits cell signalling processes that impact long-term disease progression (Humphrey 2008). Moreover, in the treatment of several cardiovascular diseases, studies have shown improved outcomes from treatments guided by haemodynamic metrics, such as flow and pressure,

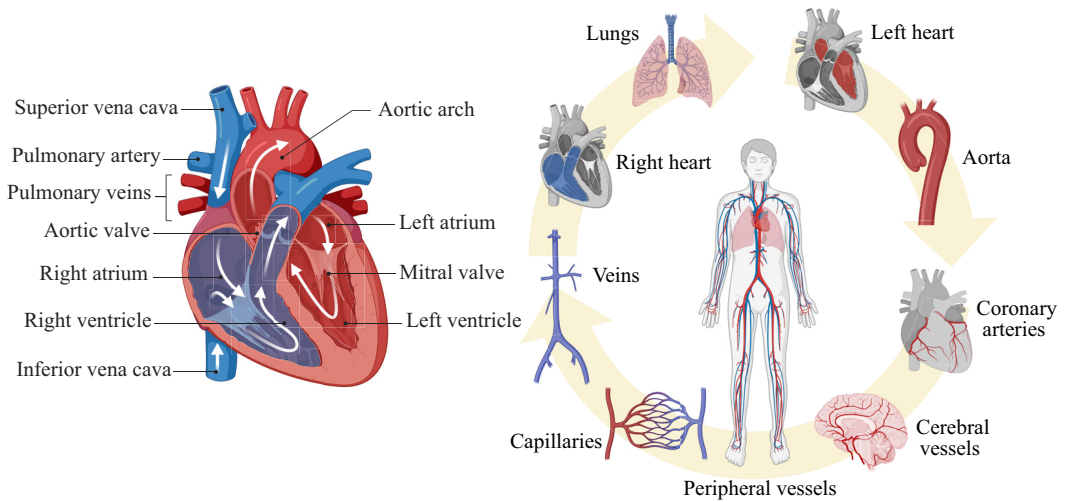


Figure 1. An overview of the key features in the human cardiovascular system that we discuss in this review. The left panel shows a cross-section of the heart with relevant anatomical features labelled. The right panel schematically shows the order in which we will visit the different parts of the cardiovascular system.

rather than anatomical imaging alone (Powers 1991; Pijls *et al.* 2010; Taylor, Fonte & Min 2013). The recognition of the importance of haemodynamics to cardiovascular health has led to the rapid growth of image-based computational fluid dynamics (CFD) models, which simulate haemodynamics in anatomical models based on patient-specific imaging data, to analyse normal and pathological blood flow in the cardiovascular system, and correlate this haemodynamics with diseases and treatments (Taylor, Hughes & Zarins 1998; Marsden 2014; Mittal *et al.* 2016).

This review aims to take the reader on a journey through the intricacies of the human cardiovascular system (figure 1). Along the way, key flow phenomena of clinical and academic interest will be discussed, and the multi-scale nature of the circulatory system will be highlighted. Although much of cardiovascular health is a result of the interaction between blood flow, tissue mechanics, cellular function, genetics and other environmental and lifestyle factors, we focus here on phenomena of interest to fluid dynamics practitioners. We will also draw attention to computational modelling techniques that have advanced our understanding of cardiovascular haemodynamics and health, as well as challenges thereof.

The journey begins at the heart of the circulatory system, so to speak, in its main pumping chamber called the left ventricle.

2. Left ventricle

The left ventricle is one of the four heart chambers, and (in the normal circulation) one of two pumps that push blood on its long journey to ensure the nourishment and oxygenation of organs and tissues. It is located in the heart's lower left portion and is roughly conical in shape, with a thick muscular wall that is essential for generating the necessary force to pump oxygen-rich blood throughout the body. During one cardiac cycle, the left ventricle undergoes roughly four phases: passive filling (diastole), isovolumetric contraction, ejection (systole) and isovolumetric relaxation. In the diastolic phase, the ventricular muscle is relaxed, with oxygenated blood flowing in from the left atrium. The mitral valve, located between the left atrium and the left ventricle, is open, while the aortic valve, which connects the left ventricle and the aorta, is sealed due to the higher pressure in the aorta. As the ventricular muscles contract, the pressure increases sharply from 3–12 to 100–140 mmHg within a short time span of 200 ms. The volume of blood within the chamber remains constant since two valves are closed in the isovolumetric contraction

phase. Then, as the left ventricular pressure exceeds that in the aorta, the aortic valve opens and blood is pumped into the aorta. A subsequent muscle relaxation lowers the pressure, and after isovolumetric relaxation, the mitral valve reopens, refilling the left ventricle. This cycle produces what is known as the ‘pressure-volume loop’, with the enclosed area quantifying the work done during each heart beat.

Due to the substantial change in one cardiac cycle, the flow inside the left ventricle is strongly unsteady. For example, during the rapid passive filling phase, the mitral jet, emanating from the mitral valve (diameter ≈ 2 cm), generally has a peak velocity of 0.8 m s^{-1} and attains a Reynolds number of 4000. For a classical jet, this would entail a turbulent dynamics. An annular vortex is formed downstream of the mitral orifice resulting from the roll-up of the shear layer emanating from the leaflets of the mitral valve. This three-dimensional vortex ring develops into a large-scale, asymmetric, clockwise rotating vortex at the centre of the left ventricle by the end of diastole (Le *et al.* 2012; Le & Sotiropoulos 2012; Fortini *et al.* 2013). This facilitates filling by reducing convective losses (Charonko *et al.* 2013). Its rotation also supports the ejection of blood flow toward the aortic outflow track during systole with minimal flow energy dissipation (Pedrizzetti & Domenichini 2005).

Considering this intricate haemodynamics, both *in vivo* imaging as well as computational modelling offer promising ways to non-invasively quantify left ventricular haemodynamics and assess both healthy and pathological behaviour. The imaging of such cardiac flows is traditionally performed using Doppler echocardiography and, more recently, using ‘four-dimensional (4-D) flow MRI’. The latter is a relatively recent development in cardiac magnetic resonance imaging (MRI) that allows the imaging of time-resolved flows and anatomies in three dimensions (Markl *et al.* 2012; Stankovic *et al.* 2014; Azarine *et al.* 2019; Garcia, Barker & Markl 2019). Four-dimensional flow MRI has been used extensively in the imaging of cardiac flows as well as flows within several large blood vessels to identify aberrant flow patterns and their relationship to cardiac, vascular and valvular diseases. While current clinical use remains confined to large academic centres, new imaging protocols and analysis techniques are poised to move this imaging into the clinical standard of care. However, a challenge with non-invasive *in vivo* flow imaging is its limited resolution, which does not allow fine-grained imaging of all flow features as well as flows in smaller blood vessels. Computational modelling is therefore a viable alternative to quantify left ventricular haemodynamics accurately and non-invasively.

However, performing realistic and accurate simulations still poses considerable challenges; accurate simulations of left ventricular flow require patient-specific geometries, physiological wall motion generated by active tissue mechanics and fully coupled fluid–solid interaction with the inclusion of the mitral and aortic valves at the inlet and outlet. Significant progress has been made by using various simplifying assumptions to reduce the complexity of these models given specific research interests. For example, the flow can be simplified using lumped-parameter models (see § 7) to efficiently obtain pressure and volume curves, but these models are inherently incapable of providing the full flow field inside the chamber (Hirschvogel *et al.* 2017; Augustin *et al.* 2021). The geometry of the left ventricle can be idealized (Cheng, Oertel & Schenkel 2005; Domenichini, Pedrizzetti & Baccani 2005; Meschini *et al.* 2018; Dedè, Menghini & Quarteroni 2021) or patient specific (Le & Sotiropoulos 2012; Vedula *et al.* 2016; Hirschvogel *et al.* 2017). In this context, it is worth noting that the interior surface of the cardiac chambers is not smooth. It features papillary muscles, trabeculae of different sizes and false tendons, presenting a sponge-like structure extending into the chamber (see § 11). From simulations that have incorporated these detailed endocardial structures from *in vivo* imaging, they are thought to play a role in ensuring complete closure of the mitral valve, efficient filling and ejection of blood as well as reduced stress in the myocardium wall (Madu & D’Cruz 1997; Kulp *et al.* 2011; Chnafa, Mendez & Nicoud 2016; Lantz *et al.* 2016; Vedula *et al.* 2016; Sacco *et al.* 2018*b*). Another simplification in studies that have focused on ventricular filling is the absence of the mitral and aortic valves (Cheng *et al.* 2005), or simplified valves incorporated as resistive lumped-parameter elements (Dedè *et al.* 2021). More recently, 3-D valves, simulated using Arbitrary Lagrangian–Eulerian or immersed boundary methods, have been used to capture realistic flow dynamics in the healthy or pathological left ventricle (Vedula *et al.* 2016; Meschini *et al.* 2018; Meschini, Viola & Verzicco 2019). Finally, the ventricular wall motion can also be simplified as prescribed motion on moving meshes or boundaries

constructed from imaging data (Domenichini *et al.* 2005; Chnafa, Mendez & Nicoud 2014). However, to model the contraction and relaxation of tissues accurately, fluid–solid interaction simulation of the left ventricle can also be expanded to include electrophysiology and active contraction (Vigmond *et al.* 2008; Quarteroni *et al.* 2017; Viola, Meschini & Verzicco 2020). We recommend the review of Verzicco (2022), which describes the physiology and numerical methods coupling electrophysiology, solid and fluids of the whole heart in detail.

The high Reynolds number in ventricular flow raises questions about the validity of the laminar flow assumption. Research, including both *in vivo* studies (Zajac *et al.* 2015) and numerical methods (Chnafa *et al.* 2014; Dedè *et al.* 2021), indicates that turbulence occurs during late diastole and is initiated by the breakup of large vortex structures. Turbulence models, such as large eddy simulation and Reynolds-averaged Navier–Stokes, have shown improved results in left ventricular haemodynamic analyses compared with laminar flow models and experimental data, due to their ability to capture transient or turbulent states involving small-scale phenomena that cannot be retrieved under the laminar hypothesis (Chnafa *et al.* 2016; Jahanzamin, Fatouraei & Nasiraei-Moghaddam 2019). In fact, a recent study by Saqr *et al.* (2020) demonstrated that turbulence is inherent to cardiovascular flows, not only in the left ventricle but throughout the body. However, it is important to note that fully developed turbulence is not typically observed under physiological conditions (Chnafa *et al.* 2014; Dedè *et al.* 2021). Large eddy simulation approaches are generally better suited for transitional flow regimes than Reynolds-averaged Navier–Stokes approaches, since the latter assume that turbulence is fully developed. In the context of finite-element modelling, the variational multiscale method (Hughes *et al.* 1998; Hughes, Mazzei & Jansen 2000; Bazilevs *et al.* 2007), which is a stabilization technique to control numerical oscillations associated with high Reynolds numbers, models turbulence in a similar manner to large eddy simulation and has been widely applied in both cardiac flow (Quarteroni *et al.* 2017; Dedè *et al.* 2021; Zingaro *et al.* 2021) and cardiovascular flow simulations (Hughes *et al.* 2020; Liu *et al.* 2020).

Left ventricular haemodynamics is significantly affected by the functioning of the mitral valve, which ensures the correct direction of blood flow from the left atrium to the left ventricle. Mitral valve disease is the most common valvular heart disorder, particularly in ageing populations, with a prevalence of more than 10 % in people over 75 years (Nkomo *et al.* 2006). The two main types of mitral valve disease are mitral valve stenosis and mitral valve regurgitation. Mitral valve stenosis occurs due to the narrowing or stiffening of the mitral valve, which prevents it from fully opening. As a result, flow from the left atrium to the left ventricle is obstructed and, in turn, the heart pumps less efficiently. Mitral valve stenosis causes a pressure increase in the left atrium, which induces atrial wall thickening and often atrial dilatation. The augmented atrial pressure may also produce blood congestion in the pulmonary veins (Maeder *et al.* 2018). From CFD simulations, the mitral jet, generated during diastole, is seen to shrink in size and strengthen when the stenosis gets more severe. As a consequence, the kinetic energy of the flow, the shear stresses acting on the tissues and the transvalvular pressure drop increase (Meschini *et al.* 2019). This also increases mitral valve regurgitation, where the incomplete closure of the mitral valve allows blood to flow backward into the atrium. As mitral valve regurgitation worsens, the heart must work harder to pump blood to the body, leading to a progressive increase in left ventricle volume with normalization of wall stress. In terms of the fluid dynamics, large-scale flow recirculation, smaller vortices scattered throughout the left ventricle and the presence of a regurgitant jet which promotes increased turbulence in left ventricle have been observed in patients with mitral regurgitation (Al-Wakeel *et al.* 2015; Bennati *et al.* 2023).

Common therapies for valvular diseases include valve repair or replacement with prosthetic heart valves. Present-day prosthetic heart valves can be classified into two broad categories, rigid-leaflet or mechanical valves, and valves with flexible leaflets made either of synthetic materials or biological tissue (the latter are called bioprosthetic valves). However, all known heart valve prostheses have been associated with various clinical complications due to the non-physiological flow patterns they induce upon implantation. Experimental techniques such as laser Doppler velocimetry and particle image velocimetry have been extensively employed to study prosthetic heart valve flows *in vitro*, showing that

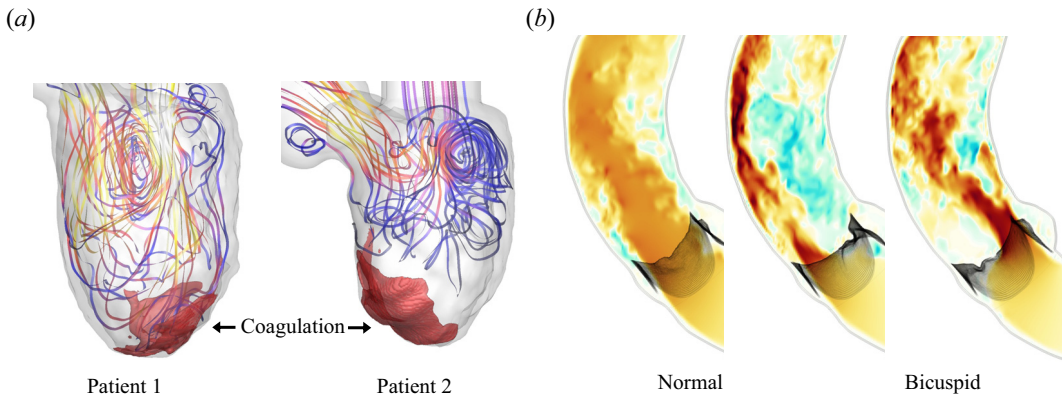


Figure 2. (a) Average flow and coagulation patterns in the left ventricle for two patients with cardiomyopathy, from patient-specific simulations of flow coupled with biochemical coagulation reactions. Note the different flow fields and coagulation patterns, highlighting the importance of patient-specific risk. Courtesy of J.-H. Seo and R. Mittal, Johns Hopkins University. (b) Simulated flow through normal and bicuspid aortic valves. Note the asymmetric jets through bicuspid valves. The middle panel shows the more common phenotype (fusion of the left and right coronary cusp leaflets) and the right panel shows the less common phenotype (fusion of the right and non-coronary cusp leaflets) (Kaiser *et al.* 2022).

the transmitral vortex formation could be influenced by the saddle annulus dynamics and also by the angle of valve opening (Kheradvar & Falahatpisheh 2012). Fluid–solid interaction simulations have also revealed drastically different flow fields created by different prosthetic heart valves, and identified non-physiologic flow patterns causing blood cell damage and platelet activation (Borazjani 2013). Moreover, studies have shown that, with impaired left ventricular function, the flow disturbances introduced by the bi-leaflet mechanical valve reduce the penetration capability of the mitral jet and weaken the recirculation in the ventricular apex (Meschini *et al.* 2018). These effects are discussed in detailed prior reviews on heart valve fluid mechanics (Peskin 1982; Yoganathan, Chandran & Sotiropoulos 2005; Sotiropoulos *et al.* 2016).

Another pathology of the left ventricle is cardiomyopathy (figure 2a), which refers to a condition where the heart muscle becomes enlarged, thickened or stiff, consequently diminishing the heart’s ability to pump blood and potentially leading to heart failure. The most prevalent type is dilated cardiomyopathy, which is characterized by progressive enlargement and deterioration of the left ventricle’s contraction capacity. The reduced cardiac function is reflected in a weaker diastolic mitral jet which penetrates less into the wider left ventricle, and a smaller vortex in the centre of the cavity that does not support flow redirection toward the outflow, resulting in increased residual volume during pumping (Mangual *et al.* 2013; Eriksson *et al.* 2016; Riva *et al.* 2022).

Left ventricular assist devices (LVADs) have become a key element for the treatment of patients suffering from terminal heart failure. These devices serve different purposes, such as a bridge to transplant (Miller *et al.* 2007; Aaronson *et al.* 2012), a bridge to recovery or as long-term therapy (Slaughter *et al.* 2009). The LVADs pump blood from the left ventricle to the aortic root, providing a mechanical counterpart that works in conjunction with the patient’s own left ventricle. Modern LVADs employ continuous flow physiology, which means they continuously pump blood throughout the cardiac cycle. The LVADs provide significant unloading of the left ventricle, manifested by decreased end-diastolic pressure, end-diastolic volume and pressure-volume area (Uriel *et al.* 2016). Simultaneously, a decrease in the left ventricular volume is evident almost immediately in patients on LVAD support (McCarthy *et al.* 1995). Besides the left ventricle, device implantation substantially modifies the haemodynamic conditions within the aorta. Due to the high velocity introduced by the pump, the aortic valve may remain persistently closed, especially when native cardiac ejection is low. Moreover, the adverse event profile of contemporary left ventricular assist devices includes suction events (where devices

unload too much so that the ventricular chamber collapses) (Vollkron *et al.* 2007; Griffin & Katz 2014), thrombosis within the device (Eckman & John 2012), right ventricular failure, device-related infections, stroke, dysrhythmia and aortic incompetence (Park *et al.* 2012; Kirklin *et al.* 2015). Computational fluid dynamics has been employed to characterize and optimize numerous different designs for LVAD functional performance towards improved long-term outcomes (Fraser *et al.* 2011). Computational fluid dynamics results identify that, with device support, the aortic root is largely a region of vascular stasis, with significantly higher shear stress on the leaflet tips in patients with aortic incompetence (Shad *et al.* 2021). Strong correlations between device outflow graft orientation and wall shear stress, pressure and turbulent energy dissipation in the ascending aorta are found. Based on these flow patterns, a more distal insertion has been recommended to produce at least occasional parallel flow through the aortic valve and ensure intermittent aortic valve opening (Osorio *et al.* 2013; Karmonik *et al.* 2014).

3. Aortic flow

Oxygenated blood pumped by the left ventricle to the rest of the circulation first passes through the aorta, the largest blood vessel in the human body at roughly 3 cm diameter. Continuing our Lagrangian journey, from the outlet of the left ventricle, the aorta ascends towards the thoracic region of the body, where it arches around and then descends into the abdomen. Along the way, several arteries branch off to carry blood to the heart, head, torso, kidneys and other organs. The aortic root features a valve which consists of three passive leaflets that are housed within three corresponding pouches in the aortic wall. These pouches are called aortic sinuses. The aortic valve, aortic sinuses and the curvature of the aortic arch interact with the flow emanating from the left ventricle to exhibit an array of interesting fluid mechanics that has fascinated scientists for centuries. This is famously evidenced by the illustrations of da Vinci in 1513 showing regions of recirculation around the aortic valve (Boon 2009).

Of particular interest has been the fluid mechanics of the opening and closure of the aortic valve and its relation to the geometry of the aortic sinus (Yoganathan, He & Jones 2004; Sotiropoulos *et al.* 2016). The three passive leaflets of the aortic valve respond to the haemodynamics within the upstream left ventricle and the downstream aorta to provide minimal flow resistance while open during ventricular contraction at systole, and to minimize backflow during ventricular filling at diastole. The opening is driven by the pressure difference between the contracting left ventricle and the aorta, i.e. the leaflets open when the pressure within the left ventricle exceeds the aortic pressure. Interestingly, the closure of the aortic valve begins before the end of this ejection phase – with an estimated 75 % of the valve closure occurring while blood continues to flow from the left ventricle to the aorta (Bellhouse & Talbot 1969). This ensures that the valve is completely closed with minimal reversed flow at the end of systole.

The hydrodynamic mechanism driving this has intrigued numerous researchers (Bellhouse & Bellhouse 1968; Peskin & Wolfe 1978), starting with the first modern study of this dynamics by Henderson & Johnson (1912). The seminal works of Bellhouse and colleagues highlighted the importance of the sinus vortex, which results from flow over the top of the aortic valves into the aortic sinuses, in initiating aortic valve closure using laboratory experiments accompanied by elegant theoretical calculations of the pressure induced by these vortices on the leaflet surfaces (Bellhouse 1969; Bellhouse & Talbot 1969). They also hypothesized the role of these vortices in maintaining the valve open position through a balance between sinus flow and the flow through the valve. While the physiological significance of the sinus vortex is still a topic of investigation (Moore & Dasi 2014, 2015), it is remarkable that the contemporary results exhibit a striking parallel with the illustrations of Da Vinci over 400 years earlier (Gharib *et al.* 2002).

The interaction of the flow with the valve leaflets and the aortic sinus is also important to the pathophysiology of aortic valve disease. Pathological conditions relating to aortic root diseases and congenital defects, such as bicuspid aortic valves where the valve forms with two leaflets instead of three, lead to abnormal flow patterns. In these cases, studies have reported asymmetric jets emanating from the valve opening, which impinge on the aortic wall to cause unphysiological shear stresses (Girdauskas *et al.* 2011; Barker *et al.* 2012; Verma & Siu 2014; Saikrishnan, Mirabella & Yoganathan

2015; Kaiser *et al.* 2022). This is shown in figure 2(b). The replacement of diseased aortic valves with mechanical and prosthetic valves also alters the haemodynamics. This is most commonly done using mechanical valves that consist of flat pivoting metal plates to mimic leaflets. The interaction of flow with the rigid leaflets gives rise to highly complex unphysiological flow within the ascending aorta, such as interacting vortex rings and shear layers emanating from the tips of the flat-plate leaflets (Dasi *et al.* 2009; Sotiropoulos *et al.* 2016). Moreover, studies have reported increased shear regions within the housing of prosthetic valves that can damage blood cells (Dasi *et al.* 2009). Prosthetic valves with flexible leaflets also exhibit the unphysiological flow patterns described above, albeit to a lesser degree depending on the properties of the leaflet and housing. In addition, geometrical alterations to the aortic root through surgical procedures to treat aortic valve diseases have been shown to result in secondary flows that exhibit turbulent transition and associated stress fluctuations (Stein & Sabbah 1976; Peacock 1990; Moore & Dasi 2014). The interaction of these unphysiological flow features with the valve leaflets is believed to exacerbate the stiffening or calcification of aortic valve leaflets as well as complications at the aortic wall. While the exact mechanism leading to leaflet calcification is not clear, there are strong correlations between flow-induced mechanical stresses, such as oscillatory shear stresses from flow recirculation, and the inflammation of endothelial cells on the leaflets (Ge & Sotiropoulos 2010; Gould *et al.* 2013). The flow through asymmetrically calcified or stenosed valves has been shown to develop into a jet that impinges on the aortic wall, where the curvature of the aortic arch introduced helical Dean vortex flows, intermittent turbulent stresses and audible sounds called murmurs (Zhu, Seo & Mittal 2018, 2019; Bailoor *et al.* 2021).

The rich haemodynamics associated with aortic flows has led to efforts to non-invasively quantify these flow *in vivo* using 4-D flow MRI in search of haemodynamic biomarkers of disease (Von Knobelsdorff-Brenkenhoff *et al.* 2014; Burris & Hope 2015; Garcia *et al.* 2019; Zimmermann *et al.* 2023). In this context, 4-D flow MRI is a promising method to non-invasively evaluate haemodynamic patterns that can aid in the diagnosis of valvular diseases as well as in the evaluation of prosthetics. However, the challenge with 4-D flow MRI is accurately resolving the flow dynamics and associated wall interactions, which has led to the emergence of computational methods to simulate these flows. The first method aimed at simulating the fluid dynamics of cardiac valves was introduced by Peskin and colleagues just over 50 years ago (Peskin 1972; Peskin & McQueen 1980). This technique, which is now referred to as the immersed boundary method, continues to be the mainstay of computational models for cardiac valves (Mittal & Iaccarino 2005; Griffith & Patankar 2020). Since its introduction, the immersed boundary method has been coupled with finite-element formulations of the mechanics and material properties of valve leaflets (Boffi *et al.* 2008; Griffith & Luo 2017; Kaiser *et al.* 2021). Sharp-interface immersed boundary methods have been developed, which can resolve the surface of the leaflets more accurately and therefore provide improved surface force estimates (Gilmanov & Sotiropoulos 2016; Seo *et al.* 2020; Bailoor *et al.* 2021). In the finite-element context, these immersed boundary fluid–structure interaction methods are broadly referred to as immersed finite-element or immersogeometric methods (Hsu *et al.* 2014, 2015; Kamensky *et al.* 2015).

These methods have been extensively used to study the haemodynamics of native as well as prosthetic valves in healthy and diseased states (see Votta *et al.* (2013) and Sun, Mao & Griffith (2019) for comprehensive reviews of applications). In fact, one such simulation-based product has recently received United States Food and Drug Administration approval to support clinical decision making for transcatheter aortic valve replacements (www.dasisim.com). However, an ongoing challenge for more widespread clinical acceptance of these simulation tools is the lack of validation with *in vivo* flow fields. The majority of validation studies have focused on the haemodynamics of mechanical heart valves measured in laboratory experiments (Dasi *et al.* 2007; Ge *et al.* 2008; Nobili *et al.* 2008; Guivier-Curien, Deplano & Bertrand 2009; Jun *et al.* 2014). In comparison, fewer studies have validated simulation models of heart valves with flexible leaflets (Wu *et al.* 2016; Sigüenza *et al.* 2018; Lee *et al.* 2020), especially with patient-specific flow fields (Emendi *et al.* 2021; Kaiser *et al.* 2023).

While a major focus of studies on aortic haemodynamics has been on the function of the aortic valve, the influence of aortic flow on the wall of the aorta has important health consequences. In particular,

shear stresses induced on the aortic wall due to the jet emanating from the aortic valve as well as the resultant turbulent flow within the aorta can damage the epithelial cell lining of the aortic wall. The peak Reynolds number in the aorta can be as high as ~ 4000 , which is significantly higher than the transitional Reynolds number in pipes (Ku 1997). However, interesting work has shown that the nature of cardiac pulsatility, including the specific waveform of aortic flow, is close to the optimal behaviour required to combine sufficient flow rates with low wall shear stresses. This is due to the combination of a short ejection phase followed by a prolonged diastolic phase that inhibits turbulence (Scarselli *et al.* 2023).

Studies have also reported that 60%–80% of patients with bicuspid aortic valves develop dilation of the aortic wall (Verma & Siu 2014). While the exact mechanism leading to aortic dilation is unknown, altered haemodynamics associated with the impinging jet arising from bicuspid valves is thought to play a role (Girdauskas *et al.* 2011; Barker *et al.* 2012; Rodríguez-Palomares *et al.* 2018; Dux-Santoy *et al.* 2020). Furthermore, aortic dilation increases the risk of aortic dissection, which is a tear in the inner wall of the aorta that introduces a parallel flow channel within the aortic wall, referred to as the false lumen (in contrast to the native ‘true’ lumen), and poses the risk of rupture of the aortic wall (Verma & Siu 2014). Although the clinical management of aortic dissections is primarily based on anatomical imaging (Spinelli *et al.* 2018), studies have shown that haemodynamics plays a significant role in the prognosis (Bäumler *et al.* 2020). For example, while the development of clots to occlude the false lumen has been shown to improve patient outcomes, the structure of these clots can cause elevated pressure within the false lumen and increase rupture risk (Tsai *et al.* 2008; Berguer *et al.* 2015).

Another pathological condition that poses the risk of aortic wall rupture is the occurrence of dilations in the abdominal aorta, referred to as abdominal aortic aneurysms (Sakalihasan, Limet & Defawe 2005). For patients with aortic dissections and aortic aneurysms, the stratification of rupture risk depends on thrombus formation due to flow stagnation as well as stress distributions induced on the aortic wall through its interaction with the haemodynamics (Bluestein *et al.* 1997; Vorp *et al.* 2001; Francis 2002; Sho *et al.* 2004). A challenge in this context is the quantification of aortic wall mechanics, which is often heterogeneous and difficult to measure *in vivo*. Conversely, there are also haemodynamic risks associated with the constriction of the aortic wall. This narrowing of the descending aorta, which is referred to as aortic coarctation and accounts for 6%–8% of congenital heart defects, can lead to aortic rupture, hypertension and stroke (Singh *et al.* 2015). These are therefore active avenues for the future application of patient-specific computational models to aid in clinical decision making (for example, Bluestein *et al.* 1997; Salsac, Sparks & Lasheras 2004; Les *et al.* 2010; Alimohammadi *et al.* 2015; Chen *et al.* 2016; Qiao *et al.* 2019; Bäumler *et al.* 2020, among many others). Mourato *et al.* (2022) provide a comprehensive review of fluid–structure interaction computational models pertinent to aortic wall diseases.

4. Coronary haemodynamics

While the pumping action of the heart ensures the delivery of blood to the far reaches of our circulatory system, the coronary arteries bear the unenviable responsibility of delivering nutrition and oxygen-laden blood to the heart muscle itself. The importance of the coronary circulation is underscored by the fact that the heart has the highest oxygen consumption per gram of any organ; it extracts 70%–80% of the oxygen delivered, compared with 30%–40% utilized by skeletal muscles (Goodwill *et al.* 2017). It is no wonder that coronary artery disease, which inhibits the transport of blood to the myocardium due to the narrowing or occlusion of coronary arteries, is the leading cause of death worldwide (Ralapanawa & Sivakanesan 2021; Tsao *et al.* 2022).

The left and right coronary arteries arise on either side of the aortic sinus and carry 3%–5% of the volume of blood pumped by the heart into the myocardial tissue (Guyton & Hall 2006). They have diameters of ≈ 3 mm at their origin on the aortic sinus, and proceed through a series of bifurcations that leads to small arteries and arterioles with diameters ≈ 100 μm , and eventually capillaries with diameters ≈ 10 μm (Lee & Smith 2012). Although the peak Reynolds number in coronary arteries is typically < 500 , coronary flow can exhibit higher Reynolds number jets downstream of constrictions that occur

due to disease. This has consequences for the progression of coronary artery disease as well as the stability of calcified plaques that cause these constrictions (Falk, Shah & Fuster 1995; Samady *et al.* 2011). A peculiar aspect of the coronary circulation is that, while maximum flow through most vascular networks in the body occurs during systole, a majority of the flow through coronary arteries occurs during diastole. This is due to the so-called ‘cross-talk’ between the contracting myocardial tissue and the coronary circulation from large vessels to arterioles and capillaries embedded within the myocardial tissue (Westerhof *et al.* 2006). The disparate length scales involved in the coronary circulation and its interaction with the beating (and moving) heart, combined with the importance of coronary flows to cardiovascular function, present a host of challenges in understanding, imaging, as well as modelling coronary artery blood flows.

Most studies on coronary artery haemodynamics have focused on the flow through the large arteries that can be clinically imaged, either invasively using coronary angiography or non-invasively using computed tomography. Efforts to measure and model coronary artery flow are motivated by several randomized clinical trials that have firmly established the importance of considering haemodynamics in clinical care. Coronary artery disease causes the narrowing and stiffening of coronary artery walls, which limits the delivery of blood to the myocardium. This has been observed to occur in regions of the vasculature that experience low and oscillating wall shear stress in laboratory experiments as well as animal models (Giddens *et al.* 1993). Coronary artery disease is usually treated either by inserting stents within affected arteries to relieve the narrowing, or in cases with more severe occlusion, surgically bypassing the location of narrowing in arteries by using grafts (Yusuf *et al.* 1994; Windecker *et al.* 2014). In both cases, the long-term outcomes for patients receiving these treatments has been shown to significantly improve when treatments are guided by haemodynamic measurements of pressure loss within the affected artery, rather than based on anatomical measures of the narrowing in the artery (Meijboom *et al.* 2008; Tonino *et al.* 2009; Pijls *et al.* 2010). There is also evidence that short as well as long-term treatment outcomes are dependent on local blood flow patterns at the site of stenting or grafting, such as flow reversal and competitive flow between the native diseased artery and bypass graft (Pagni *et al.* 1997; Sabik *et al.* 2003; Tokuda *et al.* 2008), as well as regions of stagnation or abnormal wall shear stress (Malek, Alper & Izumo 1999; Chatzizisis *et al.* 2008; Humphrey 2008).

While the major focus of studies on coronary artery blood flows has been on the flows within the coronary arteries themselves, the location of coronary arteries and their proximity to the aortic valve also raises interesting questions. Owing to their origin within the aortic sinus, researchers have long hypothesized about the influence of recirculating flow within the aortic sinus (due to interaction with the aortic valve) on coronary circulation, and *vice versa*. Bellhouse, Bellhouse & Reid (1968) used a laboratory model to relate flow stagnation on the ridge of the aortic sinus to high pressure that would be beneficial to driving coronary flow. They showed a significant drop in coronary flow when the coronary arteries originate outside the aortic sinus. There is also a difference in the fluid dynamics between the two sinus lobes that contain the origin of coronary arteries, or coronary sinuses, and the lobe that does not. Moore & Dasi (2015) showed that the presence of coronary arteries originating from the coronary sinuses pulls the sinus vortex closer to the walls. This leads to higher flow velocities, shear stresses and washout in the coronary sinuses compared with the non-coronary sinus. In addition, the aortic leaflets corresponding to coronary sinuses open farther into the sinus and exhibit better mechanics. These haemodynamic differences have physiological significance because low recirculation velocities lead to less washout in the non-coronary sinus, and low and oscillatory shear stresses have been linked to calcification (Chandra, Rajamannan & Sucosky 2012). Interestingly, these observations also present a possible mechanism for the observation that the non-coronary sinus is often the first to calcify – eventually leading to aortic valve calcification (Freeman & Otto 2005).

The importance of fluid mechanics in these critical clinical questions has spurred development of patient-specific computational models of coronary artery blood flows for personalized risk assessment and treatment planning. Current state-of-the-art methods use non-invasive clinical imaging to build patient-specific coronary artery anatomical models (Updegrove *et al.* 2017). The flow within these anatomies is simulated using either high-fidelity 3-D flow simulation methods, or reduced-order methods

that evaluate the flow field either only along the centreline of the arteries or at specifically chosen points in the anatomy, such as bifurcations, by assuming Poiseuille flow throughout (see § 7). Owing to the complex geometries of vascular trees, 3-D simulations are usually performed using stabilized finite-element methods with unstructured meshes (Taylor *et al.* 1998; Marsden & Esmaily-Moghadam 2015). A significant challenge is that these image-based models are usually restricted to the large vessels in the coronary tree that are visible from volumetric clinical imaging. Therefore, the effect of the smaller downstream arteries and their interaction with the contracting myocardium needs to be modelled appropriately. This is usually accomplished by coupling the flow within the large arteries included in these anatomical models with lumped-parameter boundary conditions at their outlets (Kim *et al.* 2010). These boundary conditions are designed to account for the resistance as well as dilation of downstream blood vessels not included in the model. They also recapitulate the key features of coronary physiology in which coronary flows peak at diastole due to the ‘intramyocardial pressure’ experienced by the coronary circulation via its interaction with myocardial contractions. In addition, the compliance of the coronary artery walls as well as their movement with the contracting myocardium pose additional challenges in the modelling of coronary haemodynamics. Although the former is commonly included in models using simplified as well as high-fidelity fluid–structure interaction techniques, such as the coupled momentum method (Figueroa *et al.* 2006) and arbitrary Lagrangian–Eulerian (Seo *et al.* 2020), studies have shown that the effect of wall compliance can be small in certain situations (Torii *et al.* 2009; Eslami *et al.* 2020). However, although the movement of coronary arteries due to myocardial contraction can have significant effects on the haemodynamics, this is rarely included in simulations (Santamarina *et al.* 1998).

As expected, the modelling techniques and boundary conditions used to simulate coronary haemodynamics include several parameters relating to the coupling between the microcirculation and large vessels that cannot be measured on a patient-specific basis. Importantly, they determine how the flow entering the coronary artery tree is split amongst all the vessels in the tree. While there are physiological and empirical measures relating coronary artery diameters to the flow splits amongst the arteries (Murray 1926; Zhou, Kassab & Molloy 1999), these are not patient specific and do not account for vascular disease. It is not surprising that parameters affecting the amount of flow through each coronary artery have a measurable impact on our ability to predict pressure losses resulting from narrowing or aneurysms in these arteries (Wellnhofer *et al.* 2010; Sankaran *et al.* 2016; Vardhan *et al.* 2019). Advances in imaging methods, combined with patient-specific modelling, are now aiming to directly measure myocardial perfusion to address this need (Nieman & Balla 2020; Menon *et al.* 2024).

In spite of the challenges outlined above, computational modelling of coronary artery haemodynamics is a powerful tool for non-invasive clinical risk assessment and treatment planning. The computation of the pressure loss resulting from diseased coronary arteries using patient-specific computational models has successfully predicted disease severity and reduced unnecessary invasive procedures in clinical trials (Koo *et al.* 2011; Min *et al.* 2012; Taylor *et al.* 2013; Mathew, Gottbrecht & Salerno 2018). This has led to the approval of the first simulation-based risk assessment tool, *FFRCT*, for clinical use by the United States Food and Drug Administration (www.heartflow.com). In addition, computational modelling also provides insights not accessible in clinical imaging. For example, the multi-directionality and topological skeleton of wall shear stress, i.e. regions of expansion and constriction in the wall shear stress field, have emerged as possible predictor of atherosclerosis (Arzani & Shadden 2018; Kok *et al.* 2019; Hoogendoorn *et al.* 2021; Mazzi *et al.* 2021). In addition, computational modelling has highlighted the role of coronary flow helicity in promoting healthy wall shear stress (Morbiducci *et al.* 2007; De Nisco *et al.* 2019), as well as other insights into wall shear stress patterns that are related to the progression of coronary artery disease and coronary artery bypass graft failure (Nordgaard *et al.* 2010; Ramachandra, Kahn & Marsden 2016; Khan *et al.* 2020; Candreva *et al.* 2022).

The importance of haemodynamics in risk assessment and treatment has also been demonstrated in other afflictions of the coronary arteries. For example, Kawasaki disease is a paediatric inflammatory condition that leads to coronary artery aneurysms in some untreated patients (McCrindle *et al.* 2017). A risk associated with these aneurysms is clot formation as a result of flow stagnation and recirculation. While current clinical guidelines recommend treatment based purely on aneurysm size, recent studies

have demonstrated the use of computational modelling to reveal blood flow patterns within aneurysms that might provide a better indicator of patients' risk (Sengupta *et al.* 2012, 2014; Grande Gutierrez *et al.* 2019; Menon *et al.* 2023). The use of computational modelling for non-invasive clinical risk assessment has also been explored in patients affected by anomalous aortic origin of coronary arteries, a congenital defect that causes the coronaries to arise from outside their normal aortic sinus location (Jiang *et al.* 2022). In addition to clinical risk stratification, there have also been efforts to employ patient-specific computational models of coronary haemodynamics for virtual planning of treatments and surgical procedures (Balossino *et al.* 2008; Sankaran *et al.* 2012; Morlacchi & Migliavacca 2013; Ballarin *et al.* 2017; Seo *et al.* 2021). Due to the importance of haemodynamics in the clinical diagnoses, treatment planning and disease progression of such a central part of our circulatory system, these efforts to develop personalized and predictive models of coronary artery haemodynamics, as well as developments in imaging methods to measure coronary flows, have the potential to make a significant impact on cardiovascular health.

5. Cerebral haemodynamics

Following the branching off of coronary arteries at the aortic sinuses, the next set of arteries to arise from the aorta is located downstream at the aortic arch. Of these, the most important are the left and right common carotid arteries, the latter bifurcating from the brachiocephalic artery. The carotid arteries are responsible for supplying the face, neck and, crucially, the brain. The left and right internal carotid arteries, which are branches of the left and right common carotid arteries, travel up the neck into the base of the skull, after which they bifurcate into a network of cerebral arteries that perfuse the brain. In humans, the brain accounts for only 2%–3% of body mass, but receives approximately 15%–20% of cardiac output and consumes 20% of the available oxygen in the body under normal conditions (Claassen *et al.* 2021). The brain's high metabolic rate and the limited ability for anaerobic metabolism in neurons underscore the importance of maintaining healthy cerebral blood flow. The disruption of cerebral blood flow therefore has severe consequences that can lead to life-threatening strokes, permanent brain damage, as well as other maladies related to impaired removal of metabolic wastes from the brain (Tarasoff-Conway *et al.* 2015).

One of the most widely investigated topics relating to cerebral circulation, is the growth, rupture and treatment of cerebral aneurysms. These aneurysms typically form in the Circle of Willis, which is a traffic circle-like junction of several arteries at the base of the brain. Research has shown that the most common locations of aneurysm development coincide with regions of elevated flow and wall shear stress, usually occurring due to pathological vessel narrowing or at bifurcations between arteries (Sforza *et al.* 2009). Haemodynamics also plays a role in the growth and rupture of cerebral aneurysms due to the interaction between flow-induced stresses and cellular function on blood vessel walls. In fact, computational modelling has revealed that a significant proportion of cerebral aneurysms exhibit flow instabilities that lead to high-frequency oscillations even at modest Reynolds numbers of ~ 300 (Khan *et al.* 2021). Interestingly, both low and high wall shear stress have been implicated in unfavourable aneurysm progression, with each pathological state being associated with a different vascular response (Shojima *et al.* 2004; Jou *et al.* 2008; Cebal *et al.* 2011; Xiang *et al.* 2011). While there is general agreement on the mechanism of aneurysm initiation – triggered by cell damage caused by high flow and wall shear stress states that have been observed in animal models (Stehbens 1989) – there is disagreement on the mechanisms associating abnormal wall shear stress with aneurysm progression and rupture (Xiang *et al.* 2014). Nevertheless, these observed links between haemodynamics and aneurysm progression, and the inability of *in vivo* imaging to measure critical haemodynamic stimuli, have accelerated the use of computational models to identify haemodynamic predictors of aneurysm progression (Chung & Cebal 2015). Studies have introduced several haemodynamic metrics to quantify aneurysm rupture risk, such as high oscillatory shear index and particle residence time (Gonzalez *et al.* 1992; Xiang *et al.* 2011). The risk of aneurysm rupture has also been correlated with the presence of complex vorticity

patterns (Xiang *et al.* 2011) as well as the size, strength and location of the jet that emanates from the neck of the aneurysm and impinges on the aneurysm wall (Cebal *et al.* 2005).

Haemodynamics has also played a central role in the treatment of cerebral aneurysms to prevent rupture. Increasingly, clinical interventions have moved away from surgery, towards the implantation of endovascular devices that promote the formation of stabilizing clots within aneurysms (Brisman, Song & Newell 2006; Brinjikji *et al.* 2011). The development of such clots, either forming spontaneously or promoted by implanted devices, has been shown to reduce the incidence of rupture (Etminan & Rinkel 2016). The most commonly implanted devices are coils and flow diverters, both of which impede flow into the aneurysm and lead to flow stagnation, low wall shear stress and, consequently, clot formation (Ngoepe *et al.* 2018). Although the biochemistry of clot formation is currently still under investigation, computational haemodynamics models have proven to be remarkably effective at predicting the potential for clot formation and its location based on flow stagnation and residence time (Sadasivan *et al.* 2002; Rayz *et al.* 2010; De Sousa *et al.* 2016), as well as simulating the process of clot formation by coupling fluid and chemical transport with models of thrombogenesis (Bedekar *et al.* 2005; Ngoepe & Ventikos 2016).

However, broader clinical acceptance of computational models for patient-specific risk stratification and thrombosis prediction has been slow. One reason for this is the lack of clear mechanobiology that relates the observed haemodynamic patterns to pathophysiology, which makes conflicting findings regarding high and low wall shear stress difficult to interpret (Xiang *et al.* 2014). In the prediction of thrombosis, an interesting challenge is the wide range of time scales involved – the fluid transport occurs at the scale of seconds, clot formation occurs in minutes, while clot maturation and stabilization occurs over months (Szikora, Turányi & Marosfoi 2015). Moreover, these interacting time scales influence the properties of blood itself, which changes during the process of clotting. Cerebral haemodynamics models also contend with the familiar challenges of patient specificity in terms of model parameters and boundary conditions (Levitt *et al.* 2014; Steinman & Pereira 2019). An added difficulty is that the biochemical coagulation profile of each person is different, and this needs to be accounted for in patient-specific simulations of clot formation (Ngoepe *et al.* 2018). Finally, the lack of many large patient cohort studies has hampered their translation to clinical use (Sforza *et al.* 2009).

A unique aspect of the cerebral circulation that also benefits from patient-specific haemodynamic measurements and simulations is the presence of collateral arteries due to the anatomy of the Circle of Willis. Collaterals provide alternate flow paths that allow cerebral circulation to be robust to occlusions in specific parts of the vascular anatomy. However, they also complicate the clinical management of cerebral stenoses, because anatomical measurements of vessel narrowing do not correlate well with their effect on cerebral blood flow due to the presence of alternate flow paths via collaterals (Powers 1991). Furthermore, cerebral circulation exhibits a high degree of autoregulation, i.e. the blood vessels adapt to changes in upstream pressure and flow to preserve homeostatic cerebral blood flow volumes (Claassen *et al.* 2021). The study of the haemodynamics associated with cerebral and carotid stenosis and their treatments at the patient-specific level has therefore emerged as another area for the application of personalized imaging and computational simulations based on imaging of patient-specific cerebral artery anatomies (Birchall *et al.* 2006; Liang *et al.* 2011).

Of particular interest is the haemodynamics of the growth and rupture of atherosclerotic plaque in carotid stenosis due to the risk of dislodged plaque travelling downstream, occluding other parts of the circulation and causing stroke (Carr *et al.* 2013; Mukherjee *et al.* 2016). The location of these plaques has been shown to most often correlate with regions of low wall shear stress and flow disruption (Zarins *et al.* 1983; Ku *et al.* 1985). The development of carotid re-stenosis following treatment has also been correlated with wall shear stress patterns that exhibit high temporal variation and strong expansion/contraction through the analysis of the wall shear stress topological skeleton (Morbiducci *et al.* 2020). In addition, the narrowing of these arteries due to the presence of plaque leads to accelerated and highly transient downstream flows that exhibit elevated shear stress and stress gradients as well as turbulent fluctuations, all of which are thought to cause cell damage and plaque rupture (Davies *et al.* 1986; Gertz & Roberts 1990; Loree *et al.* 1991; DePaola *et al.* 1992; Lee *et al.* 2008).

Finally, a fascinating and relatively unexplored haemodynamic phenomenon associated with cerebral circulation is the transport and clearance of brain interstitial fluid, which occupies interstitial regions of the brain surrounding blood vessels and neurons and carries metabolic wastes and toxins (Shetty & Zanirati 2020). In particular, the impaired clearance of amyloid betas is a hallmark of Alzheimer's disease (Tarasoff-Conway *et al.* 2015). While the bulk flow of interstitial fluid has recently been identified as one of several simultaneous mechanisms for the clearance of such wastes, the mechanisms driving this flow are currently unknown. Due to the fact that interstitial fluid envelopes cerebral vasculature, studies have suggested that arterial wave propagation as a result of pulsatile blood flow are a major driver of interstitial fluid transport (Ilf *et al.* 2013; Ladrón-de Guevara *et al.* 2022). However, this has been debated due to the strength of these pulsations, with larger amplitude and lower-frequency motions caused by vasomotion proposed as an alternate mechanism (Diem *et al.* 2017; van Veluw *et al.* 2020). In spite of these disagreements, the role of circulatory phenomena in the clearance of toxins, as well as the aforementioned haemodynamic phenomena associated with aneurysms and strokes, have important consequences for brain health and are promising avenues for ongoing and future research.

6. Peripheral vascular flows

As we travel beyond the main arteries discussed so far, the circulatory system begins to branch off into the peripheral vascular system, which consists of the blood vessels outside of the heart and brain. The peripheral vascular system plays a critical role in transporting blood to and from the body's tissues, and it can be affected by various conditions. The most notable is peripheral artery disease, which affects over 8 million individuals aged 40 and older in the United States (Aday & Matsushita 2021). This disease is a slow and progressive disorder characterized by narrowing, blockage or spasms in the arteries, commonly caused by atherosclerosis – a condition marked by plaque accumulation on the arterial walls. This buildup of plaque narrows the arteries, impeding blood flow and often leading to complete occlusion. Since peripheral artery disease is a subtype of atherosclerotic disease, it is not surprising that people with peripheral artery disease have a higher risk of other atherosclerotic diseases such as coronary artery disease and stroke (Aday & Matsushita 2021).

Similar to the cerebral flow, wall shear stress has been emphasized to play an important role in peripheral artery disease: low wall shear stress may promote the build-up of plaque while high wall shear stress could increase the vulnerability of plaques (Samady *et al.* 2011; Casa, Deaton & Ku 2015). Simulations of local flow through thrombosis have quantified abnormal mean and oscillatory wall shear stress, which, when combined, may serve as risk factors for rupture (Xu *et al.* 2016; Ferrarini *et al.* 2021; Wang, Serracino-Ingloft & Feng 2021). Additionally, simulations have highlighted the importance of patient specificity of peripheral vascular anatomies. Wood *et al.* (2006) investigated the differences in flow patterns, curvature and tortuosity in the superficial femoral artery between young men and women. Their MRI-based computational modelling revealed that men exhibited greater tortuosity and curvature in the superficial femoral artery, along with lower mean wall shear stress, compared with women, which might contribute to the understanding of the two- to five-fold higher incidence of peripheral vascular disease in men.

Finally, a unique challenge of modelling peripheral artery blood flow is that lower limb movement significantly affects the haemodynamics in the lower peripheral vessel. To study this, Colombo *et al.* (2020) mimicked hip rotation, knee flexion and complete movement of walking with idealized femoropopliteal arteries and moving-boundary models. Interestingly, they showed that leg movements induce higher time-averaged wall shear stress, with flow rate amplitude and walking period being the most influential parameters that affect wall shear stress.

7. Microvascular and capillary flows

From centimetre-scale blood vessels arising from the heart, to micron-scale capillaries perfusing the various organs in the body, the interacting scales in the circulatory system span roughly six orders of

magnitude. For example, distal capillary beds, consisting of millions of micron-sized blood vessels, respond to biomechanical stimuli and metabolic demand to change the flow within upstream millimetre-sized blood vessels, which can be as much as four-fold in the coronary circulation (Wilson *et al.* 1990), via autoregulatory mechanisms (Goodwill *et al.* 2017). The flow of blood, which enters the aorta and its branches exhibiting Newtonian-like flow in the large vessels, ceases to behave as a continuum fluid as it traverses the μm -sized arterioles and capillaries. This leads to a nonlinear as well as non-monotonic relationship between fluid viscosity and vessel diameter (Secomb 2017). The study of such multi-scale interaction necessitates multi-scale and multi-physics modelling approaches to tackle the prohibitive computational cost associated with simulating blood flow in these disparate scales.

The earliest physiologically motivated models of flow in the circulatory system considered the system as a so-called ‘lumped-parameter network’, drawing analogies between electric and hydraulic circuits (Westerhof *et al.* 1969). These highly simplified models, also known as ‘zero-dimensional models’, have basic building blocks comprising resistors (R) to model viscous resistance within blood vessels derived from Poiseuille flow, capacitors (C) to model vessel wall distensibility and inductors (L) to model fluid inertia. The simplified equations that encapsulate these physical phenomena to relate flow (Q) and pressure (P), which are analogous to electric current and voltage, respectively, of blood with density ρ and viscosity μ within a blood vessel with length l , radius r , wall thickness h and Young’s modulus E are given by

$$\left. \begin{aligned} \text{Resistance: } \Delta P &= RQ, \quad \text{where } R = \frac{8\mu l}{\pi r^4}, \\ \text{Capacitance: } \Delta \dot{P} &= \frac{Q}{C}, \quad \text{where } C = \frac{3\pi l r^3}{2Eh}, \\ \text{Inductance: } \Delta P &= L\dot{Q}, \quad \text{where } L = \frac{\rho l}{\pi r^2}. \end{aligned} \right\} \quad (7.1)$$

Lumped-parameter models use suitable arrangements of the above resistors, capacitors and inductors to provide macroscopic descriptions of blood flow rates and pressures at specific locations in hydraulic circuits via a set of ordinary differential equations satisfying global mass conservation but only partial momentum conservation (Pfaller *et al.* 2022). Figure 3 shows two examples of such zero-dimensional models. Although the simplicity of these models does not conventionally allow accurate modelling of complex flow topologies, such as vessel bifurcations and curvature, several studies have proposed improvements and corrections to account for flow nonlinearities while preserving the simplicity of these models (Mynard & Valen-Sendstad 2015; Chnafa *et al.* 2017; Mirramezani & Shadden 2020). The minimal computational expense of zero-dimensional models has led to their wide use in low-order modelling of multi-scale circulatory phenomena by effectively ‘lumping’ together the resistance and capacitance of entire micro-vascular/capillary beds into single electric circuit-like components (Vignon-Clementel *et al.* 2006; Kim *et al.* 2010).

Another class of simplified vascular flow models that has enabled the modelling in large, multi-scale circulatory networks at reasonable computational expense are so-called ‘one-dimensional’ flow models (Formaggia *et al.* 1999, 2001). The description of flow within blood vessels is obtained by averaging the 3-D Navier–Stokes equations across the vessel cross-section and projecting this on the 1-D curve tracing the centre of blood vessels (z). This yields partial differential equations describing the flow rate, $Q(t, z)$, and pressure, $P(t, z)$, within vessels of cross-sectional area $S(t, z)$

$$\left. \begin{aligned} \frac{\partial Q}{\partial t} + \frac{4}{3} \frac{\partial}{\partial z} \left(\frac{Q^2}{S} \right) + \frac{S}{\rho} \frac{\partial p}{\partial z} &= Sf - \frac{8\mu Q}{\rho S} + \frac{\mu}{\rho} \frac{\partial^2 Q}{\partial z^2}, \\ \frac{\partial S}{\partial t} + \frac{\partial Q}{\partial z} &= 0. \end{aligned} \right\} \quad (7.2)$$

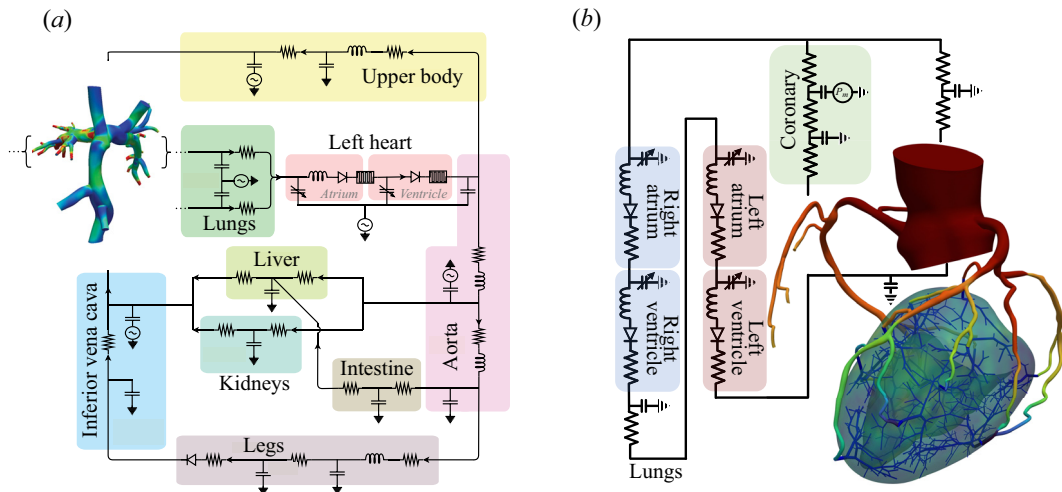


Figure 3. Examples of multiscale computational models. (a) A model of Fontan surgery that allows the quantification of local as well as whole-body haemodynamics (Schwarz *et al.* 2021). (b) A coronary flow model coupling 3-D flow in the aorta and large coronary vessels, 0-D flow in smaller myocardial vessels (shown in blue) and systemic circulation and Darcy flow in the myocardial microvasculature (Menon *et al.* 2024).

The above equations are closed using constitutive models for the wall deformation that relate $P(t, z)$ to $S(t, z)$. These models provide higher-fidelity descriptions of the fluid dynamics than lumped-parameter models, particularly in vasculature with more complicated topology, while still remaining significantly less computationally expensive than full 3-D flow simulations.

These 0-D and 1-D descriptions of the circulation have been widely used in multi-scale flow simulations of extensive vascular networks (Westerhof *et al.* 1969; Avolio 1980; Olufsen 1999). They are most often used in conjunction with high-fidelity 3-D models of blood flow in a multi-scale manner, where 3-D blood flow simulations are performed in limited vascular segments of interest and 0-D or 1-D models approximate downstream/upstream circulatory behaviour that is not included in 3-D blood flow simulations (Migliavacca *et al.* 2006; Vignon-Clementel *et al.* 2006; Kim *et al.* 2010; Sankaran *et al.* 2016; Grande Gutierrez *et al.* 2019; Grande Gutiérrez, Sinno & Diamond 2022; Menon *et al.* 2024). This is shown in figure 3. Such multi-scale models have allowed researchers to investigate the relationship between widely disparate circulatory scales, such as the effect of exercise on changes in cardiac function and pulmonary circulation (Kung *et al.* 2014), haemodynamic changes in distal/proximal circulation to compensate for local abnormalities within specific vascular regions (Balossino *et al.* 2009; Schwarz *et al.* 2021) and the effects of local surgical interventions (e.g. shunt sizing) on global physiologic parameters such as oxygen delivery and cardiac workload in patients with congenital heart disease (Migliavacca *et al.* 2006; Moghadam *et al.* 2012; Esmaily-Moghadam, Hsia & Marsden 2015).

Although their minimal computational expense has allowed the study of physiological interactions amongst different scales, the primary challenge associated with such multi-scale models is the relationship between their parametrization and the associated physiology they aim to capture. For example, in models consisting of 3-D descriptions of vascular haemodynamics coupled with reduced-order representations of the beating heart, it is not immediately obvious how the parameters of the heart model, usually consisting of resistors, time-varying capacitors and valves, relate to patients' physiological cardiac volume, ejection fraction and other clinically relevant metrics. The need to associate these low-order flow models with clinical measurements for personalized modelling has led to development of parameter estimation and automated tuning schemes, which ideally should account for uncertainties (Tran *et al.* 2017; Fleeter *et al.* 2020; Seo *et al.* 2020; Menon *et al.* 2024).

While the above low-order modelling strategies can be used to provide macroscopic descriptions of flow and pressure through lumped-parameter representations of microvasculature, they are computationally intractable when modelling flow that is resolved at the scale of each blood vessel in dense capillary networks within tissues. This is due to the complexity and computational expense of modelling millions of interconnected vessels, as well as the network-like structure of capillary beds where simplified Poiseuille flow, without accounting for viscous effects at junctions between blood vessels, may not be valid. A spatially averaged/coarse-grained description of flow is therefore required in such microvascular networks. In fact, dimensional analysis as well as microfluidic measurements have shown a linear relationship between the pressure gradient and spatially averaged flow within microvasculature (Fung 1997; Stauber *et al.* 2017) – akin to Darcy’s law governing flow through porous materials. Recent work has therefore led to the development of computational models for microvascular/capillary tissue perfusion that represent dense capillary networks and interstitial regions of tissues as porous materials.

These models have been applied to study capillary flows, oxygen or nutrient exchange, as well as the transport of therapeutics in various organs such as in alveoli within the lungs (Erbertseder *et al.* 2012; Zurita & Hurtado 2022), within tumours (Secomb *et al.* 2004; Stylianopoulos & Jain 2013; d’Esposito *et al.* 2018), in the brain (Sweeney, Walker-Samuel & Shipley 2018; Kim *et al.* 2023) and in the heart (Chapelle *et al.* 2010; Cookson *et al.* 2012; Michler *et al.* 2013; Di Gregorio *et al.* 2021, 2022; Papamanolis *et al.* 2021; Kim *et al.* 2023). While the development of tissue perfusion models is relatively nascent compared with the 3-D and lumped-parameter models discussed above, in the context of flow through cardiac tissue, porous medium flow models have been coupled with high-fidelity and reduced-order models of flow in upstream coronary arteries (Hyde *et al.* 2014; Di Gregorio *et al.* 2021; Papamanolis *et al.* 2021; Kim *et al.* 2023; Menon *et al.* 2024) as well as the elasto-mechanics describing cardiac contraction and its effect on the pressure driving coronary flow within the cardiac tissue (Chapelle *et al.* 2010; Cookson *et al.* 2012; Di Gregorio *et al.* 2021). Figure 3(b) shows an example of a Darcy myocardial flow model coupled to upstream 3-D flow in coronary arteries and 0-D distal circulation models. However, as with the low-order micro-circulation models discussed above, a challenge with these approaches is the correspondence between modelling parameters, such as Darcy permeability and pressure, with quantities that can be measured *in vivo* using current clinical techniques. Recent advances in imaging methods hold promise for more accurate prescription of these parameters.

Delving even deeper into smallest scales of the circulatory system, i.e. the cellular level, fluid dynamics continues to play a prominent role. Typical Reynolds numbers in capillaries are $O(10^{-3})$, where Stokes flow assumptions are valid (Secomb 2017). However, the challenge at these scales is that the continuum description of blood breaks down. It is more accurately characterized as a complex fluid or suspension of predominantly red blood cells, white blood cells and platelets within plasma. These constituents exhibit a complex dynamics, such as migration away from vessel walls (creating a cell-free layer), intricate orientations and motions, as well as non-uniform concentrations within vessels as well as between different branching vessels (Chien *et al.* 1967a,b; Chien 1970; Fedosov, Noguchi & Gompper 2014; Takeishi *et al.* 2019). This occurs in response to various factors including their concentration, which varies with scale from $\sim 50\%$ in most of the body to $\sim 20\%$ in small vessels with $30\mu\text{m}$ diameters, flow-induced shear forces within vessels and their different material properties (Zhao, Shaqfeh & Narsimhan 2012; Qi & Shaqfeh 2017). The cell-scale dynamics within small vessels has several implications, including for clot formation, drug delivery and, most importantly, blood viscosity (Chien 1970). Interestingly, the dynamics and deformability of blood’s constituents lead to the effective viscosity of blood being only 4–5 times that of plasma, compared with an equivalent suspension of rigid spheres which would be 10–100 times as viscous as its solvent (Verzicco 2022). Shear-induced cell migration and deformation within vessels also leads to blood acting as a shear-thinning fluid and produces a non-monotonic trend in blood viscosity with respect to vessel diameter (Pries, Neuhaus & Gaehtgens 1992). Effective blood viscosity first decreases with increasing diameter due to the cell-free near vessel walls. This is referred to as the Fåhræus–Lindqvist effect (Fåhræus & Lindqvist 1931). It reaches a minimum in vessels with diameters of the order of red blood cell diameters, where red blood cells line up in a single-file-like motion, and then increases in vessels with smaller diameters due to the

deformation of red blood cells. A review of these effects is available in [Secomb \(2017\)](#), and efforts to simulate them are discussed in [Freund \(2014\)](#).

8. Venous flow

After perfusing tissues throughout the body, blood begins its return journey to the heart via the venous system. The venous circulation consists of veins that carry blood depleted of oxygen and nutrients, and stowed with metabolic wastes, from deep within organs, tissues and cells to the great veins that return to the heart. Compared with arteries, veins operate under lower pressure with low pulsatility, and therefore have thinner walls. For the large veins close to the heart, such as the vena cava, there is some mild pulsatility due to right atrial contraction and respiratory effects.

A unique feature of venous haemodynamics is the presence of one-way valves within most veins in the body, adding complexity to venous flow simulation. These valves are essential for maintaining unidirectional venous flow, especially given the low pressure under which they operate. Their dysfunction, which impairs the ability of the venous network to return blood to the heart, is a primary cause of chronic venous inefficiency and venous hypertension ([Bergan *et al.* 2006](#)). Although these valves operate in very low-speed flows, the formation of an axial and helical jet, the presence of flow recirculation within the sinus, and the pulsatility of flow resulting from the opening and closure of valves have been observed and are hypothesized to play roles in healthy venous function ([Hamer, Malone & Silver 1981](#); [Lurie *et al.* 2003](#); [Lurie & Kistner 2013](#)). In this context, another interesting feature is that when multiple valves are present at venous junctions, the valve openings are consistently observed to be at an angle to each other and this angle correlates with the distance between the valves ([Lurie & Kistner 2012](#)). This asymmetry naturally gives rise to helical flows that have been shown to improve efficiency and reduce flow stagnation – thus preventing thrombosis/clotting ([Lurie & Kistner 2013](#); [Chen *et al.* 2018](#)).

The formation of clots within veins – or deep venous thrombosis – presents a significant health concern, with an annual incidence of approximately 1 per 1000 adults in the United States ([Cushman 2007](#)). Physical immobility is one of the most significant risk factor for deep venous thrombosis because the absence of muscular activity leads to a loss of oscillatory blood flow around valve areas in veins, thereby promoting thrombus or clot formation ([Welsh *et al.* 2019](#)). Subsequently, these clots can travel to the lungs and get lodged in the pulmonary arteries, leading to a potentially fatal pulmonary embolism. In its prevention, alongside anticoagulation therapy, placing a filter in the inferior vena cava serves as an alternative strategy. This mechanical device is designed to filter thrombi carried by the blood flow within the vein. Using *in vitro* experiments and numerical simulation, the design of these filters has been characterized and optimized with a focus on maximizing thrombus capture efficiency, minimizing areas of low wall shear stress, and ensuring minimal disruption to blood flow ([Singer, Wang & Diachin 2010](#); [Feng, Li & Feng 2022](#)). We recommend the recent review by [Watson *et al.* \(2024\)](#) for a discussion of modelling efforts in this domain to understand flow-mediated mechanisms driving deep vein thrombosis.

Beyond the pulmonary circulation, abnormalities in venous flow can have far-reaching health effects because the entire circulatory system is intricately linked with other bodily fluid systems. For instance, global multi-scale models of human circulation with its interactions with central nervous system fluids have been developed to explore how venous irregularities might influence the development and progression of neurological diseases ([Müller & Toro 2014](#); [Toro *et al.* 2022](#)).

A theme of central focus, with regard to the haemodynamics of the venous system, is palliative approaches for patients with single ventricle physiology. This is a group of congenital heart defects in which one ventricle (either the left or right) is too underdeveloped to function normally. Typically, these patients undergo a series of three surgeries between birth and 4 years of age to reconfigure their systemic and pulmonary circulations sequentially so that they are driven by the single functioning ventricle. These surgeries are primarily centred around the great veins that return blood to the heart, with the aim of maintaining passive flow in these and the pulmonary vessels due to the absence of the second functioning ventricle. While these surgeries are life saving, the associated complications have spurred the use of

CFD for improving surgical designs virtually. In these applications, 3-D computational models are often integrated with lumped-parameter networks, thus offering insights into the local haemodynamics while also capturing the interactions with the broader circulatory system (Corsini *et al.* 2011; Kung *et al.* 2020; Schwarz *et al.* 2021).

During the stage one, Norwood surgery, the pulmonary circulation is connected to the aorta with a shunt to provide blood flow to the lungs. Early computational studies proposed and examined several variations in the position and size of the shunt, and found the larger shunts result in poorer oxygen delivery while leading to increased pulmonary flow (Migliavacca *et al.* 2001; Hsia *et al.* 2011). The effect of various degrees of pulmonary banding in the hybrid procedure has been simulated to determine the optimal systemic to pulmonary flow ratio and oxygen delivery (Corsini *et al.* 2011). Moreover, modelling provides valuable quantitative insight into the optimization of the neo-aortic reconstruction. With patient specific geometries, a smooth aortic arch and a larger anastomosis have been shown to result in higher energy efficiency in the blood flow (Qian *et al.* 2010; Itatani *et al.* 2012).

In the second stage, the Glenn procedure, the superior vena cava is directly connected to the pulmonary arteries. By allowing passive blood flow to the lungs from the upper body, it reduces the workload on the single ventricle. The connection can be achieved through either the hemi-Fontan or bidirectional Glenn (Douglas *et al.* 1999; Kogon *et al.* 2008), but questions remain as to which results in the best haemodynamic results. Patient-specific simulation initially indicated that the Glenn connection is haemodynamically more efficient compared with hemi-Fontan, due to its direct end-to-side anastomosis (Pekkan *et al.* 2009). Despite what appears to be significant local power loss differences, follow up studies found no notable distinctions in haemodynamic or physiological parameters between the two models (Kung *et al.* 2020).

After the third surgery, known as the Fontan procedure, the total cavopulmonary connection is established with inferior and superior vena cava connected to the pulmonary arteries. This distinct circulation causes elevated central venous pressure and reduced pulmonary pulsatility, which are associated with morbidities such as liver fibrosis, exercise intolerance and heart failure (Goldberg *et al.* 2011). Besides assessing the cavopulmonary connection at rest, computational frameworks have also offered valuable insights into the impacts of respiration and exercise in Fontan patients (Marsden *et al.* 2007; Kung *et al.* 2014). They reveal that the elevated resistance at connection and nonlinearly increased energy loss significantly restrict the Fontan circulation's capacity to augment cardiac output during exercise, demonstrating a limited ability to accommodate exercise conditions (Whitehead *et al.* 2007; Sundaeswaran *et al.* 2008). The connection was then proposed to be offset to prevent the head-on collision of flow (De Leval *et al.* 1996), but this design introduces uneven hepatic flow distribution and therefore uneven growth in pulmonary vascular tree. Subsequently, the bifurcated Y-graft was introduced and improved energy loss and hepatic flow distribution compared with the offset design in computational studies that were later validated clinically (Marsden *et al.* 2009; Yang *et al.* 2012; Martin *et al.* 2015; Trusty *et al.* 2019, 2020). Figure 4(a) shows examples of flow fields resulting from these offset and Y-graft configurations. It is worth mentioning that, although power loss is a major focus of these computational studies, Fontan haemodynamics from 100 patients showed that Fontan power loss varies from patient to patient, and elevated levels are correlated with lower systemic flow and cardiac index (Haggerty *et al.* 2014). As their predictive power has grown, computational simulations continue to be used in investigations of new palliative techniques, such as models of tissue-engineered vascular grafts in the Fontan pathway (Schwarz *et al.* 2021).

9. Right heart

After its long journey from large blood vessels through the depths of tissues and eventually through the venous system, de-oxygenated blood returns to the right side of the heart, which consists of the right atrium and the right ventricle. The superior and inferior vena cava first direct de-oxygenated blood into the right atrium. From there, it flows into the right ventricle, which is the secondary pumping chamber of the heart, responsible for driving flow to the lungs to be re-oxygenated. Blood moving from the right

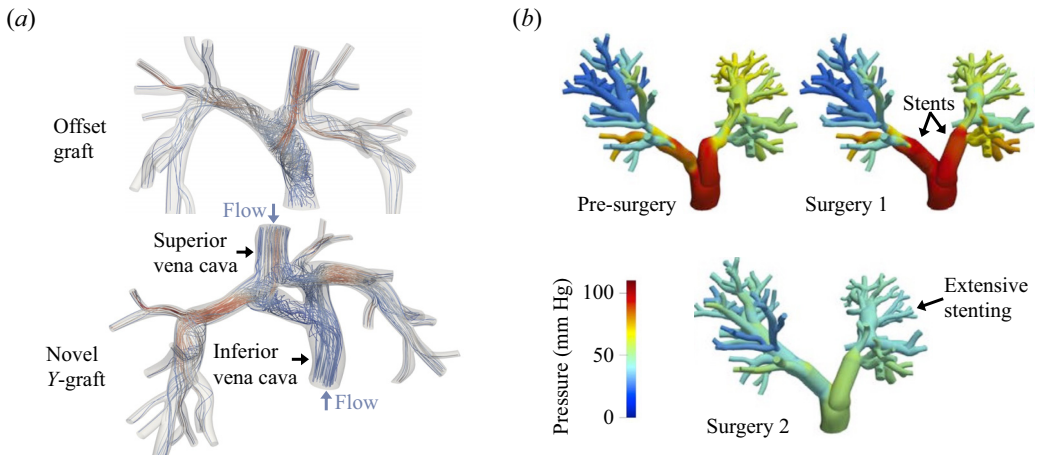


Figure 4. (a) Haemodynamics associated with standard offset grafts and novel Y-grafts in the Fontan procedure to treat single ventricle physiology (Marsden *et al.* 2010; Yang *et al.* 2015). The highly disturbed flow and the split between left and right pulmonary arteries are ongoing challenges. (b) Patient-specific models for treating pulmonary stenoses. Comparing exclusively proximal stenting vs more extensive stenting showed improved pressure alleviation with extensive stenting (Lan *et al.* 2022).

atrium to the right ventricle flows through the tricuspid valve that separates these chambers, and is initially driven by its own inertia. Eventually, an active right atrial contraction completes the ventricular filling. Subsequently, the right ventricle contracts to increase the blood pressure therein, thus closing the tricuspid valve and opening the pulmonary valve to pump blood into the lungs. The left and right sides of the heart, working in parallel, operate synchronously to ensure equal volumes of blood flow, maintaining equilibrium in the circulatory system. The atrial and ventricular septums separate the right and left atria and ventricles, respectively.

Despite similarities to the left heart, the right atrium possess unique anatomical and functional traits. The right atrium connects to the right ventricle through the tricuspid valve, while the left atrium links to the left ventricle via the bicuspid mitral valve. Both atria feature trabeculated appendages that may enhance stagnant flow and promote clot formation (or thrombosis). However, the right atrial appendage has a larger junction than its left counterpart, which likely accounts for reduced thrombosis in the right atrial appendage compared with the left (see § 11) (Lang *et al.* 2022). Flow patterns within the right atrium are significantly influenced by the inflows from the superior and inferior vena cava. Studies have observed that these incoming flows engage in a circular motion rather than colliding directly, which results in predominantly rotational energy that tends to form a single vortex in the right atrium (Kilner *et al.* 2000). The kinetic energy is better preserved compared with configurations with multiple vortices or less prevalent helical flow, and conversely, atria without this single vortex flow tend to rely more on energy from atrial contractions (Dewhurst *et al.* 2020).

Often termed the ‘forgotten ventricle’, the right ventricle also exhibits distinct characteristics from the left ventricle. It is a thin-walled crescent-shaped chamber that wraps around the left ventricle and pumps against the low-impedance pulmonary circuit at a lower pressure of approximately 5–20 mmHg (667–2650 Pa). As such, its mass is roughly 1/6th that of the left ventricle, and its stroke work is approximately a quarter that of the left ventricle. Interestingly, although both right and left ventricular contractions are predominantly driven by shortening of the long-axis, left ventricular contractions significantly affect right ventricular function. The bulging of the ventricular septum due to high pressure in left ventricle reduces the right ventricle volume, and about 20% to 40% of the right ventricular systolic pressure and volume outflow result from left ventricular contraction (Santamore & Dell’Italia 1998; Gaine *et al.* 2014). The right ventricle is also more afterload sensitive. When afterload rises, the

right ventricle experiences a significant surge in energy use and a decrease in efficiency compared with the left ventricle, causing the right ventricle's stroke volume to decrease more rapidly. This sensitivity could explain why systemic arterial hypertension is better tolerated than pulmonary arterial hypertension (Bravo *et al.* 2022).

The flow field in the right ventricle differs from the left ventricle largely due to its different geometry. A number of MRI and CFD studies have shown that the general flow path through the right ventricle is dominated by the smooth curvature of the chamber with a less acute change in direction between the inflow and the outflow tract (Kilner *et al.* 2000; Fredriksson *et al.* 2011). A ring-like vortex forms behind the tricuspid valve at the early diastole, which interacts with the narrower boundaries of the right ventricle, particularly on the septal side that is flatter, quickly breaking into a weakly turbulent flow pattern (Kilner *et al.* 2000; Markl, Kilner & Ebbers 2011). Thus, the flow in the right ventricle features a higher dissipative state, whereas the left ventricle preserves more circulation and kinetic energy throughout diastole. Additionally, its shape helps streamline the flow, promoting the formation of a helical flow towards the pulmonary orifice (Mangual, Domenichini & Pedrizzetti 2012). During systolic contraction, the residual vorticity extends along the outflow tract, adding a slightly helical pattern to the largely irrotational velocity field, and assists in mixing of the blood (Collia *et al.* 2021). A number of CFD simulations have also characterized the effect of endocardial structures, such as trabeculae and papillary muscles, on disrupting the main vortex ring and dissipating energy in intra-ventricular flows (Sacco *et al.* 2018a). However, as with the left ventricle, this is usually ignored in both simulations and imaging due to the challenge of simultaneously resolving both the macro-scale flow features and the geometric details of the endocardial surface.

Flow modelling techniques have also been expanded to describe changes linked to pathological conditions, serving as markers for impaired right ventricular function. For example, pulmonary arterial hypertension patients, who have increased pressure and diminished ejection fraction, exhibit a significant increase in right ventricle kinetic energy work density and pronounced pulmonary artery energy loss across the cardiac cycle, which correlates with right ventricle ejection fraction (Han *et al.* 2015). Moreover, haemodynamic analysis has revealed an increase in both right atrium and right ventricle vorticity at late diastole in pulmonary artery hypertension patients, suggesting its potential interplay between right ventricle fluid dynamics and tissue mechanics leading to pulmonary artery hypertension (Fenster *et al.* 2015).

10. Pulmonary circulation

The pulmonary circulation carries oxygen-depleted blood from the right side of the heart to the lungs for oxygen enrichment, and then channels the oxygen-saturated blood back to the left side of the heart. Starting from the right ventricular outflow tract, blood is pumped into the main pulmonary artery, which splits into the left and right pulmonary arteries. As these arteries penetrate the lungs, they further subdivide into smaller vessels, following a pattern analogous to the bronchial tree in the respiratory system. At their finest level, these vessels sprawl out across the alveoli, the tiny air sacs where the critical process of gas exchange occurs. Here, carbon dioxide is expelled from the blood and replaced with fresh oxygen. This newly oxygenated blood is then collected by the pulmonary veins and directed back to the left atrium of the heart, ready to be pumped to the rest of the body.

Owing to the central role of blood oxygenation and its subsequent transport, the focus of pulmonary haemodynamics studies has generally revolved around two important pathologies – pulmonary arterial hypertension and pulmonary stenosis. Pulmonary arterial hypertension is a chronic disease characterized by progressive elevation in pulmonary artery pressure due to increased pulmonary vascular resistance. The progression of pulmonary artery hypertension is driven by the remodelling of vascular tissue in response to elevated haemodynamic pressure. The wall thickness and vascular compliance decrease during this remodelling, which leads to increased right ventricle afterload and ventricle–vascular decoupling (Kheifets *et al.* 2013). A primary clinical diagnostic indicator of pulmonary arterial hypertension is the pulmonary vascular resistance. It is calculated as the ratio of the pressure drop through the pulmonary

circulation to pulmonary blood flow and signifies the structural changes at the pulmonary arteriole level. Interestingly, this widely used clinical metric does not reflect the fact that blood flow is pulsatile with reflective waves. Therefore, several studies have proposed pulmonary impedance to better predict patient outcomes by taking into account not only resistance but also elasticity and inertia to characterize the steady and oscillatory behaviours of blood flow and dynamic interactions between the heart and the lungs, especially under varying physiological conditions (Hunter *et al.* 2008; Naeije 2012; Kheyfets *et al.* 2015).

Pulmonary stenosis, or narrowing of the pulmonary vessel lumen, is another significant cause of pulmonary flow disruption. Peripheral pulmonary artery stenosis is commonly associated with congenital heart diseases, including Williams syndrome, Alagille syndrome and tetralogy of Fallot. Severe peripheral pulmonary artery stenosis results in right ventricular hypertension, right ventricular hypertrophy and eventually right ventricular failure. Additionally, if pulmonary blood flow is not promptly restored, it can lead to irreversible damage to the pulmonary artery (Mainwaring & Hanley 2016). Interventional procedures alleviate the stenosis with catheter-based angioplasty or surgical homograft patches. Nonetheless, such surgeries are challenging since they require long hours of cardiopulmonary bypass and address only the most proximal pulmonary arteries. Moreover, post-operative complications include persistent right ventricle hypertension, tears in the vessel wall, aneurysm formation, in-stent restenosis and even death (Cunningham *et al.* 2013; Felmly *et al.* 2023).

In light of these debilitating pathologies, both CFD and 4-D flow MRI have been used to investigate blood flow patterns that provide insights into the physiological mechanisms behind disease progression and clinical outcomes. For example, MRI data have revealed that pulmonary artery hypertension patients exhibit reduced flow, peak velocities, wall shear stress, helicity, vorticity and strain (Tang *et al.* 2012; Barker *et al.* 2015; Schäfer *et al.* 2017; Sieren *et al.* 2019). Increased recirculation and large vortex formation along the inferior curvature of the main pulmonary artery are also reported in pulmonary artery hypertension patients, which can serve as marker for pulmonary artery hypertension risk stratification. This formation of large-scale vortices stems from vessel dilation and diminished right ventricular function, creating shear layers with dramatically different velocities resulting in flow instabilities. This also explains the decreased wall shear stress at the proximal artery wall, which leads to endothelial dysfunction and maladaptive mechanobiological responses (Reiter *et al.* 2008, 2013).

While the resolution limitations of MRI hinder its effectiveness in distal branches where disease is thought to initiate, computational simulations can provide an in-depth assessment of haemodynamics in these farther reaches of the pulmonary arterial tree. Automatic algorithms have been developed to segment the pulmonary vasculature below 1 mm resolution (Doel, Gavaghan & Grau 2015). With more detailed anatomical models, blood flow simulations have reported decreased wall shear stress in the proximal arterial tree in severe pulmonary artery hypertension, as well as increased oscillatory shear index and relative residence time in the distal arteries, which indicate more stagnant blood flow (Tang *et al.* 2012; Kheyfets *et al.* 2015; Yang *et al.* 2019; Pillalamarri *et al.* 2021). Computational models have allowed the exploration of pulmonary artery hypertension linked to congenital heart defects, and found increased wall shear stress with increasing ventricular septal defect size in paediatric pulmonary artery trees (Dong *et al.* 2021). Moreover, recent work has attempted to couple models of pulmonary haemodynamics with vascular growth and remodelling to simulate mechanobiological metrics of interest and potential treatment strategies for pulmonary artery hypertension patients (Szafron *et al.* 2023). Image-based CFD can also serve as a virtual platform to evaluate interventions on a patient-specific basis to optimize surgical procedures. Yang, Feinstein & Vignon-Clementel (2016) and Yang *et al.* (2018) performed virtual pulmonary artery reconstruction for patients with Alagille syndrome and achieved accurate predictions of postoperative pulmonary artery flows via adaptive outflow boundary conditions. Recently, Lan *et al.* (2022) performed virtual intervention in Williams and Alagille syndrome patients and showed that stenting only proximal lesions is often insufficient to reduce overall vascular resistance and thus right ventricular pressures (figure 4b).

A challenge in such computational models is that of prescribing the boundary conditions required to accurately simulate the haemodynamics both before and after clinical interventions. For example, outflow

boundary conditions substantially impact the flow distribution in the distal vessels, which is a significant predictor of pulmonary hypertension severity (Kheifets *et al.* 2015). Models also need to consider flow autoregulation in distal pulmonary vasculature to correctly predict haemodynamics post-treatments (Yang *et al.* 2016, 2018). Another challenge is assessing blood flow in distal pulmonary arteries with diameters between 50 and 500 μm , which are beyond typical modelling resolution. To address this, 3-D models have been combined with 0-D morphometric trees that consist of resistances in parallel and series based on existing pulmonary artery morphometric data of vessel segment diameters, lengths and branching patterns (Huang *et al.* 1996). Results from models with morphometric trees have uncovered increased wall shear stress in the distal small vessels compared with controls (Yang *et al.* 2019), as well as elevated pulmonary vascular resistance and hypertension due to rarefaction in the pulmonary circulation (Olufsen *et al.* 2012). They have also reported decreased shear stress along with increased cyclic stretch due to pulmonary vascular resistance at the microvascular level (Bartolo *et al.* 2022). While it is challenging to accurately recapitulate the wide spatial scales and physiological responses at these scales in computational models, continued progress is important for clinical translation, especially due to the difficulty in accurately resolving these scales using clinical imaging.

11. Left atrium

At the end of our tour, we return to the left side of the heart where oxygen-rich blood returning from the lungs via the pulmonary veins collects in the left atrium. From here, blood is directed back into the left ventricle, via contraction of the left atrium, to restart its journey through the circulatory system.

Haemodynamic studies have revealed intricate flow patterns within the left atrium. The inflow from pulmonary veins are asymmetric, with left pulmonary veins forming a rotational loop while right pulmonary veins are more aligned with the wall (Fyrenius *et al.* 2001). Such asymmetric filling generates asymmetric atrial flow pathways and tends to preserve blood momentum during the cardiac cycle (Kilner *et al.* 2000). During systole and mid-diastole, discrete left atrial vortices have been observed both from clinical (Fyrenius *et al.* 2001; Park *et al.* 2013) and computational data (Vedula *et al.* 2015; Zingaro *et al.* 2021). The formation of atrial vortices is conjectured to produce a better ‘washout’ effect in the left atrium and avoid intra-atrial flow stasis (Fyrenius *et al.* 2001).

In terms of the haemodynamics, the most interesting feature of the left atrium is the left atrial appendage. Anatomically, the left atrium has a smooth-walled interior, except for the left atrial appendage protruding from its upper left corner. The left atrial appendage is a small and ear-shaped pouch, featuring a ridged interior due to the presence of pectinate muscles. It is more distensible than the rest of the left atrium and is hypothesized to act as a decompression chamber during left ventricular systole and periods of high atrial pressure (Al-Saady, Obel & Camm 1999). However, its structure has a propensity to cause increased flow stasis – which can lead to the formation of blood clots and the risk of stroke. This is particularly important in the context of atrial fibrillation, which is the most prevalent and clinically important cardiac arrhythmia. In patients with this condition, the heart’s electrical signals are chaotic, leading to the inefficient atrial pumping. This can result in an irregular and frequently rapid heart rate, along with the risk of the blood pooling and potential clotting. If untreated, atrial fibrillation increases the risk of heart-related complications, such as stroke or heart failure. Notably, over 90 % of left atrial thrombi (or blood clots) originate in the left atrial appendage (Al-Saady *et al.* 1999). Flow patterns within the left atrial appendage have long been suggested as potential predictors for these events (Agmon *et al.* 1999; Kamp *et al.* 1999).

Therefore, the integration of computational methods with medical imaging has been used to provide a comprehensive view of the haemodynamics within the left atrial appendage. Decreased mean and peak velocities in left atrial appendage have been reported for atrial fibrillation patients, thus making the washout field incomplete and more prone to fluid stagnation. A large vortex has been observed in the centre of the left atrium for atrial fibrillation patients, instead of the multiple discrete vortices in healthy left atrium (Park *et al.* 2013). Four typical left atrial appendage morphologies and their impacts

on the haemodynamics have been investigated using CFD, showing the close relation between morphology and thrombosis, in agreement with clinical reports. By modelling flow in distinct left atrial appendage morphologies, simulation results have underscored the critical importance of patient-specific left atrial appendage geometric characteristics in influencing thromboembolic risks (Bosi *et al.* 2018; Masci *et al.* 2019). While various CFD models have been employed for the left atrium to address potential shifts from transitional to turbulent flows, it is noteworthy that, in atrial fibrillation contexts, models without turbulence remain viable (Dueñas-Pamplona *et al.* 2021). For more details about computational modelling of the left atrium and the left atrial appendage, we refer to the review by Valvez *et al.* (2023).

12. Future outlook

As we conclude our journey through the human circulatory system, we hope to have impressed upon the reader the central role that fluid dynamics plays in a wide range of circulatory phenomena. The decades of research that have uncovered these insights have been primarily motivated by one goal – to use physics and engineering insights in advancing clinical care. To that end, several ongoing challenges remain – especially in the context of widespread clinical translation of computational models.

Chief amongst these is the pressing need for more comprehensive verification and validation of realistic patient-specific computational models and their associated insights in large-scale clinical studies (Steinman *et al.* 2012). This is a theme that was discussed several times in preceding sections of this review, which highlights its importance in all areas of the circulation. While there have been efforts to validate computational models with *in vitro* flows (Emendi *et al.* 2021; Kaiser *et al.* 2023; Zimmermann *et al.* 2023), there is an urgent need for *in vivo* validation using patient-specific clinical data.

A related ongoing challenge is the need to develop methods for more personalized computational models that are informed by a variety of patient-specific clinical measurements – not just anatomical imaging, as is currently the norm. This requires the combination of accurate models with data-driven methods to tune model parameters based on routine as well as novel clinical measurements/imaging (Tran *et al.* 2017; Menon *et al.* 2024). The translation of such models to clinical use also critically depends on the use of rigorous uncertainty quantification techniques (Fleeter *et al.* 2020).

We should also highlight emerging tools to process and interpret the fluid dynamics of cardiovascular function. This includes methods that enable new and higher quality insights from clinical imaging, such as super-resolution and de-noising (Fathi *et al.* 2020). In this context, there have also been several recent efforts to enhance the utility of low-resolution clinical imaging by augmenting such measurements with physics-based and data-enabled techniques to extract the clinically relevant haemodynamics that is otherwise under-resolved (Bakhshinejad *et al.* 2017; Habibi *et al.* 2021; Zhang *et al.* 2022a,b). Finally, new analysis techniques focused on topological features of the flow field itself, including Lagrangian coherent structures and the topology of the wall shear stress field, have recently been shown to provide promising clinical indicators for clinical risk and disease progression (Arzani *et al.* 2017; Arzani & Shadden 2018; Morbiducci *et al.* 2020; Mazzi *et al.* 2021).

As important as fluid dynamics is to cardiovascular health, future treatments will hinge on more comprehensive predictive models that incorporate new findings from a range of different disciplines, including mechanobiology, genetics, and cell signalling (Schwarz *et al.* 2023a). This has led to the development of multi-physics models, such as whole-heart models, which combine haemodynamics with the spatio-temporal behaviour of the heart at molecular, cellular and tissue scale – from ionic activation in electrophysiology to the tissue mechanics leading to cardiac contraction – to provide a more detailed description of cardiac function (Sugiura *et al.* 2022; Verzicco 2022; Bucelli *et al.* 2023). Models combining haemodynamics with mechanobiology are also being developed to predict vascular growth and remodelling, which occur due to the interplay between haemodynamics and biomechanical stimuli experienced by vessel walls, in realistic patient-specific models (Schwarz *et al.* 2023b). Finally, while computational modelling has provided many of the crucial insights discussed in this review, such modelling is often not possible in time frames that allow their widespread clinical uptake. To address this, machine learning methods are being developed to automatically construct patient-specific

anatomical models as well as extract new insights from routine imaging (Fathi *et al.* 2020; Kong, Wilson & Shadden 2021; Arzani *et al.* 2022). There is also a need for real-time cardiovascular simulations, through reduced-order modelling and machine learning methods (Pegolotti *et al.* 2023).

Efforts to address these challenges will yield validated, accurate and robust digital twins that will accelerate the promise of personalized and non-invasive *in silico* medicine.

Acknowledgement. We are grateful to A. Kaiser, E. Schwarz, L. Pegolotti and W. Yang from Stanford University, and J.-H. Seo and R. Mittal from Johns Hopkins University for providing flow-field data and images for this manuscript.

Declaration of interests. The authors declare no conflict of interest.

Funding statement. This work was supported by NIH grant R01HL141712 and the Additional Ventures Cures Collaborative.

Data availability statement. Not applicable.

References

- AARONSON, K.D., *et al.* 2012 Use of an intrapericardial, continuous-flow, centrifugal pump in patients awaiting heart transplantation. *Circulation* **125** (25), 3191–3200.
- ADAY, A.W. & MATSUSHITA, K. 2021 Epidemiology of peripheral artery disease and polyvascular disease. *Circ. Res.* **128** (12), 1818–1832.
- AGMON, Y., KHANDHERIA, B.K., GENTILE, F. & SEWARD, J.B. 1999 Echocardiographic assessment of the left atrial appendage. *J. Am. Coll. Cardiol.* **34** (7), 1867–1877.
- AL-SAADY, N.M., OBEL, O.A. & CAMM, A.J. 1999 Left atrial appendage: structure, function, and role in thromboembolism. *Heart* **82** (5), 547–554.
- AL-WAKEEL, N., FERNANDES, J.F., AMIRI, A., SINIAWSKI, H., GOUBERGRIETS, L., BERGER, F. & KUEHNE, T. 2015 Haemodynamic and energetic aspects of the left ventricle in patients with mitral regurgitation before and after mitral valve surgery. *J. Magn. Reson. Imag.* **42** (6), 1705–1712.
- ALIMOHAMMADI, M., SHERWOOD, J.M., KARIMPOUR, M., AGU, O., BALABANI, S. & DÍAZ-ZUCCARINI, V. 2015 Aortic dissection simulation models for clinical support: fluid-structure interaction vs. rigid wall models. *Biomed. Engng Online* **14** (1), 1–16.
- ARZANI, A., GAMBARUTO, A.M., CHEN, G. & SHADDEN, S.C. 2017 Wall shear stress exposure time: a Lagrangian measure of near-wall stagnation and concentration in cardiovascular flows. *Biomech. Model. Mechanobiol.* **16** (3), 787–803.
- ARZANI, A. & SHADDEN, S.C. 2018 Wall shear stress fixed points in cardiovascular fluid mechanics. *J. Biomech.* **73**, 145–152.
- ARZANI, A., WANG, J.X., SACKS, M.S. & SHADDEN, S.C. 2022 Machine learning for cardiovascular biomechanics modeling: challenges and beyond. *Ann. Biomed. Engng* **50** (6), 615–627.
- AUGUSTIN, C.M., GSELL, M.A., KARABELAS, E., WILLEMEN, E., PRINZEN, F.W., LUMENS, J., VIGMOND, E.J. & PLANK, G. 2021 A computationally efficient physiologically comprehensive 3D–0D closed-loop model of the heart and circulation. *Comput. Meth. Appl. Mech. Engng* **386**, 114092.
- AVOLIO, A.P. 1980 Multi-branched model of the human arterial system. *Med. Biol. Engng Comput.* **18** (6), 709–718.
- AZARINE, A., GARÇON, P., STANSAL, A., CANEPA, N., ANGELOPOULOS, G., SILVERA, S., SIDI, D., MARTEAU, V. & ZINS, M. 2019 Four-dimensional flow MRI: principles and cardiovascular applications. *Radiographics* **39** (3), 632–648.
- BAILLOOR, S., SEO, J.H., DASI, L.P., SCHENA, S. & MITTAL, R. 2021 A computational study of the haemodynamic of bioprosthetic aortic valves with reduced leaflet motion. *J. Biomech.* **120**, 110350.
- BAKHSHINEJAD, A., BAGHAIE, A., VALI, A., SALONER, D., RAYZ, V.L. & D'SOUZA, R.M. 2017 Merging computational fluid dynamics and 4D flow MRI using proper orthogonal decomposition and ridge regression. *J. Biomech.* **58**, 162–173.
- BALLARIN, F., FAGGIANO, E., MANZONI, A., QUARTERONI, A., ROZZA, G., IPPOLITO, S., ANTONA, C. & SCROFANI, R. 2017 Numerical modeling of haemodynamic scenarios of patient-specific coronary artery bypass grafts. *Biomech. Model. Mechanobiol.* **16** (4), 1373–1399.
- BALOSSINO, R., GERVASO, F., MIGLIAVACCA, F. & DUBINI, G. 2008 Effects of different stent designs on local haemodynamic in stented arteries. *J. Biomech.* **41** (5), 1053–1061.
- BALOSSINO, R., PENNATI, G., MIGLIAVACCA, F., FORMAGGIA, L., VENEZIANI, A., TUVERI, M. & DUBINI, G. 2009 Computational models to predict stenosis growth in carotid arteries: which is the role of boundary conditions? *Comput. Meth. Biomech. Biomed. Engng* **12** (1), 113–123.
- BARKER, A.J., MARKL, M., BÜRK, J., LORENZ, R., BOCK, J., BAUER, S., SCHULZ-MENGER, J. & VON KNOBELSDORFF-BRENKENHOFF, F. 2012 Bicuspid aortic valve is associated with altered wall shear stress in the ascending aorta. *Circulation* **5** (4), 457–466.
- BARKER, A.J., ROLDÁN-ALZATE, A., ENTEZARI, P., SHAH, S.J., CHESLER, N.C., WIEBEN, O., MARKL, M. & FRANÇOIS, C.J. 2015 Four-dimensional flow assessment of pulmonary artery flow and wall shear stress in adult pulmonary arterial hypertension: results from two institutions. *Magn. Reson. Med.* **73** (5), 1904–1913.
- BARTOLO, M.A., QURESHI, M.U., COLEBANK, M.J., CHESLER, N.C. & OLUFSEN, M.S. 2022 Numerical predictions of shear stress and cyclic stretch in pulmonary hypertension due to left heart failure. *Biomech. Model. Mechanobiol.* **21** (1), 363–381.

- BÄUMLER, K., VEDULA, V., SAILER, A.M., SEO, J., CHIU, P., MISTELBAUER, G., CHAN, F.P., FISCHBEIN, M.P., MARSDEN, A.L. & FLEISCHMANN, D. 2020 Fluid–structure interaction simulations of patient-specific aortic dissection. *Biomech. Model. Mechanobiol.* **19** (5), 1607–1628.
- BAZILEVS, Y., CALO, V., COTTRELL, J., HUGHES, T., REALI, A. & SCOVAZZI, G. 2007 Variational multiscale residual-based turbulence modeling for large eddy simulation of incompressible flows. *Comput. Meth. Appl. Mech. Engng* **197** (1–4), 173–201.
- BEDEKAR, A.S., PANT, K., VENTIKOS, Y. & SUNDARAM, S. 2005 A computational model combining vascular biology and haemodynamics for thrombosis prediction in anatomically accurate cerebral aneurysms. *Food Bioprod. Process.* **83** (2 C), 118–126.
- BEERE, P.A., GLAGOV, S. & ZARINS, C.K. 1984 Retarding effect of lowered heart rate on coronary atherosclerosis. *Science* **226** (4671), 180–182.
- BELLHOUSE, B.J. 1969 Velocity and pressure distributions in the aortic valve. *J. Fluid Mech.* **37** (3), 587–600.
- BELLHOUSE, B.J. & BELLHOUSE, F.H. 1968 Mechanism of closure of the aortic valve. *Nature* **217** (5123), 86–87.
- BELLHOUSE, B.J., BELLHOUSE, F.H. & REID, K.G. 1968 Fluid mechanics of the aortic root with application to coronary flow. *Nature* **219** (5158), 1059–1061.
- BELLHOUSE, B.J. & TALBOT, L. 1969 The fluid mechanics of the aortic valve. *J. Fluid Mech.* **35** (4), 721–735.
- BENNATI, L., GIAMBRUNO, V., RENZI, F., DI NICOLA, V., MAFFEIS, C., PUPPINI, G., LUCIANI, G.B. & VERGARA, C. 2023 Turbulent blood dynamics in the left heart in the presence of mitral regurgitation: a computational study based on multi-series cine-MRI. *Biomech. Model. Mechanobiol.* **22**, 1829–1846.
- BERGAN, J.J., SCHMID-SCHÖNBEIN, G.W., SMITH, P.D.C., NICOLAIDES, A.N., BOISSEAU, M.R. & EKLOF, B. 2006 Chronic venous disease. *New Engl. J. Med.* **355** (5), 488–498.
- BERGUER, R., PARODI, J.C., SCHLICHT, M. & KHANAFAER, K. 2015 Experimental and clinical evidence supporting septectomy in the primary treatment of acute type B thoracic aortic dissection. *Ann. Vasc. Surg.* **29** (2), 167–173.
- BIRCHALL, D., ZAMAN, A., HACKER, J., DAVIES, G. & MENDELOW, D. 2006 Analysis of haemodynamic disturbance in the atherosclerotic carotid artery using computational fluid dynamics. *Eur. Radiol.* **16** (5), 1074–1083.
- BLUESTEIN, D., NIU, L., SCHOEPHOERSTER, R.T. & DEWANJEE, M.K. 1997 Fluid mechanics of arterial stenosis: relationship to the development of mural thrombus. *Ann. Biomed. Engng* **25**, 344–356.
- BOFFI, D., GASTALDI, L., HELTAI, L. & PESKIN, C.S. 2008 On the hyper-elastic formulation of the immersed boundary method. *Comput. Meth. Appl. Mech. Engng* **197** (25–28), 2210–2231.
- BOON, B. 2009 Leonardo da Vinci on atherosclerosis and the function of the sinuses of Valsalva. *Neth. Heart J.* **17** (12), 496–499.
- BORAZJANI, I. 2013 Fluid–structure interaction, immersed boundary-finite element method simulations of bio-prosthetic heart valves. *Comput. Meth. Appl. Mech. Engng* **257**, 103–116.
- BOSI, G.M., COOK, A., RAI, R., MENEZES, L.J., SCHIEVANO, S., TORII, R. & BURRIESCI, G. 2018 Computational fluid dynamic analysis of the left atrial appendage to predict thrombosis risk. *Front. Cardiovasc. Med.* **5**, 34.
- BRAVO, C.A., NAVARRO, A.G., DHALIWAL, K.K., KHORSANDI, M., KEENAN, J.E., MUDIGONDA, P., O'BRIEN, K.D. & MAHR, C. 2022 Right heart failure after left ventricular assist device: from mechanisms to treatments. *Front. Cardiovasc. Med.* **9**, 1023549.
- BRINJKIJ, W., RABINSTEIN, A.A., NASR, D.M., LANZINO, G., KALLMES, D.F. & CLOFT, H.J. 2011 Better outcomes with treatment by coiling relative to clipping of unruptured intracranial aneurysms in the United States, 2001–2008. *Am. J. Neuroradiol.* **32** (6), 1071–1075.
- BRISMAN, J.L., SONG, J.K. & NEWELL, D.W. 2006 Cerebral aneurysms. *New Engl. J. Med.* **355**, 928–939.
- BUCCELLI, M., ZINGARO, A., AFRICA, P.C., FUMAGALLI, I., DEDE', L. & QUARTERONI, A. 2023 A mathematical model that integrates cardiac electrophysiology, mechanics, and fluid dynamics: application to the human left heart. *Intl J. Numer. Meth. Biomed. Engng* **39** (3), e3678.
- BURRIS, N.S. & HOPE, M.D. 2015 4D flow MRI applications for aortic disease. *Magn. Reson. Imag. Clin. N. Am.* **23** (1), 15–23.
- CANDREVA, A., *et al.* 2022 Risk of myocardial infarction based on endothelial shear stress analysis using coronary angiography. *Atherosclerosis* **342**, 28–35.
- CARR, I.A., NEMOTO, N., SCHWARTZ, R.S. & SHADDEN, S.C. 2013 Size-dependent predilections of cardiogenic embolic transport. *Am. J. Physiol. Heart Circ. Physiol.* **305** (5), 732–739.
- CASA, L.D., DEATON, D.H. & KU, D.N. 2015 Role of high shear rate in thrombosis. *J. Vasc. Surg.* **61** (4), 1068–1080.
- CEBRAL, J.R., CASTRO, M.A., BURGESS, J.E., PERGOLIZZI, R.S., SHERIDAN, M.J. & PUTMAN, C.M. 2005 Characterization of cerebral aneurysms for assessing risk of rupture by using patient-specific computational haemodynamic models. *Am. J. Neuroradiol.* **26** (10), 2550–2559.
- CEBRAL, J.R., MUT, F., WEIR, J. & PUTMAN, C. 2011 Quantitative characterization of the haemodynamic environment in ruptured and unruptured brain aneurysms. *Am. J. Neuroradiol.* **32** (1), 145–151.
- CHANDRA, S., RAJAMANNAN, N.M. & SUCOSKY, P. 2012 Computational assessment of bicuspid aortic valve wall-shear stress: implications for calcific aortic valve disease. *Biomech. Model. Mechanobiol.* **11** (7), 1085–1096.
- CHAPELLE, D., GERBEAU, J.F., SAINTE-MARIE, J. & VIGNON-CLEMENTEL, I.E. 2010 A poroelastic model valid in large strains with applications to perfusion in cardiac modeling. *Comput. Mech.* **46** (1), 91–101.
- CHARONKO, J.J., KUMAR, R., STEWART, K., LITTLE, W.C. & VLACHOS, P.P. 2013 Vortices formed on the mitral valve tips aid normal left ventricular filling. *Ann. Biomed. Engng* **41**, 1049–1061.
- CHATZIZISIS, Y.S., *et al.* 2008 Prediction of the localization of high-risk coronary atherosclerotic plaques on the basis of low endothelial shear stress—an intravascular ultrasound and histopathology natural history study. *Circulation* **117** (8), 993–1002.

- CHEN, H.Y., DIAZ, J.A., LURIE, F., CHAMBERS, S.D. & KASSAB, G.S. 2018 Haemodynamics of venous valve pairing and implications on helical flow. *J. Vasc. Surg. Venous Lymphat. Disord.* **6** (4), 517–522.
- CHEN, H.Y., PEELUKHANA, S.V., BERWICK, Z.C., KRATZBERG, J., KRIEGER, J.F., ROEDER, B., CHAMBERS, S. & KASSAB, G.S. 2016 Editor's choice – fluid–structure interaction simulations of aortic dissection with bench validation. *Eur. J. Vasc. Endovasc. Surg.* **52** (5), 589–595.
- CHENG, Y., OERTEL, H. & SCHENKEL, T. 2005 Fluid–structure coupled CFD simulation of the left ventricular flow during filling phase. *Ann. Biomed. Engng* **33** (5), 567–576.
- CHIEN, S. 1970 Shear dependence of effective cell volume as a determinant of blood viscosity. *Science* **168** (3934), 977–979.
- CHIEN, S., USAMI, S., DELLENBACK, R.J. & GREGERSEN, M.I. 1967a Blood viscosity: influence of erythrocyte deformation. *Science* **157** (3790), 827–829.
- CHIEN, S., USAMI, S., DELLENBACK, R.J., GREGERSEN, M.I., NANNINGA, L.B. & GUEST, M.M. 1967b Blood viscosity: influence of erythrocyte aggregation. *Science* **157** (3790), 829–831.
- CHNAFA, C., MENDEZ, S. & NICLOUD, F. 2014 Image-based large-eddy simulation in a realistic left heart. *Comput. Fluids* **94**, 173–187.
- CHNAFA, C., MENDEZ, S. & NICLOUD, F. 2016 Image-based simulations show important flow fluctuations in a normal left ventricle: what could be the implications? *Ann. Biomed. Engng* **44** (11), 3346–3358.
- CHNAFA, C., VALEN-SENDSTAD, K., BRINA, O., PEREIRA, V.M. & STEINMAN, D.A. 2017 Improved reduced-order modelling of cerebrovascular flow distribution by accounting for arterial bifurcation pressure drops. *J. Biomech.* **51**, 83–88.
- CHUNG, B. & CEBRAL, J.R. 2015 CFD for evaluation and treatment planning of aneurysms: review of proposed clinical uses and their challenges. *Ann. Biomed. Engng* **43** (1), 122–138.
- CLAASSEN, J.A., THIJSSSEN, D.H., PANERAI, R.B. & FARACI, F.M. 2021 Regulation of cerebral blood flow in humans: physiology and clinical implications of autoregulation. *Physiol. Rev.* **101** (4), 1487–1559.
- COLLIA, D., ZOVATTO, L., TONTI, G. & PEDRIZZETTI, G. 2021 Comparative analysis of right ventricle fluid dynamics. *Front. Bioeng. Biotechnol.* **9**, 667408.
- COLOMBO, M., LURAGHI, G., CESTARIOLO, L., RAVASI, M., AIROLDI, A., CHIASTRA, C. & PENNATI, G. 2020 Impact of lower limb movement on the haemodynamic of femoropopliteal arteries: a computational study. *Med. Engng Phys.* **81**, 105–117.
- COOKSON, A.N., LEE, J., MICHLER, C., CHABINIOK, R., HYDE, E., NORDSLETTEN, D.A., SINCLAIR, M., SIEBES, M. & SMITH, N.P. 2012 A novel porous mechanical framework for modelling the interaction between coronary perfusion and myocardial mechanics. *J. Biomech.* **45** (5), 850–855.
- CORSINI, C., COSENTINO, D., PENNATI, G., DUBINI, G., HSIA, T.-Y. & MIGLIAVACCA, F. 2011 Multiscale models of the hybrid palliation for hypoplastic left heart syndrome. *J. Biomech.* **44** (4), 767–770.
- CUNNINGHAM, J.W., MCELHINNEY, D.B., GAUVREAU, K., BERGERSEN, L., LACRO, R.V., MARSHALL, A.C., SMOOT, L. & LOCK, J.E. 2013 Outcomes after primary transcatheter therapy in infants and young children with severe bilateral peripheral pulmonary artery stenosis. *Circulation* **6** (4), 460–467.
- CUSHMAN, M. 2007 Epidemiology and risk factors for venous thrombosis. In *Seminars in Hematology*, vol. 44, pp. 62–69. Elsevier.
- DASI, L.P., GE, L., SIMON, A.H., SOTIROPOULOS, F. & YOGANATHAN, P.A. 2007 Vorticity dynamics of a bileaflet mechanical heart valve in an axisymmetric aorta. *Phys. Fluids* **19** (6), 067105.
- DASI, L.P., SIMON, H.A., SUCOSKY, P. & YOGANATHAN, A.P. 2009 Fluid mechanics of artificial heart valves. *Clin. Exp. Pharmacol. Physiol.* **36** (2), 225–237.
- DAVIES, P.F., REMUZZI, A., GORDON, E.J., DEWEY, C.F. & GIMBRONE, M.A. 1986 Turbulent fluid shear stress induces vascular endothelial cell turnover in vitro. *Proc. Natl Acad. Sci. USA* **83** (7), 2114–2117.
- DE LEVAL, M., DUBINI, G., MIGLIAVACCA, F., JALALI, H., CAMPORINI, G., REDINGTON, A. & PIETRABISSA, R. 1996 Use of computational fluid dynamics in the design of surgical procedures: application to the study of competitive flows in cavopulmonary connections. *J. Thorac. Cardiovasc. Surg.* **111** (3), 502–513.
- DE NISCO, G., KOK, A.M., CHIASTRA, C., GALLO, D., HOOGENDOORN, A., MIGLIAVACCA, F., WENTZEL, J.J. & MORBIDUCCI, U. 2019 The atheroprotective nature of helical flow in coronary arteries. *Ann. Biomed. Engng* **47** (2), 425–438.
- DE SOUSA, D.R., *et al.* 2016 Determination of a shear rate threshold for thrombus formation in intracranial aneurysms. *J. Neurointerv. Surg.* **8** (8), 853–858.
- DEDE, L., MENGHINI, F. & QUARTERONI, A. 2021 Computational fluid dynamics of blood flow in an idealized left human heart. *Intl J. Numer. Meth. Biomed. Engng* **37** (11), e3287.
- DEPAOLA, N., GIMBRONE, M.A., DAVIES, P.F. & DEWEY, C.F. 1992 Vascular endothelium responds to fluid shear stress gradients. *Arterioscler. Thromb.* **12** (11), 1254–1257.
- DEWHURST, P., COATS, L., PARIKH, J.D., HOLLINGSWORTH, K.G. & GAN, L. 2020 The role of flow rotation in the adult right atrium: a 4D flow cardiovascular magnetic resonance study. *Physiol. Meas.* **41** (3), 035007.
- DIEM, A.K., SHARP, M.M.G., GATHERER, M., BRESSLOFF, N.W., CARARE, R.O. & RICHARDSON, G. 2017 Arterial pulsations cannot drive intramural periarterial drainage: significance for $\alpha\beta$ drainage. *Front. Neurosci.* **11**, 274820.
- DI GREGORIO, S., FEDELE, M., PONTONE, G., CORNO, A.F., ZUNINO, P., VERGARA, C. & QUARTERONI, A. 2021 A computational model applied to myocardial perfusion in the human heart: from large coronaries to microvasculature. *J. Comput. Phys.* **424**, 109836.
- DI GREGORIO, S., *et al.* 2022 Prediction of myocardial blood flow under stress conditions by means of a computational model. *Eur. J. Nucl. Med. Mol. Imag.* **49**, 1894–1905.

- DOEL, T., GAVAGHAN, D.J. & GRAU, V. 2015 Review of automatic pulmonary lobe segmentation methods from CT. *Comput. Med. Imag. Graph* **40**, 13–29.
- DOMENICHINI, F., PEDRIZZETTI, G. & BACCANI, B. 2005 Three-dimensional filling flow into a model left ventricle. *J. Fluid Mech.* **539**, 179–198.
- DONG, M.L., LAN, I.S., YANG, W., RABINOVITCH, M., FEINSTEIN, J.A. & MARSDEN, A.L. 2021 Computational simulation-derived haemodynamic and biomechanical properties of the pulmonary arterial tree early in the course of ventricular septal defects. *Biomech. Model. Mechanobiol.* **20**, 2471–2489.
- DOUGLAS, W.I., GOLDBERG, C.S., MOSCA, R.S., LAW, I.H. & BOVE, E.L. 1999 Hemi-Fontan procedure for hypoplastic left heart syndrome: outcome and suitability for Fontan. *Ann. Thorac. Surg.* **68** (4), 1361–1367.
- DUEÑAS-PAMPLONA, J., GARCÍA, J.G., SIERRA-PALLARES, J., FERRERA, C., AGUJETAS, R. & LOPEZ-MINGUEZ, J.R. 2021 A comprehensive comparison of various patient-specific CFD models of the left atrium for atrial fibrillation patients. *Comput. Biol. Med.* **133**, 104423.
- DUX-SANTOY, L., *et al.* 2020 Low and oscillatory wall shear stress is not related to aortic dilation in patients with bicuspid aortic valve: a time-resolved 3-dimensional phase-contrast magnetic resonance imaging study. *Arterioscler. Thromb. Vasc. Biol.* **40** (1), e10–e20.
- ECKMAN, P.M. & JOHN, R. 2012 Bleeding and thrombosis in patients with continuous-flow ventricular assist devices. *Circulation* **125** (24), 3038–3047.
- EMENDI, M., STURLA, F., GHOSH, R.P., BIANCHI, M., PIATTI, F., PLUCHINOTTA, F.R., GIESE, D., LOMBARDI, M., REDAELLI, A. & BLUESTEIN, D. 2021 Patient-specific bicuspid aortic valve biomechanics: a magnetic resonance imaging integrated fluid–structure interaction approach. *Ann. Biomed. Engng* **49** (2), 627–641.
- ERBERTSEDER, K., REICHHOLD, J., FLEMISCH, B., JENNY, P. & HELMIG, R. 2012 A coupled discrete/continuum model for describing cancer-therapeutic transport in the lung. *PLoS ONE* **7** (3), 31966.
- ERIKSSON, J., BOLGER, A.F., EBBERS, T. & CARLHÄLL, C.-J. 2016 Assessment of left ventricular haemodynamic forces in healthy subjects and patients with dilated cardiomyopathy using 4D flow MRI. *Physiol. Rep.* **4** (3), e12685.
- ESLAMI, P., TRAN, J., JIN, Z., KARADY, J., SOTOODEH, R., LU, M.T., HOFFMANN, U. & MARSDEN, A. 2020 Effect of wall elasticity on haemodynamic and wall shear stress in patient-specific simulations in the coronary arteries. *J. Biomech. Engng* **142** (2), 1–10.
- ESMAILY-MOGHADAM, M., HSIA, T.Y. & MARSDEN, A.L. 2015 The assisted bidirectional Glenn: a novel surgical approach for first-stage single-ventricle heart palliation. *J. Thoracic Cardiovasc. Surg.* **149** (3), 699–705.
- D'ESPOSITO, A., *et al.* 2018 Computational fluid dynamics with imaging of cleared tissue and of in vivo perfusion predicts drug uptake and treatment responses in tumours. *Nat. Biomed. Engng* **2** (10), 773–787.
- ETMINAN, N. & RINKEL, G.J. 2016 Unruptured intracranial aneurysms: development, rupture and preventive management. *Nat. Rev. Neurol.* **12** (12), 699–713.
- FÄHRÆUS, R. & LINDQVIST, T. 1931 The viscosity of the blood in narrow capillary tubes. *Am. J. Physiol.* **96** (3), 562–568.
- FALK, E., SHAH, P.K. & FUSTER, V. 1995 Coronary plaque disruption. *Circulation* **92** (3), 657–671.
- FATHI, M.F., PEREZ-RAYA, I., BAGHAIE, A., BERG, P., JANIGA, G., ARZANI, A. & D'SOUZA, R.M. 2020 Super-resolution and denoising of 4D-flow MRI using physics-informed deep neural nets. *Comput. Meth. Programs Biomed.* **197**, 105729.
- FEDOSOV, D.A., NOGUCHI, H. & GOMPPER, G. 2014 Multiscale modeling of blood flow: from single cells to blood rheology. *Biomech. Model. Mechanobiol.* **13** (2), 239–258.
- FELMLY, L.M., MAINWARING, R.D., COLLINS, R.T., LECHICH, K., MARTIN, E., MA, M. & HANLEY, F.L. 2023 Surgical repair of peripheral pulmonary artery stenosis: a 2-decade experience with 145 patients. *J. Thorac. Cardiovasc. Surg.* **165** (4), 1493–1502.e2.
- FENG, H., LI, C. & FENG, H. 2022 Numerical simulation and in vitro experimental study of thrombus capture efficiency of a new retrievable vena cava filter. *Comput. Meth. Biomech. Biomed. Engng* **26** (16), 2034–2046.
- FENSTER, B.E., BROWNING, J., SCHROEDER, J.D., SCHAFFER, M., PODGORSKI, C.A., SMYSER, J., SILVEIRA, L.J., BUCKNER, J.K. & HERTZBERG, J.R. 2015 Vorticity is a marker of right ventricular diastolic dysfunction. *Am. J. Physiol. Heart Circ. Physiol.* **309** (6), H1087–H1093.
- FERRARINI, A., FINOTELLO, A., SALSANO, G., AURICCHIO, F., PALOMBO, D., SPINELLA, G., PANE, B. & CONTI, M. 2021 Impact of leg bending in the patient-specific computational fluid dynamics of popliteal stenting. *Acta Mechanica Sin.* **37**, 279–291.
- FIGUEROA, C.A., VIGNON-CLEMENTEL, I.E., JANSEN, K.E., HUGHES, T.J. & TAYLOR, C.A. 2006 A coupled momentum method for modeling blood flow in three-dimensional deformable arteries. *Comput. Meth. Appl. Mech. Engng* **195** (41–43), 5685–5706.
- FLEETER, C.M., GERACI, G., SCHIAVAZZI, D.E., KAHN, A.M. & MARSDEN, A.L. 2020 Multilevel and multifidelity uncertainty quantification for cardiovascular haemodynamic. *Comput. Meth. Appl. Mech. Engng* **365**, 113030.
- FORMAGGIA, L., GERBEAU, J.F., NOBILE, F. & QUARTERONI, A. 2001 On the coupling of 3D and 1D Navier–Stokes equations for flow problems in compliant vessels. *Comput. Meth. Appl. Mech. Engng* **191** (6–7), 561–582.
- FORMAGGIA, L., NOBILE, F., QUARTERONI, A. & VENEZIANI, A. 1999 Multiscale modelling of the circulatory system: a preliminary analysis. *Comput. Vis. Sci.* **2** (2–3), 75–83.
- FORTINI, S., QUERZOLI, G., ESPA, S. & CENEDESE, A. 2013 Three-dimensional structure of the flow inside the left ventricle of the human heart. *Exp. Fluids* **54**, 1–9.
- FRANCIS, F.J. 2002 Aortic aneurysms: it's all about the stress. *Arterioscler. Thromb. Vasc. Biol.* **22** (12), 1948–1949.
- FRASER, K.H., TASKIN, M.E., GRIFFITH, B.P. & WU, Z.J. 2011 The use of computational fluid dynamics in the development of ventricular assist devices. *Med. Engng Phys.* **33** (3), 263–280.

- FREDRIKSSON, A.G., ZAJAC, J., ERIKSSON, J., DYVERFELDT, P., BOLGER, A.F., EBBERS, T. & CARLHÄLL, C.-J. 2011 4-D blood flow in the human right ventricle. *Am. J. Physiol. Heart Circ. Physiol.* **301** (6), H2344–H2350.
- FREEMAN, R.V. & OTTO, C.M. 2005 Spectrum of calcific aortic valve disease: pathogenesis, disease progression, and treatment strategies. *Circulation* **111** (24), 3316–3326.
- FREUND, J.B. 2014 Numerical simulation of flowing blood cells. *Annu. Rev. Fluid Mech.* **46**, 67–95.
- FUNG, Y.C. 1984 Blood flow in arteries. In *Biodynamics*. Springer. Available at: https://link.springer.com/chapter/10.1007/978-1-4757-3884-1_3.
- FUNG, Y.C. 1997 *Biomechanics*. Springer.
- FYRENIUS, A., WIGSTRÖM, L., EBBERS, T., KARLSSON, M., ENGVALL, J. & BOLGER, A.F. 2001 Three dimensional flow in the human left atrium. *Heart* **86** (4), 448–455.
- GAINES, S.P., NAEIJE, R. & PEACOCK, A.J. 2014 *The Right Heart*. Springer.
- GARCIA, J., BARKER, A.J. & MARKL, M. 2019 The role of imaging of flow patterns by 4D flow MRI in aortic stenosis. *Cardiovasc. Imag.* **12** (2), 252–266.
- GE, L., DASI, L.P., SOTIROPOULOS, F. & YOGANATHAN, A.P. 2008 Characterization of haemodynamic forces induced by mechanical heart valves: Reynolds vs. viscous stresses. *Ann. Biomed. Engng* **36** (2), 276–297.
- GE, L. & SOTIROPOULOS, F. 2010 Direction and magnitude of blood flow shear stresses on the leaflets of aortic valves: is there a link with valve calcification? *J. Biomech. Engng* **132** (1), 014505.
- GERTZ, S.D. & ROBERTS, W.C. 1990 Haemodynamic shear force in rupture of coronary arterial atherosclerotic plaques. *Am. J. Cardiol.* **66** (19), 1368–1372.
- GHARIB, M., KREMERS, D., KOOCHESFAHANI, M. & KEMP, M. 2002 Leonardo's vision of flow visualization. *Exp. Fluids* **33** (1), 219–223.
- GIDDENS, D.P., ZARINS, C.K. & GLAGOV, S. 1993 The role of fluid mechanics in the localization and detection of atherosclerosis. *J. Biomech. Engng* **115** (4), 588–594.
- GILMANOV, A. & SOTIROPOULOS, F. 2016 Comparative haemodynamic in an aorta with bicuspid and trileaflet valves. *Theor. Comput. Fluid Dyn.* **30** (1–2), 67–85.
- GIRDAUSKAS, E., BORGER, M.A., SECKNUS, M.A., GIRDAUSKAS, G. & KUNTZE, T. 2011 Is aortopathy in bicuspid aortic valve disease a congenital defect or a result of abnormal haemodynamic? A critical reappraisal of a one-sided argument. *Eur. J. Cardiothorac. Surg.* **39** (6), 809–814.
- GOLDBERG, D.J., SHADY, R.E., RAVISHANKAR, C. & RYCHIK, J. 2011 The failing Fontan: etiology, diagnosis and management. *Expert Rev. Cardiovasc. Ther.* **9** (6), 785–793.
- GONZALEZ, C.F., CHO, Y.I., ORTEGA, H.V. & MORET, J. 1992 Intracranial aneurysms: flow analysis of their origin and progression. *Am. J. Neuroradiol.* **13** (1), 181–188.
- GOODWILL, A.G., DICK, G.M., KIEL, A.M. & TUNE, J.D. 2017 Regulation of coronary blood flow. *Compr. Physiol.* **7** (2), 321–382.
- GOULD, S.T., SRIGUNAPALAN, S., SIMMONS, C.A. & ANSETH, K.S. 2013 Haemodynamic and cellular response feedback in calcific aortic valve disease. *Circ. Res.* **113** (2), 186–197.
- GRANDE GUTIERREZ, N., MATHEW, M., MCCRINDLE, B.W., TRAN, J.S., KAHN, A.M., BURNS, J.C. & MARSDEN, A.L. 2019 Haemodynamic variables in aneurysms are associated with thrombotic risk in children with Kawasaki disease. *Intl J. Cardiol.* **281**, 15–21.
- GRANDE GUTIÉRREZ, N., SINNO, T. & DIAMOND, S.L. 2022 A 1D–3D hybrid model of patient-specific coronary haemodynamic. *Cardiovasc. Engng Technol.* **13** (2), 331–342.
- GRIFFIN, J.M. & KATZ, J.N. 2014 The burden of ventricular arrhythmias following left ventricular assist device implantation. *Arrhythm Electrophysiol. Rev.* **3** (3), 145.
- GRIFFITH, B.E. & LUO, X. 2017 Hybrid finite difference/finite element immersed boundary method. *Intl J. Numer. Meth. Biomed. Engng* **33** (12), e2888.
- GRIFFITH, B.E. & PATANKAR, N.A. 2020 Immersed methods for fluid-structure interaction. *Annu. Rev. Fluid Mech.* **52**, 421–448.
- GUIVIER-CURIEN, C., DEPLANO, V. & BERTRAND, E. 2009 Validation of a numerical 3-D fluid-structure interaction model for a prosthetic valve based on experimental PIV measurements. *Med. Engng Phys.* **31** (8), 986–993.
- GUYTON, A. & HALL, J.E. 2006 *Textbook of Medical Physiology*. Elsevier Saunders.
- HA, H., ZIEGLER, M., WELANDER, M., BJARNEGÅRD, N., CARLHÄLL, C.J., LINDENBERGER, M., LÄNNE, T., EBBERS, T. & DYVERFELDT, P. 2018 Age-related vascular changes affect turbulence in aortic blood flow. *Front. Physiol.* **9**, 310199.
- HABIBI, M., D'SOUZA, R.M., DAWSON, S.T. & ARZANI, A. 2021 Integrating multi-fidelity blood flow data with reduced-order data assimilation. *Comput. Biol. Med.* **135**, 104566.
- HAGGERTY, C.M., RESTREPO, M., TANG, E., DE ZÉLICOURT, D.A., SUNDARESWARAN, K.S., MIRABELLA, L., BETHEL, J., WHITEHEAD, K.K., FOGEL, M.A. & YOGANATHAN, A.P. 2014 Fontan haemodynamic from 100 patient-specific cardiac magnetic resonance studies: a computational fluid dynamics analysis. *J. Thorac. Cardiovasc. Surg.* **148** (4), 1481–1489.
- HAMER, J.D., MALONE, P.C. & SILVER, I.A. 1981 The PO₂ in venous valve pockets: its possible bearing on thrombogenesis. *Brit. J. Surg.* **68** (3), 166–170.
- HAN, Q.J., WITSCHY, W.R., FANG-YEN, C.M., ARKLES, J.S., BARKER, A.J., FORFIA, P.R. & HAN, Y. 2015 Altered right ventricular kinetic energy work density and viscous energy dissipation in patients with pulmonary arterial hypertension: a pilot study using 4D flow MRI. *PLoS ONE* **10** (9), e0138365.

- HE, X. & KU, D.N. 1996 Pulsatile flow in the human left coronary artery bifurcation: average conditions. *J. Biomech. Engng* **118** (1), 74–82.
- HENDERSON, Y. & JOHNSON, F. 1912 Two modes of closure of the heart valves. *Heart* **4**, 69–82.
- HIRSCHVOGEL, M., BASSILIOUS, M., JAGSCHIES, L., WILDHIRT, S.M. & GEE, M.W. 2017 A monolithic 3D-0D coupled closed-loop model of the heart and the vascular system: experiment-based parameter estimation for patient-specific cardiac mechanics. *Intl J. Numer. Meth. Biomed. Engng* **33** (8), 1–22.
- HOOGENDOORN, A., *et al.* 2021 Multidirectional wall shear stress promotes advanced coronary plaque development: comparing five shear stressmetrics. *Cardiovasc. Res.* **116** (6), 1136–1146.
- Hsia, T.-Y., COSENTINO, D., CORSINI, C., PENNATI, G., DUBINI, G., MIGLIAVACCA, F. & MODELING OF CONGENITAL HEARTS ALLIANCE (MOCHA) INVESTIGATORS 2011 Use of mathematical modeling to compare and predict haemodynamic effects between hybrid and surgical norwood palliations for hypoplastic left heart syndrome. *Circulation* **124** (11_suppl_1), S204–S210.
- HSU, M.C., KAMENSKY, D., BAZILEVS, Y., SACKS, M.S. & HUGHES, T.J. 2014 Fluid–structure interaction analysis of bioprosthetic heart valves: significance of arterial wall deformation. *Comput. Mech.* **54** (4), 1055–1071.
- HSU, M.C., KAMENSKY, D., XU, F., KIENDL, J., WANG, C., WU, M.C., MINEROFF, J., REALI, A., BAZILEVS, Y. & SACKS, M.S. 2015 Dynamic and fluid–structure interaction simulations of bioprosthetic heart valves using parametric design with T-splines and Fung-type material models. *Comput. Mech.* **55** (6), 1211–1225.
- HUANG, W., YEN, R., MCLAURINE, M. & BLEDSOE, G. 1996 Morphometry of the human pulmonary vasculature. *J. Appl. Physiol. Respir. Environ. Exerc. Physiol.* **81** (5), 2123–2133.
- HUGHES, T.J., FEIJÓO, G.R., MAZZEI, L. & QUINCY, J.-B. 1998 The variational multiscale method—a paradigm for computational mechanics. *Comput. Meth. Appl. Mech. Engng* **166** (1–2), 3–24.
- HUGHES, T.J., MAZZEI, L. & JANSEN, K.E. 2000 Large eddy simulation and the variational multiscale method. *Comput. Vis. Sci.* **3**, 47–59.
- HUGHES, T.J., TAKIZAWA, K., BAZILEVS, Y., TEZDUYAR, T.E. & Hsu, M.-C. 2020 Computational cardiovascular analysis with the variational multiscale methods and isogeometric discretization. In *Parallel Algorithms Comput. Sci. Engng* (ed. A. Grama & A. Sameh), pp. 151–193. Birkhauser.
- HUMPHREY, J.D. 2008 Mechanisms of arterial remodeling in hypertension: coupled roles of wall shear and intramural stress. *Hypertension* **52** (2), 195–200.
- HUNTER, K.S., LEE, P.-F., LANNING, C.J., IVY, D.D., KIRBY, K.S., CLAUSSEN, L.R., CHAN, K.C. & SHANDAS, R. 2008 Pulmonary vascular input impedance is a combined measure of pulmonary vascular resistance and stiffness and predicts clinical outcomes better than pulmonary vascular resistance alone in pediatric patients with pulmonary hypertension. *Am. Heart J.* **155** (1), 166–174.
- HYDE, E.R., *et al.* 2014 Multi-scale parameterisation of a myocardial perfusion model using whole-organ arterial networks. *Ann. Biomed. Engng* **42** (4), 797–811.
- ILIFF, J.J., WANG, M., ZEPPEFELD, D.M., VENKATARAMAN, A., PLOG, B.A., LIAO, Y., DEANE, R. & NEDERGAARD, M. 2013 Cerebral arterial pulsation drives paravascular CSF–interstitial fluid exchange in the murine brain. *J. Neurosci.* **33** (46), 18190–18199.
- ITATANI, K., MIYAJI, K., QIAN, Y., LIU, J.L., MIYAKOSHI, T., MURAKAMI, A., ONO, M. & UMEZU, M. 2012 Influence of surgical arch reconstruction methods on single ventricle workload in the norwood procedure. *J. Thorac. Cardiovasc. Surg.* **144** (1), 130–138.
- JAHAZAMIN, J., FATOURAEE, N. & NASIRAEI-MOGHADDAM, A. 2019 Effect of turbulent models on left ventricle diastolic flow patterns simulation. *Comput. Meth. Biomech. Biomed. Engng* **22** (15), 1229–1238.
- JIANG, M.X., KHAN, M.O., GHOBRIAL, J., ROGERS, I.S., PETERSSON, G.B., BLACKSTONE, E.H. & MARSDEN, A.L. 2022 Patient-specific fluid–structure simulations of anomalous aortic origin of right coronary arteries. *JTCVS Tech.* **13**, 144–162.
- JONES, R.T. 1969 Blood flow. *Annu. Rev. Fluid Mech.* **1**, 223–244.
- JOSEPH, A.A., VOIT, D. & FRAHM, J. 2020 Inferior vena cava revisited – real-time flow MRI of respiratory maneuvers. *NMR Biomed.* **33** (4), e4232.
- JOU, L.D., LEE, D.H., MORSI, H. & MAWAD, M.E. 2008 Wall shear stress on ruptured and unruptured intracranial aneurysms at the internal carotid artery. *Am. J. Neuroradiol.* **29** (9), 1761–1767.
- JUN, B.H., SAIKRISHNAN, N., ARJUNON, S., YUN, B.M. & YOGANATHAN, A.P. 2014 Effect of hinge gap width of a St. Jude medical bileaflet mechanical heart valve on blood damage potential—an in vitro micro particle image velocimetry study. *J. Biomech. Engng* **136** (9), 091008.
- KAISER, A.D., SCHIAVONE, N.K., ELKINS, C.J., MCELHINNEY, D.B., EATON, J.K. & MARSDEN, A.L. 2023 Comparison of immersed boundary simulations of heart valve haemodynamic against in vitro 4D flow MRI data. *Ann. Biomed. Engng* **51**, 2267–2288.
- KAISER, A.D., SHAD, R., HIESINGER, W. & MARSDEN, A.L. 2021 A design-based model of the aortic valve for fluid–structure interaction. *Biomech. Model. Mechanobiol.* **20** (6), 2413–2435.
- KAISER, A.D., SHAD, R., SCHIAVONE, N., HIESINGER, W. & MARSDEN, A.L. 2022 Controlled comparison of simulated haemodynamic across tricuspid and bicuspid aortic valves. *Ann. Biomed. Engng* **50** (9), 1053–1072.
- KAJIYA, F., TSUJIOKA, K., OGASAWARA, Y., WADA, Y., MATSUOKA, S., KANAZAWA, S., HIRAMATSU, O., TADAOKA, S.I., GOTO, M. & FUJIWARA, T. 1987 Analysis of flow characteristics in poststenotic regions of the human coronary artery during bypass graft surgery. *Circulation* **76** (5), 1092–1100.
- KAMENSKY, D., Hsu, M.C., SCHILLINGER, D., EVANS, J.A., AGGARWAL, A., BAZILEVS, Y., SACKS, M.S. & HUGHES, T.J. 2015 An immersogeometric variational framework for fluid–structure interaction: application to bioprosthetic heart valves. *Comput. Meth. Appl. Mech. Engng* **284**, 1005–1053.

- KAMP, O., VERHORST, P., WELLING, R. & VISSER, C. 1999 Importance of left atrial appendage flow as a predictor of thromboembolic events in patients with atrial fibrillation. *Eur. Heart J.* **20** (13), 979–985.
- KARMONIK, C., PARTOVI, S., LOEBE, M., SCHMACK, B., WEYMANN, A., LUMSDEN, A.B., KARCK, M. & RUHPARWAR, A. 2014 Computational fluid dynamics in patients with continuous-flow left ventricular assist device support show haemodynamic alterations in the ascending aorta. *J. Thorac. Cardiovasc. Surg.* **147** (4), 1326–1333.
- KHAN, M.O., TORO ARANA, V., NAJAFI, M., MACDONALD, D.E., NATARAJAN, T., VALEN-SENDSTAD, K. & STEINMAN, D.A. 2021 On the prevalence of flow instabilities from high-fidelity computational fluid dynamics of intracranial bifurcation aneurysms. *J. Biomech.* **127**, 110683.
- KHAN, M.O., TRAN, J.S., ZHU, H., BOYD, J., PACKARD, R.R., KARLSBERG, R.P., KAHN, A.M. & MARSDEN, A.L. 2020 Low wall shear stress is associated with saphenous vein graft stenosis in patients with coronary artery bypass grafting. *J. Cardiovasc. Transl. Res.* **14**, 770–781.
- KHERADVAR, A. & FALAHATPISHEH, A. 2012 The effects of dynamic saddle annulus and leaflet length on transmitral flow pattern and leaflet stress of a bileaflet bioprosthetic mitral valve. *J. Heart Valve Dis.* **21** (2), 225.
- KHEYFETS, V., O'DELL, W., SMITH, T., REILLY, J. & FINOL, E. 2013 Considerations for numerical modeling of the pulmonary circulation—a review with a focus on pulmonary hypertension. *J. Biomech. Engng* **135** (6), 061011.
- KHEYFETS, V.O., *et al.* 2015 Patient-specific computational modeling of blood flow in the pulmonary arterial circulation. *Comput. Meth. Programs. Biomed.* **120** (2), 88–101.
- KILNER, P.J., YANG, G.-Z., WILKES, A.J., MOHIADDIN, R.H., FIRMIN, D.N. & YACOB, M.H. 2000 Asymmetric redirection of flow through the heart. *Nature* **404** (6779), 759–761.
- KIM, H.J., RUNDFELDT, H.C., LEE, I. & LEE, S. 2023 Tissue-growth-based synthetic tree generation and perfusion simulation. *Biomech. Model. Mechanobiol.* **22** (3), 1095–1112.
- KIM, H.J., VIGNON-CLEMENTEL, I.E., COOGAN, J.S., FIGUEROA, C.A., JANSEN, K.E. & TAYLOR, C.A. 2010 Patient-specific modeling of blood flow and pressure in human coronary arteries. *Ann. Biomed. Engng* **38** (10), 3195–3209.
- KIRKLIN, J.K., NAFTEL, D.C., PAGANI, F.D., KORMOS, R.L., STEVENSON, L.W., BLUME, E.D., MYERS, S.L., MILLER, M.A., BALDWIN, J.T. & YOUNG, J.B. 2015 Seventh intermacs annual report: 15 000 patients and counting. *J. Heart Lung Transpl.* **34** (12), 1495–1504.
- KOGON, B.E., PLATTNER, C., LEONG, T., SIMSIC, J., KIRSHBOM, P.M. & KANTER, K.R. 2008 The bidirectional glenn operation: a risk factor analysis for morbidity and mortality. *J. Thorac. Cardiovasc. Surg.* **136** (5), 1237–1242.
- KOK, A.M., MOLONY, D.S., TIMMINS, L.H., KO, Y.A., BOERSMA, E., ESHTEHARDI, P., WENTZEL, J.J. & SAMADY, H. 2019 The influence of multidirectional shear stress on plaque progression and composition changes in human coronary arteries. *EuroIntervention* **15** (8), 692–699.
- KONG, F., WILSON, N. & SHADDEN, S. 2021 A deep-learning approach for direct whole-heart mesh reconstruction. *Med. Image Anal.* **74**, 102222.
- KOO, B.K., *et al.* 2011 Diagnosis of ischemia-causing coronary stenoses by noninvasive fractional flow reserve computed from coronary computed tomographic angiograms: results from the prospective multicenter DISCOVER-FLOW (diagnosis of Ischemia-causing Stenoses obtained via Noni. *J. Am. Coll. Cardiol.* **58** (19), 1989–1997.
- KU, D.N. 1997 Blood flow in arteries. *Annu. Rev. Fluid Mech.* **29**, 399–434.
- KU, D.N. & GIDDENS, D.P. 1983 Pulsatile flow in a model carotid bifurcation. *Arteriosclerosis* **3** (1), 31–39.
- KU, D.N., GIDDENS, D.P., ZARINS, C.K. & GLAGOV, S. 1985 Pulsatile flow and atherosclerosis in the human carotid bifurcation. Positive correlation between plaque location and low and oscillating shear stress. *Arteriosclerosis* **5** (3), 293–302.
- KULP, S., GAO, M., ZHANG, S., QIAN, Z., VOROS, S., METAXAS, D. & AXEL, L. 2011 Using high resolution cardiac CT data to model and visualize patient-specific interactions between trabeculae and blood flow. In *Medical Image Computing and Computer-Assisted Intervention—MICCAI 2011: 14th International Conference, Toronto, Canada, September 18–22, 2011, Proceedings, Part I 14*, pp. 468–475. Springer.
- KUNG, E., PENNATI, G., MIGLIAVACCA, F., HSIA, T.-Y., FIGLIOLA, R., MARSDEN, A., GIARDINI, A. & MOCHA INVESTIGATORS 2014 A simulation protocol for exercise physiology in Fontan patients using a closed loop lumped-parameter model. *J. Biomech. Engng* **136** (8), 081007.
- KUNG, E., *et al.* 2020 Multiscale modeling of superior cavopulmonary circulation: hemi-Fontan and bidirectional Glenn are equivalent. In *Seminars in Thoracic and Cardiovascular Surgery*, vol. 32, pp. 883–892. Elsevier.
- LADRÓN-DE GUEVARA, A., SHANG, J.K., NEDERGAARD, M. & KELLEY, D.H. 2022 Perivascular pumping in the mouse brain: improved boundary conditions reconcile theory, simulation, and experiment. *J. Theor. Biol.* **542**, 111103.
- LAN, I.S., YANG, W., FEINSTEIN, J.A., KREUTZER, J., COLLINS, R.T., MA, M., ADAMSON, G.T. & MARSDEN, A.L. 2022 Virtual transcatheter interventions for peripheral pulmonary artery stenosis in Williams and Alagille syndromes. *J. Am. Heart Assoc.* **11** (6), e023532.
- LANG, R.M., CAMELI, M., SADE, L.E., FALETRA, F.F., FORTUNI, F., ROSSI, A. & SOULAT-DUFOUR, L. 2022 Imaging assessment of the right atrium: anatomy and function. *Eur. Heart J. Cardiovasc. Imag.* **23** (7), 867–884.
- LANTZ, J., HENRIKSSON, L., PERSSON, A., KARLSSON, M. & EBBERS, T. 2016 Patient-specific simulation of cardiac blood flow from high-resolution computed tomography. *J. Biomech. Engng* **138** (12), 121004.
- LE, T.B. & SOTIROPOULOS, F. 2012 On the three-dimensional vortical structure of early diastolic flow in a patient-specific left ventricle. *Eur. J. Mech. (B/Fluids)* **35**, 20–24.

- LE, T.B., SOTIROPOULOS, F., COFFEY, D. & KEEFE, D. 2012 Vortex formation and instability in the left ventricle. *Phys. Fluids* **24** (9), 091110.
- LEE, S.E., LEE, S.W., FISCHER, P.F., BASSIOUNY, H.S. & LOTH, F. 2008 Direct numerical simulation of transitional flow in a stenosed carotid bifurcation. *J. Biomech.* **41** (11), 2551–2561.
- LEE, J.H., RYGG, A.D., KOLAHDOUZ, E.M., ROSSI, S., RETTA, S.M., DURAISWAMY, N., SCOTTEN, L.N., CRAVEN, B.A. & GRIFFITH, B.E. 2020 Fluid–structure interaction models of bioprosthetic heart valve dynamics in an experimental pulse duplicator. *Ann. Biomed. Engng* **48** (5), 1475–1490.
- LEE, J. & SMITH, N.P. 2012 The multi-scale modelling of coronary blood flow. *Ann. Biomed. Engng* **40** (11), 2399–2413.
- LEMONNIER, N., ZHOU, G.-B., PRASHER, B., MUKERJI, M., CHEN, Z., BRAHMACHARI, S.K., NOBLE, D., AUFRAY, C. & SAGNER, M. 2017 Traditional knowledge-based medicine: a review of history, principles, and relevance in the present context of P4 systems medicine. *Prog. Prev. Med.* **2** (7), e0011.
- LES, A.S., SHADDEN, S.C., FIGUEROA, C.A., PARK, J.M., TEDESCO, M.M., HERFKENS, R.J., DALMAN, R.L. & TAYLOR, C.A. 2010 Quantification of haemodynamic in abdominal aortic aneurysms during rest and exercise using magnetic resonance imaging and computational fluid dynamics. *Ann. Biomed. Engng* **38** (4), 1288–1313.
- LEVITT, M.R., MCGAH, P.M., ALISEDA, A., MOURAD, P.D., NERVA, J.D., VAIDYA, S.S., MORTON, R.P., GHODKE, B.V. & KIM, L.J. 2014 Cerebral aneurysms treated with flow-diverting stents: computational models with intravascular blood flow measurements. *Am. J. Neuroradiol.* **35** (1), 143–148.
- LIANG, F., FUKASAKU, K., LIU, H. & TAKAGI, S. 2011 A computational model study of the influence of the anatomy of the circle of willis on cerebral hyperperfusion following carotid artery surgery. *Biomed. Engng Online* **10** (1), 1–22.
- LIU, X., SUN, A., FAN, Y. & DENG, X. 2015 Physiological significance of helical flow in the arterial system and its potential clinical applications. *Ann. Biomed. Engng* **43** (1), 3–15.
- LIU, J., YANG, W., LAN, I.S. & MARSDEN, A.L. 2020 Fluid-structure interaction modeling of blood flow in the pulmonary arteries using the unified continuum and variational multiscale formulation. *Mech. Res. Commun.* **107**, 103556.
- LOGERFO, F.W., NOWAK, M.D., QUIST, W.C., CRAWSHAW, H.M. & BHARADVAJ, B.K. 1981 Flow studies in a model carotid bifurcation. *Arteriosclerosis* **1** (4), 235–241.
- LOREE, H.M., KAMM, R.D., ATKINSON, C.M. & LEE, R.T. 1991 Turbulent pressure fluctuations on surface of model vascular stenoses. *Am. J. Physiol. Heart Circ. Physiol.* **261** (3), H644–H650.
- LURIE, F. & KISTNER, R.L. 2012 The relative position of paired valves at venous junctions suggests their role in modulating three-dimensional flow pattern in veins. *Eur. J. Vasc. Endovasc. Surg.* **44** (3), 337–340.
- LURIE, F. & KISTNER, R.L. 2013 On the existence of helical flow in veins of the lower extremities. *J. Vasc. Surg. Venous Lymphat. Disord.* **1** (2), 134–138.
- LURIE, F., KISTNER, R.L., EKLOF, B. & KESSLER, D. 2003 Mechanism of venous valve closure and role of the valve in circulation: a new concept. *J. Vasc. Surg.* **38** (5), 955–961.
- MADU, E.C. & D'CRUZ, I.A. 1997 The vital role of papillary muscles in mitral and ventricular function: echocardiographic insights. *Clin. Cardiol.* **20** (2), 93–98.
- MAEDER, M.T., WEBER, L., BUSER, M., GERHARD, M., HAAGER, P.K., MAISANO, F. & RICKLI, H. 2018 Pulmonary hypertension in aortic and mitral valve disease. *Front. Cardiovasc. Med.* **5**, 40.
- MAINWARING, R.D. & HANLEY, F.L. 2016 Surgical techniques for repair of peripheral pulmonary artery stenosis. In *Seminars in Thoracic and Cardiovascular Surgery*, vol. 28, pp. 418–424. Elsevier.
- MALEK, A.M., ALPER, S.L. & IZUMO, S. 1999 Haemodynamic shear stress and its role in atherosclerosis. *J. Am. Med. Assoc.* **282** (21), 2035–2042.
- MANGUAL, J., DOMENICHINI, F. & PEDRIZZETTI, G. 2012 Describing the highly three dimensional right ventricle flow. *Ann. Biomed. Engng* **40**, 1790–1801.
- MANGUAL, J.O., KRAIGHER-KRAINER, E., DE LUCA, A., TONCELLI, L., SHAH, A., SOLOMON, S., GALANTI, G., DOMENICHINI, F. & PEDRIZZETTI, G. 2013 Comparative numerical study on left ventricular fluid dynamics after dilated cardiomyopathy. *J. Biomech.* **46** (10), 1611–1617.
- MARKL, M., FRYDRYCHOWICZ, A., KOZERKE, S., HOPE, M. & WIEBEN, O. 2012 4D flow MRI. *J. Magn. Reson. Imag.* **36** (5), 1015–1036.
- MARKL, M., KILNER, P.J. & EBBERS, T. 2011 Comprehensive 4D velocity mapping of the heart and great vessels by cardiovascular magnetic resonance. *J. Cardiovasc. Magn. Reson.* **13**, 1–22.
- MARSDEN, A.L. 2014 Optimization in cardiovascular modeling. *Annu. Rev. Fluid Mech.* **46**, 519–546.
- MARSDEN, A.L., BERNSTEIN, A.J., REDDY, V.M., SHADDEN, S.C., SPILKER, R.L., CHAN, F.P., TAYLOR, C.A. & FEINSTEIN, J.A. 2009 Evaluation of a novel Y-shaped extracardiac Fontan baffle using computational fluid dynamics. *J. Thorac. Cardiovasc. Surg.* **137** (2), 394–403.
- MARSDEN, A.L. & ESMAILY-MOGHADAM, M. 2015 Multiscale modeling of cardiovascular flows for clinical decision support. *Appl. Mech. Rev.* **67** (3), 030804.
- MARSDEN, A.L., REDDY, V.M., SHADDEN, S.C., CHAN, F.P., TAYLOR, C.A. & FEINSTEIN, J.A. 2010 A new multiparameter approach to computational simulation for Fontan assessment and redesign. *Congenit. Heart Dis.* **5** (2), 104–117.
- MARSDEN, A.L., VIGNON-CLEMENTEL, I.E., CHAN, F.P., FEINSTEIN, J.A. & TAYLOR, C.A. 2007 Effects of exercise and respiration on haemodynamic efficiency in CFD simulations of the total cavopulmonary connection. *Ann. Biomed. Engng* **35**, 250–263.

- MARTIN, M.H., FEINSTEIN, J.A., CHAN, F.P., MARSDEN, A.L., YANG, W. & REDDY, V.M. 2015 Technical feasibility and intermediate outcomes of using a handcrafted, area-preserving, bifurcated Y-graft modification of the Fontan procedure. *J. Thorac. Cardiovasc. Surg.* **149** (1), 239–245.
- MASCI, A., BARONE, L., DEDÈ, L., FEDELE, M., TOMASI, C., QUARTERONI, A. & CORSI, C. 2019 The impact of left atrium appendage morphology on stroke risk assessment in atrial fibrillation: a computational fluid dynamics study. *Front. Physiol.* **9**, 1938.
- MATHEW, R.C., GOTTBRECHT, M. & SALERNO, M. 2018 Computed tomography fractional flow reserve to guide coronary angiography and intervention. *Interv. Cardiol. Clin.* **7** (3), 345–354.
- MAZZI, V., DE NISCO, G., HOOGENDOORN, A., CALÒ, K., CHIASTRA, C., GALLO, D., STEINMAN, D.A., WENTZEL, J.J. & MORBIDUCCI, U. 2021 Early atherosclerotic changes in coronary arteries are associated with endothelium shear stress contraction/expansion variability. *Ann. Biomed. Engng* **49** (9), 2606–2621.
- MCCARTHY, P.M., NAKATANI, S., VARGO, R., KOTTKE-MARCHANT, K., HARASAKI, H., JAMES, K.B., SAVAGE, R.M. & THOMAS, J.D. 1995 Structural and left ventricular histologic changes after implantable LVAD insertion. *Ann. Thorac. Surg.* **59** (3), 609–613.
- MCCRINDLE, B.W., *et al.* 2017 Diagnosis, treatment, and long-term management of Kawasaki disease: a scientific statement for health professionals from the American Heart Association. *Circulation* **135** (17), e927–e999.
- MEIJBOOM, W.B., *et al.* 2008 Comprehensive assessment of coronary artery stenoses: computed tomography coronary angiography versus conventional coronary angiography and correlation with fractional flow reserve in patients with stable angina. *J. Am. Coll. Cardiol.* **52** (8), 636–643.
- MENON, K., KHAN, M.O., SEXTON, Z.A., RICHTER, J., NIEMAN, K. & MARSDEN, A.L. 2024 Personalized coronary and myocardial blood flow models incorporating CT perfusion imaging and synthetic vascular trees. *NPJ Imaging* **2**, 9.
- MENON, K., SEO, J., FUKAZAWA, R., OGAWA, S., KAHN, A.M., BURNS, J.C. & MARSDEN, A.L. 2023 Predictors of myocardial ischemia in patients with Kawasaki disease: insights from patient-specific simulations of coronary haemodynamic. *J. Cardiovasc. Transl. Res.* **16**, 1099–1109.
- MESCHINI, V., DE TULLIO, M.D., QUERZOLI, G. & VERZICCO, R. 2018 Flow structure in healthy and pathological left ventricles with natural and prosthetic mitral valves. *J. Fluid Mech.* **834**, 271–307.
- MESCHINI, V., VIOLA, F. & VERZICCO, R. 2019 Modeling mitral valve stenosis: a parametric study on the stenosis severity level. *J. Biomech.* **84**, 218–226.
- MICHLER, C., *et al.* 2013 A computationally efficient framework for the simulation of cardiac perfusion using a multi-compartment Darcy porous-media flow model. *Intl J. Numer. Meth. Biomed. Engng* **29** (2), 217–232.
- MIGLIAVACCA, F., BALOSSINO, R., PENNATI, G., DUBINI, G., HSIA, T.Y., DE LEVAL, M.R. & BOVE, E.L. 2006 Multiscale modelling in biofluidynamics: application to reconstructive paediatric cardiac surgery. *J. Biomech.* **39** (6), 1010–1020.
- MIGLIAVACCA, F., PENNATI, G., DUBINI, G., FUMERO, R., PIETRABISSA, R., URCELAY, G., BOVE, E.L., HSIA, T.-Y. & DE LEVAL, M.R. 2001 Modeling of the norwood circulation: effects of shunt size, vascular resistances, and heart rate. *Am. J. Physiol. Heart Circ. Physiol.* **280** (5), H2076–H2086.
- MILLER, L.W., *et al.* 2007 Use of a continuous-flow device in patients awaiting heart transplantation. *New Engl. J. Med.* **357** (9), 885–896.
- MIN, J.K., *et al.* 2012 Diagnostic accuracy of fractional flow reserve from anatomic CT angiography. *J. Am. Med. Assoc.* **308** (12), 1237–1245.
- MIRRAMAZANI, M. & SHADDEN, S.C. 2020 A distributed lumped parameter model of blood flow. *Ann. Biomed. Engng* **48** (12), 2870–2886.
- MITTAL, R. & IACCARINO, G. 2005 Immersed boundary methods. *Annu. Rev. Fluid Mech.* **37** (1), 239–261.
- MITTAL, R., SEO, J.H., VEDULA, V., CHOI, Y.J., LIU, H., HUANG, H.H., JAIN, S., YOUNES, L., ABRAHAM, T. & GEORGE, R.T. 2016 Computational modeling of cardiac haemodynamic: current status and future outlook. *J. Comput. Phys.* **305**, 1065–1082.
- MOGHADAM, M.E., MIGLIAVACCA, F., VIGNON-CLEMENTEL, I.E., HSIA, T.Y. & MARSDEN, A.L. 2012 Optimization of shunt placement for the norwood surgery using multi-domain modeling. *J. Biomech. Engng* **134** (5), 051002.
- MOORE, B. & DAS, L.P. 2014 Spatiotemporal complexity of the aortic sinus vortex. *Exp. Fluids* **55** (7), 1–12.
- MOORE, B.L. & DAS, L.P. 2015 Coronary flow impacts aortic leaflet mechanics and aortic sinus haemodynamic. *Ann. Biomed. Engng* **43** (9), 2231–2241.
- MORBIDUCCI, U., MAZZI, V., DOMANIN, M., DE NISCO, G., VERGARA, C., STEINMAN, D.A. & GALLO, D. 2020 Wall shear stress topological skeleton independently predicts long-term restenosis after carotid bifurcation endarterectomy. *Ann. Biomed. Engng* **48** (12), 2936–2949.
- MORBIDUCCI, U., PONZINI, R., GRIGIONI, M. & REDAELLI, A. 2007 Helical flow as fluid dynamic signature for atherogenesis risk in aortocoronary bypass. A numeric study. *J. Biomech.* **40** (3), 519–534.
- MORBIDUCCI, U., PONZINI, R., RIZZO, G., CADIOLI, M., ESPOSITO, A., MONTEVECCHI, F.M. & REDAELLI, A. 2011 Mechanistic insight into the physiological relevance of helical blood flow in the human aorta: an in vivo study. *Biomech. Model. Mechanobiol.* **10** (3), 339–355.
- MORLACCHI, S. & MIGLIAVACCA, F. 2013 Modeling stented coronary arteries: where we are, where to go. *Ann. Biomed. Engng* **41** (7), 1428–1444.
- MOURATO, A., VALENTE, R., XAVIER, J., BRITO, M., AVRIL, S., DE SÁ, J.C., TOMÁS, A. & FRAGATA, J. 2022 Computational modelling and simulation of fluid structure interaction in aortic aneurysms: a systematic review and discussion of the clinical potential. *Appl. Sci.* **12** (16), 8049.

- MUKHERJEE, D., JANI, N.D., SELVAGANESAN, K., WENG, C.L. & SHADDEN, S.C. 2016 Computational assessment of the relation between embolism source and embolus distribution to the circle of Willis for improved understanding of Stroke etiology. *J. Biomech. Engng* **138** (8), 081008.
- MÜLLER, L.O. & TORO, E.F. 2014 A global multiscale mathematical model for the human circulation with emphasis on the venous system. *Intl J. Numer. Meth. Biomed. Engng* **30** (7), 681–725.
- MURRAY, C.D. 1926 The physiological principle of minimum work I: the vascular system and the cost of blood volume. *Proc. Natl Acad. Sci.* **12** (3), 207–214.
- MYNARD, J.P. & VALEN-SENDSTAD, K. 2015 A unified method for estimating pressure losses at vascular junctions. *Intl J. Numer. Meth. Biomed. Engng* **31** (7), 1–23.
- NAEIJE, R. 2012 Pulmonary vascular resistance: a meaningless variable? In *Applied Physiology in Intensive Care Medicine 1: Physiological Notes-Technical Notes-Seminal Studies in Intensive Care*, pp. 79–82. Springer.
- NGOEPE, M.N., FRANGI, A.F., BYRNE, J.V. & VENTIKOS, Y. 2018 Thrombosis in cerebral aneurysms and the computational modeling thereof: a review. *Front. Physiol.* **9**, 259981.
- NGOEPE, M.N. & VENTIKOS, Y. 2016 Computational modelling of clot development in patient-specific cerebral aneurysm cases. *J. Thromb. Haemost.* **14** (2), 262–272.
- NIEMAN, K. & BALLA, S. 2020 Dynamic CT myocardial perfusion imaging. *J. Cardiovasc. Comput. Tomogr.* **14** (4), 303–306.
- NKOMO, V.T., GARDIN, J.M., SKELTON, T.N., GOTTDIENER, J.S., SCOTT, C.G. & ENRIQUEZ-SARANO, M. 2006 Burden of valvular heart diseases: a population-based study. *Lancet* **368** (9540), 1005–1011.
- NOBILI, M., MORBIDUCCI, U., PONZINI, R., DEL GAUDIO, C., BALDUCCI, A., GRIGIONI, M., MARIA MONTEVECCHI, F. & REDAELLI, A. 2008 Numerical simulation of the dynamics of a bileaflet prosthetic heart valve using a fluid-structure interaction approach. *J. Biomech.* **41** (11), 2539–2550.
- NORDGAARD, H., SWILLEN, A., NORDHAUG, D., KIRKEBY-GARSTAD, I., VAN LOO, D., VITALE, N., SEGERS, P., HAAVERSTAD, R. & LØVSTAKKEN, L. 2010 Impact of competitive flow on wall shear stress in coronary surgery: computational fluid dynamics of a LIMA-LAD model. *Cardiovasc. Res.* **88** (3), 512–519.
- OLUFSEN, M.S. 1999 Structured tree outflow condition for blood flow in larger systemic arteries. *Am. J. Physiol. Heart Circ. Physiol.* **276** (1), H257–H268.
- OLUFSEN, M.S., HILL, N., VAUGHAN, G.D., SAINSBURY, C. & JOHNSON, M. 2012 Rarefaction and blood pressure in systemic and pulmonary arteries. *J. Fluid Mech.* **705**, 280–305.
- OSORIO, A.F., OSORIO, R., CEBALLOS, A., TRAN, R., CLARK, W., DIVO, E.A., ARGUETA-MORALES, I.R., KASSAB, A.J. & DECAMPLI, W.M. 2013 Computational fluid dynamics analysis of surgical adjustment of left ventricular assist device implantation to minimise stroke risk. *Comput. Meth. Biomech. Biomed. Engng* **16** (6), 622–638.
- PAGNI, S., STOREY, J., BALLEEN, J., MONTGOMERY, W., CHIANG, B.Y., ETOCH, S. & SPENCE, P.A. 1997 ITA versus SVG: a comparison of instantaneous pressure and flow dynamics during competitive flow. *Eur. J. Cardiothorac. Surg.* **11** (6), 1086–1092.
- PAPAMANOLIS, L., *et al.* 2021 Myocardial perfusion simulation for coronary artery disease: a coupled patient-specific multiscale model. *Ann. Biomed. Engng* **49** (5), 1432–1447.
- PARK, S.J., *et al.* 2012 Outcomes in advanced heart failure patients with left ventricular assist devices for destination therapy. *Circ. Heart Fail.* **5** (2), 241–248.
- PARK, K.-H., *et al.* 2013 Characterization of the left atrial vortex flow by two-dimensional transesophageal contrast echocardiography using particle image velocimetry. *Ultrasound Med. Biol.* **39** (1), 62–71.
- PATWARDHAN, K. 2012 The history of the discovery of blood circulation: unrecognized contributions of Ayurveda masters. *Am. J. Physiol. Adv. Physiol. Educ.* **36** (2), 77–82.
- PEACOCK, J.A. 1990 An in vitro study of the onset of turbulence in the sinus of Valsalva. *Circ. Res.* **67** (2), 448–460.
- PEDRIZZETTI, G. & DOMENICHINI, F. 2005 Nature optimizes the swirling flow in the human left ventricle. *Phys. Rev. Lett.* **95** (10), 108101.
- PEGOLOTTI, L., PFALLER, M.R., RUBIO, N.L., DING, K., BRUFAU, R.B., DARVE, E. & MARSDEN, A.L. 2023 Learning reduced-order models for cardiovascular simulations with graph neural networks. Available at: <http://arxiv.org/abs/2303.07310>.
- PEKKAN, K., DASI, L.P., DE ZÉLICOURT, D., SUNDARESWARAN, K.S., FOGEL, M.A., KANTER, K.R. & YOGANATHAN, A.P. 2009 Haemodynamic performance of stage-2 univentricular reconstruction: Glenn vs. hemi-Fontan templates. *Ann. Biomed. Engng* **37**, 50–63.
- PERKTOLD, K., NEREM, R.M. & PETER, R.O. 1991 A numerical calculation of flow in a curved tube model of the left main coronary artery. *J. Biomech.* **24** (3–4), 175–189.
- PESKIN, C.S. 1972 Flow patterns around heart valves: a numerical method. *J. Comput. Phys.* **10** (2), 252–271.
- PESKIN, C.S. 1982 The fluid dynamics of heart valves: experimental, theoretical, and computational methods. *Annu. Rev. Fluid Mech.* **14** (1), 235–259.
- PESKIN, C.S. & MCQUEEN, D.M. 1980 Modeling prosthetic heart valves for numerical analysis of blood flow in the heart. *J. Comput. Phys.* **37** (1), 113–132.
- PESKIN, C.S. & WOLFE, A.W. 1978 The aortic sinus vortex. *Fed. Proc.* **37** (14), 2784–2792.
- PFALLER, M.R., PHAM, J., VERMA, A., PEGOLOTTI, L., WILSON, N.M., PARKER, D.W., YANG, W. & MARSDEN, A.L. 2022 Automated generation of 0D and 1D reduced-order models of patient-specific blood flow. *Intl J. Numer. Meth. Biomed. Engng* **38** (10), e3639.

- PIJLS, N.H., *et al.* 2010 Fractional flow reserve versus angiography for guiding percutaneous coronary intervention in patients with multivessel coronary artery disease: 2-year follow-up of the FAME (fractional flow reserve versus angiography for multivessel evaluation) study. *J. Am. Coll. Cardiol.* **56** (3), 177–184.
- PILLALAMARRI, N.R., PISKIN, S., PATNAIK, S.S., MURALI, S. & FINOL, E.A. 2021 Patient-specific computational analysis of haemodynamic in adult pulmonary hypertension. *Ann. Biomed. Engng* **49** (12), 3465–3480.
- POELMA, C., WATTON, P.N. & VENTIKOS, Y. 2015 Transitional flow in aneurysms and the computation of haemodynamic parameters. *J. R. Soc. Interface* **12**, 20141394.
- POWERS, W.J. 1991 Cerebral haemodynamic in ischemic cerebrovascular disease. *Ann. Neurol.* **29** (3), 231–240.
- PRIES, A.R., NEUHAUS, D. & GAETGENS, P. 1992 Blood viscosity in tube flow: dependence on diameter and hematocrit. *Am. J. Physiol. Heart Circ. Physiol.* **263** (6), H1770–H1778.
- QI, Q.M. & SHAQFEH, E.S. 2017 Theory to predict particle migration and margination in the pressure-driven channel flow of blood. *Phys. Rev. Fluids* **2**, 093102.
- QIAN, Y., LIU, J., ITATANI, K., MIYAJI, K. & UMEZU, M. 2010 Computational haemodynamic analysis in congenital heart disease: simulation of the norwood procedure. *Ann. Biomed. Engng* **38**, 2302–2313.
- QIAO, Y., ZENG, Y., DING, Y., FAN, J., LUO, K. & ZHU, T. 2019 Numerical simulation of two-phase non-Newtonian blood flow with fluid-structure interaction in aortic dissection. *Comput. Meth. Biomech. Biomed. Engng* **22** (6), 620–630.
- QUARTERONI, A., LASSILA, T., ROSSI, S. & RUIZ-BAIER, R. 2017 Integrated heart–coupling multiscale and multiphysics models for the simulation of the cardiac function. *Comput. Meth. Appl. Mech. Engng* **314**, 345–407.
- RALAPANAWA, U. & SIVAKANESAN, R. 2021 Epidemiology and the magnitude of coronary artery disease and acute coronary syndrome: a narrative review. *J. Epidemiol. Glob. Health.* **11** (2), 169–177.
- RAMACHANDRA, A.B., KAHN, A.M. & MARSDEN, A.L. 2016 Patient-specific simulations reveal significant differences in mechanical stimuli in venous and arterial coronary grafts. *J. Cardiovasc. Transl. Res.* **9** (4), 279–290.
- RAYZ, V.L., BOUSSEL, L., GE, L., LEACH, J.R., MARTIN, A.J., LAWTON, M.T., MCCULLOCH, C. & SALONER, D. 2010 Flow residence time and regions of intraluminal thrombus deposition in intracranial aneurysms. *Ann. Biomed. Engng* **38** (10), 3058–3069.
- REITER, G., REITER, U., KOVACS, G., KAINZ, B., SCHMIDT, K., MAIER, R., OLSCHESKI, H. & RIENMUELLER, R. 2008 Magnetic resonance–derived 3-dimensional blood flow patterns in the main pulmonary artery as a marker of pulmonary hypertension and a measure of elevated mean pulmonary arterial pressure. *Circ. Cardiovasc. Imag.* **1** (1), 23–30.
- REITER, U., REITER, G., KOVACS, G., STALDER, A.F., GULSUN, M.A., GREISER, A., OLSCHESKI, H. & FUCHSJÄGER, M. 2013 Evaluation of elevated mean pulmonary arterial pressure based on magnetic resonance 4D velocity mapping: comparison of visualization techniques. *PLoS ONE* **8** (12), e82212.
- RITNER, R.K. 2006 The cardiovascular system in ancient Egyptian thought. *J. Near East. Stud.* **65** (2), 99–109.
- RIVA, A., *et al.* 2022 Comparison of four-dimensional magnetic resonance imaging analysis of left ventricular fluid dynamics and energetics in ischemic and restrictive cardiomyopathies. *J. Magn. Reson. Imag.* **56** (4), 1157–1170.
- RODRÍGUEZ-PALOMARES, J.F., *et al.* 2018 Aortic flow patterns and wall shear stress maps by 4D-flow cardiovascular magnetic resonance in the assessment of aortic dilatation in bicuspid aortic valve disease. *J. Cardiovasc. Magn. Reson.* **20** (1), 28.
- SABIK, J.F., LYTLE, B.W., BLACKSTONE, E.H., KHAN, M., HOUGHTALING, P.L., COSGROVE, D.M., SHUMWAY, S.J., TATOULIS, J. & BEDNARSKI, P. 2003 Does competitive flow reduce internal thoracic artery graft patency? *Ann. Thorac. Surg.* **76** (5), 1490–1497.
- SACCO, F., PAUN, B., LEHMKUHL, O., ILES, T.L., IAIZZO, P.A., HOUZEUX, G., VÁZQUEZ, M., BUTAKOFF, C. & AGUADO-SIERRA, J. 2018a Evaluating the roles of detailed endocardial structures on right ventricular haemodynamics by means of CFD simulations. *Intl J. Numer. Meth. Biomed. Engng* **34** (9), e3115.
- SACCO, F., PAUN, B., LEHMKUHL, O., ILES, T.L., IAIZZO, P.A., HOUZEUX, G., VÁZQUEZ, M., BUTAKOFF, C. & AGUADO-SIERRA, J. 2018b Left ventricular trabeculations decrease the wall shear stress and increase the intra-ventricular pressure drop in CFD simulations. *Front. Physiol.* **9**, 458.
- SADASIVAN, C., LIEBER, B.B., GOUNIS, M.J., LOPES, D.K. & HOPKINS, L.N. 2002 Angiographic quantification of contrast medium washout from cerebral aneurysms after stent placement. *Am. J. Neuroradiol.* **23** (7), 1214–1221.
- SAIKRISHNAN, N., MIRABELLA, L. & YOGANATHAN, A.P. 2015 Bicuspid aortic valves are associated with increased wall and turbulence shear stress levels compared to trileaflet aortic valves. *Biomech. Model. Mechanobiol.* **14** (3), 577–588.
- SAKALIHASAN, N., LIMET, R. & DEFAWE, O.D. 2005 Abdominal aortic aneurysm. *Lancet* **365** (9470), 1577–1589.
- SALSAC, A.V., SPARKS, S.R. & LASHERAS, J.C. 2004 Haemodynamic changes occurring during the progressive enlargement of abdominal aortic aneurysms. *Ann. Vasc. Surg.* **18** (1), 14–21.
- SAMADY, H., ESHTEHARDI, P., MCDANIEL, M.C., SUO, J., DHAWAN, S.S., MAYNARD, C., TIMMINS, L.H., QUYYUMI, A.A. & GIDDENS, D.P. 2011 Coronary artery wall shear stress is associated with progression and transformation of atherosclerotic plaque and arterial remodeling in patients with coronary artery disease. *Circulation* **124** (7), 779–788.
- SANKARAN, S., KIM, H.J., CHOI, G. & TAYLOR, C.A. 2016 Uncertainty quantification in coronary blood flow simulations: impact of geometry, boundary conditions and blood viscosity. *J. Biomech.* **49** (12), 2540–2547.
- SANKARAN, S., MOGHADAM, M.E., KAHN, A.M., TSENG, E.E., GUCCIONE, J.M. & MARSDEN, A.L. 2012 Patient-specific multiscale modeling of blood flow for coronary artery bypass graft surgery. *Ann. Biomed. Engng* **40** (10), 2228–2242.
- SANTAMARINA, A., WEYDAHL, E., SIEGEL, J.M. & MOORE, J.E. 1998 Computational analysis of flow in a curved tube model of the coronary arteries: effects of time-varying curvature. *Ann. Biomed. Engng* **26** (6), 944–954.
- SANTAMORE, W.P. & DELL’ITALIA, L.J. 1998 Ventricular interdependence: significant left ventricular contributions to right ventricular systolic function. *Prog. Cardiovasc. Dis.* **40** (4), 289–308.

- SAQR, K.M., TUPIN, S., RASHAD, S., ENDO, T., NIIZUMA, K., TOMINAGA, T. & OHTA, M. 2020 Physiologic blood flow is turbulent. *Sci. Rep.* **10** (1), 1–12.
- SCARSELLI, D., LOPEZ, J.M., VARSHNEY, A. & HOF, B. 2023 Turbulence suppression by cardiac-cycle-inspired driving of pipe flow. *Nature* **621** (7977), 71–74.
- SCHÄFER, M., BARKER, A.J., KHEYFETS, V., STENMARK, K.R., CRAPO, J., YEAGER, M.E., TRUONG, U., BUCKNER, J.K., FENSTER, B.E. & HUNTER, K.S. 2017 Helicity and vorticity of pulmonary arterial flow in patients with pulmonary hypertension: quantitative analysis of flow formations. *J. Am. Heart Assoc.* **6** (12), e007010.
- SCHWARZ, E.L., *et al.* 2021 Haemodynamic performance of tissue-engineered vascular grafts in Fontan patients. *NPJ Reg. Med.* **6** (1), 38.
- SCHWARZ, E.L., PEGOLOTTI, L., PFALLER, M.R. & MARSDEN, A.L. 2023a Beyond CFD: emerging methodologies for predictive simulation in cardiovascular health and disease. *Biophys. Rev.* **4** (1), 011301.
- SCHWARZ, E.L., PFALLER, M.R., SZAFRON, J.M., LATORRE, M., LINDSEY, S.E., BREUER, C.K., HUMPHREY, J.D. & MARSDEN, A.L. 2023b A fluid-solid-growth solver for cardiovascular modeling. *Comput. Meth. Appl. Mech. Engng* **417**, 116312.
- SECOMB, T.W. 2017 Blood flow in the microcirculation. *Annu. Rev. Fluid Mech.* **49**, 443–461.
- SECOMB, T.W., HSU, R., PARK, E.Y. & DEWHRIST, M.W. 2004 Green's function methods for analysis of oxygen delivery to tissue by microvascular networks. *Ann. Biomed. Engng* **32** (11), 1519–1529.
- SENGUPTA, D., KAHN, A.M., BURNS, J.C., SANKARAN, S., SHADDEN, S.C. & MARSDEN, A.L. 2012 Image-based modeling of haemodynamic in coronary artery aneurysms caused by Kawasaki disease. *Biomech. Model. Mechanobiol.* **11** (6), 915–932.
- SENGUPTA, D., KAHN, A.M., KUNG, E., ESMAILY MOGHADAM, M., SHIRINSKY, O., LYSKINA, G.A., BURNS, J.C. & MARSDEN, A.L. 2014 Thrombotic risk stratification using computational modeling in patients with coronary artery aneurysms following Kawasaki disease. *Biomech. Model. Mechanobiol.* **13** (6), 1261–1276.
- SEO, J., RAMACHANDRA, A.B., BOYD, J., MARSDEN, A.L. & KAHN, A.M. 2021 Computational evaluation of venous graft geometries in coronary artery bypass surgery. *Semin. Thorac. Cardiovasc. Surg.* **34** (2), 521–532.
- SEO, J., SCHIAVAZZI, D.E., KAHN, A.M. & MARSDEN, A.L. 2020 The effects of clinically-derived parametric data uncertainty in patient-specific coronary simulations with deformable walls. *Intl J. Numer. Meth. Biomed. Engng* **36** (8), 1–27.
- SEO, J.H., VEDULA, V., ABRAHAM, T., LARDO, A.C., DAWOUD, F., LUO, H. & MITTAL, R. 2014 Effect of the mitral valve on diastolic flow patterns. *Phys. Fluids* **26** (12), 121901.
- SEO, J.H., ZHU, C., RESAR, J. & MITTAL, R. 2020 Flow physics of normal and abnormal bioprosthetic aortic valves. *Intl J. Heat Fluid Flow* **86**, 108740.
- SFORZA, D.M., PUTMAN, C.M. & CEBRAL, J.R. 2009 Haemodynamics of cerebral aneurysms. *Annu. Rev. Fluid Mech.* **41**, 91–107.
- SHAD, R., *et al.* 2021 Patient-specific computational fluid dynamics reveal localized flow patterns predictive of post-left ventricular assist device aortic incompetence. *Circ. Heart Fail.* **14** (7), e008034.
- SHETTY, A.K. & ZANIRATI, G. 2020 The interstitial system of the brain in health and disease. *Aging Dis.* **11** (1), 200–211.
- SHO, E., SHO, M., HOSHINA, K., KIMURA, H., NAKAHASHI, T.K. & DALMAN, R.L. 2004 Haemodynamic forces regulate mural macrophage infiltration in experimental aortic aneurysms. *Exp. Mol. Pathol.* **76** (2), 108–116.
- SHOJIMA, M., OSHIMA, M., TAKAGI, K., TORII, R., HAYAKAWA, M., KATADA, K., MORITA, A. & KIRINO, T. 2004 Magnitude and role of wall shear stress on cerebral aneurysm: computational fluid dynamic study of 20 middle cerebral artery aneurysms. *Stroke* **35** (11), 2500–2505.
- SIEREN, M.M., BERLIN, C., OECHTERING, T.H., HUNOLD, P., DRÖMANN, D., BARKHAUSEN, J. & FRYDRYCHOWICZ, A. 2019 Comparison of 4D flow MRI to 2D flow MRI in the pulmonary arteries in healthy volunteers and patients with pulmonary hypertension. *PLoS ONE* **14** (10), e0224121.
- SIGÜENZA, J., POTT, D., MENDEZ, S., SONNTAG, S.J., KAUFMANN, T.A., STEINSEIFER, U. & NICLOUD, F. 2018 Fluid-structure interaction of a pulsatile flow with an aortic valve model: a combined experimental and numerical study. *Intl J. Numer. Meth. Biomed. Engng* **34** (4), e2945.
- SINGER, M.A., WANG, S.L. & DIACHIN, D.P. 2010 Design optimization of vena cava filters: an application to dual filtration devices. *J. Biomech. Eng.* **132** (10), 101006.
- SINGH, S., HAKIM, F.A., SHARMA, A., ROY, R.R., PANSE, P.M., CHANDRASEKARAN, K., ALEGRIA, J.R. & MOOKADAM, F. 2015 Hypoplasia, pseudocoarctation and coarctation of the aorta - a systematic review. *Heart Lung Circ.* **24** (2), 110–118.
- SLAUGHTER, M.S., *et al.* 2009 Advanced heart failure treated with continuous-flow left ventricular assist device. *New Engl. J. Med.* **361** (23), 2241–2251.
- SLOTH, E., HOULIND, K.C., OYRE, S., YONG KIM, W., PEDERSEN, E.M., JØRGENSEN, H.S. & HASENKAM, J.M. 1994 Three-dimensional visualization of velocity profiles in the human main pulmonary artery with magnetic resonance phase-velocity mapping. *Am. Heart J.* **128** (6 PART 1), 1130–1138.
- SOTIROPOULOS, F., LE, T.B. & GILMANOV, A. 2016 Fluid mechanics of heart valves and their replacements. *Annu. Rev. Fluid Mech.* **48** (1), 259–283.
- SPINELLI, D., BENEDETTO, F., DONATO, R., PIFFARETTI, G., MARROCCO-TRISCHITTA, M.M., PATEL, H.J., EAGLE, K.A. & TRIMARCHI, S. 2018 Current evidence in predictors of aortic growth and events in acute type B aortic dissection. *J. Vasc. Surg.* **68** (6), 1925–1935.
- STALDER, A.F., FRYDRYCHOWICZ, A., RUSSE, M.F., KORVINK, J.G., HENNIG, J., LI, K. & MARKL, M. 2011 Assessment of flow instabilities in the healthy aorta using flow-sensitive MRI. *J. Magn. Reson. Imag.* **33** (4), 839–846.

- STANKOVIC, Z., ALLEN, B.D., GARCIA, J., JARVIS, K.B. & MARKL, M. 2014 4D flow imaging with MRI. *Cardiovasc. Diagn. Ther.* **4** (2), 1–20.
- STAUBER, H., WAISMAN, D., KORIN, N. & SZNITMAN, J. 2017 Red blood cell dynamics in biomimetic microfluidic networks of pulmonary alveolar capillaries. *Biomicrofluidics* **11** (1), 14103.
- STEBBENS, W.E. 1989 Etiology of intracranial berry aneurysms. *J. Neurosurg.* **70** (6), 823–831.
- STEIN, P.D. & SABBAB, H.N. 1976 Turbulent blood flow in the ascending aorta of humans with normal and diseased aortic valves. *Circ. Res.* **39** (1), 58–65.
- STEINMAN, D.A. & PEREIRA, V.M. 2019 How patient specific are patient-specific computational models of cerebral aneurysms? An overview of sources of error and variability. *Neurosurg. Focus* **47** (1), E14.
- STEINMAN, D.A., *et al.* 2012 Summer bioengineering conference CFD challenge. *J. Biomech. Engng* **135** (2), 2013.
- STYLIANOPOULOS, T. & JAIN, R.K. 2013 Combining two strategies to improve perfusion and drug delivery in solid tumors. *Proc. Natl Acad. Sci. USA* **110** (46), 18632–18637.
- SUGIURA, S., OKADA, J.I., WASHIO, T. & HISADA, T. 2022 UT-heart: a finite element model designed for the multiscale and multiphysics integration of our knowledge on the human heart. *Meth. Mol. Biol.* **2399**, 221–245.
- SUN, W., MAO, W. & GRIFFITH, B.E. 2019 Computer modeling and simulation of heart valve function and intervention. In *Principles of Heart Valve Engineering*, pp. 177–211. Elsevier.
- SUNDARESWARAN, K.S., PEKKAN, K., DAS, L.P., WHITEHEAD, K., SHARMA, S., KANTER, K.R., FOGEL, M.A. & YOGANATHAN, A.P. 2008 The total cavopulmonary connection resistance: a significant impact on single ventricle haemodynamic at rest and exercise. *Am. J. Physiol. Heart Circ. Physiol.* **295** (6), H2427–H2435.
- SWEENEY, P.W., WALKER-SAMUEL, S. & SHIPLEY, R.J. 2018 Insights into cerebral haemodynamics and oxygenation utilising in vivo mural cell imaging and mathematical modelling. *Sci. Rep.* **8** (1), 1–15.
- SZAFRON, J.M., YANG, W., FEINSTEIN, J.A., RABINOVITCH, M. & MARSDEN, A.L. 2023 A computational growth and remodeling framework for adaptive and maladaptive pulmonary arterial haemodynamic. *Biomech. Model. Mechanobiol.* **22**, 1935–1951.
- SZIKORA, I., TURÁNYI, E. & MAROSFOI, M. 2015 Evolution of flow-diverter endothelialization and thrombus organization in giant fusiform aneurysms after flow diversion: a histopathologic study. *Am. J. Neuroradiol.* **36** (9), 1716–1720.
- TAKEISHI, N., ROSTI, M.E., IMAI, Y., WADA, S. & BRANDT, L. 2019 Haemorheology in dilute, semi-dilute and dense suspensions of red blood cells. *J. Fluid Mech.* **872**, 818–848.
- TANG, B.T., PICKARD, S.S., CHAN, F.P., TSAO, P.S., TAYLOR, C.A. & FEINSTEIN, J.A. 2012 Wall shear stress is decreased in the pulmonary arteries of patients with pulmonary arterial hypertension: an image-based, computational fluid dynamics study. *Pulm. Circ.* **2** (4), 470–476.
- TARASOFF-CONWAY, J.M., *et al.* 2015 Clearance systems in the brain - implications for Alzheimer disease. *Nat. Rev. Neurol.* **11** (8), 457–470.
- TAYLOR, C.A., FONTE, T.A. & MIN, J.K. 2013 Computational fluid dynamics applied to cardiac computed tomography for noninvasive quantification of fractional flow reserve: scientific basis. *J. Am. Coll. Cardiol.* **61** (22), 2233–2241.
- TAYLOR, C.A., HUGHES, T.J. & ZARINS, C.K. 1998 Finite element modeling of blood flow in arteries. *Comput. Meth. Appl. Mech. Engng* **158** (1–2), 155–196.
- TOKUDA, Y., SONG, M.H., OSHIMA, H., USUI, A. & UEDA, Y. 2008 Predicting midterm coronary artery bypass graft failure by intraoperative transit time flow measurement. *Ann. Thorac. Surg.* **86** (2), 532–536.
- TONINO, P.A., *et al.* 2009 Fractional flow reserve versus angiography for guiding percutaneous coronary intervention. *New Engl. J. Med.* **360** (3), 213–223.
- TORII, R., *et al.* 2009 Fluid-structure interaction analysis of a patient-specific right coronary artery with physiological velocity and pressure waveforms. *Commun. Numer. Meth. Engng* **25** (5), 565–580.
- TORO, E.F., CELANT, M., ZHANG, Q., CONTARINO, C., AGARWAL, N., LINNINGER, A. & MÜLLER, L.O. 2022 Cerebrospinal fluid dynamics coupled to the global circulation in holistic setting: mathematical models, numerical methods and applications. *Intl J. Numer. Meth. Biomed. Engng* **38** (1), e3532.
- TRAN, J.S., SCHIAVAZZI, D.E., RAMACHANDRA, A.B., KAHN, A.M. & MARSDEN, A.L. 2017 Automated tuning for parameter identification and uncertainty quantification in multi-scale coronary simulations. *Comput. Fluids* **142**, 128–138.
- TRUSTY, P.M., WEI, Z., SALES, M., KANTER, K.R., FOGEL, M.A., YOGANATHAN, A.P. & SLESNICK, T.C. 2020 Y-graft modification to the Fontan procedure: increasingly balanced flow over time. *J. Thorac. Cardiovasc. Surg.* **159** (2), 652–661.
- TRUSTY, P.M., WEI, Z.A., SLESNICK, T.C., KANTER, K.R., SPRAY, T.L., FOGEL, M.A. & YOGANATHAN, A.P. 2019 The first cohort of prospective Fontan surgical planning patients with follow-up data: how accurate is surgical planning? *J. Thorac. Cardiovasc. Surg.* **157** (3), 1146–1155.
- TSAI, T.T., SCHLICHT, M.S., KHANAFAER, K., BULL, J.L., VALASSIS, D.T., WILLIAMS, D.M., BERGUER, R. & EAGLE, K.A. 2008 Tear size and location impacts false lumen pressure in an ex vivo model of chronic type B aortic dissection. *J. Vasc. Surg.* **47** (4), 844–851.
- TSAO, C.W., *et al.* 2022 Heart disease and stroke statistics-2022 update: a report from the American Heart Association. *Circulation* **145** (8), E153–E639.
- UNITED NATIONS 2022 *World Population Prospects 2022 Summary of Results*. United Nations, Department of Economic and Social Affairs Population Division.
- UPDEGROVE, A., WILSON, N.M., MERKOW, J., LAN, H., MARSDEN, A.L. & SHADDEN, S.C. 2017 SimVascular: an open source pipeline for cardiovascular simulation. *Ann. Biomed. Engng* **45** (3), 525–541.

- URIEL, N., *et al.* 2016 Haemodynamic ramp tests in patients with left ventricular assist devices. *JACC Heart Fail.* **4** (3), 208–217.
- VALVEZ, S., OLIVEIRA-SANTOS, M., PIEDADE, A.P., GONÇALVES, L. & AMARO, A.M. 2023 Computational flow dynamic analysis in left atrial appendage thrombus formation risk: a review. *Appl. Sci.* **13** (14), 8201.
- VARDHAN, M., GOUNLEY, J., CHEN, S.J., KAHN, A.M., LEOPOLD, J.A. & RANDLES, A. 2019 The importance of side branches in modeling 3D haemodynamic from angiograms for patients with coronary artery disease. *Sci. Rep.* **9** (1), 1–10.
- VEDULA, V., GEORGE, R., YOUNES, L. & MITTAL, R. 2015 Haemodynamics in the left atrium and its effect on ventricular flow patterns. *J. Biomech. Engng* **137** (11), 111003.
- VEDULA, V., SEO, J.-H., LARDO, A.C. & MITTAL, R. 2016 Effect of trabeculae and papillary muscles on the haemodynamic of the left ventricle. *Theor. Comput. Fluid Dyn.* **30** (1–2), 3–21.
- VAN VELUW, S.J., HOU, S.S., CALVO-RODRIGUEZ, M., ARBEL-ORNATH, M., SNYDER, A.C., FROSCHE, M.P., GREENBERG, S.M. & BACSKAI, B.J. 2020 Vasomotion as a driving force for paravascular clearance in the awake mouse brain. *Neuron* **105** (3), 549–561.
- VERMA, S. & SIU, S.C. 2014 Aortic dilatation in patients with bicuspid aortic valve. *New Engl. J. Med.* **370** (20), 1920–1929.
- VERZICCO, R. 2022 Electro-fluid-mechanics of the heart. *J. Fluid Mech.* **941**, P1.
- VIGMOND, E.J., CLEMENTS, C., MCQUEEN, D.M. & PESKIN, C.S. 2008 Effect of bundle branch block on cardiac output: a whole heart simulation study. *Prog. Biophys. Mol. Biol.* **97** (2–3), 520–542.
- VIGNON-CLEMENTEL, I.E., ALBERTO FIGUEROA, C., JANSEN, K.E. & TAYLOR, C.A. 2006 Outflow boundary conditions for three-dimensional finite element modeling of blood flow and pressure in arteries. *Comput. Meth. Appl. Mech. Engng* **195** (29–32), 3776–3796.
- VIOLA, F., MESCHINI, V. & VERZICCO, R. 2020 Fluid–structure–electrophysiology interaction (FSEI) in the left-heart: a multi-way coupled computational model. *Eur. J. Mech. (B/Fluids)* **79**, 212–232.
- VOLLKRON, M., VOITL, P., TA, J., WIESELTHALER, G. & SCHIMA, H. 2007 Suction events during left ventricular support and ventricular arrhythmias. *J. Heart Lung Transplant.* **26** (8), 819–825.
- VON KNOBELSDORFF-BRENKENHOFF, F., TRAUZEDDEL, R.F., BARKER, A.J., GRUETTNER, H., MARKL, M. & SCHULZ-MENGER, J. 2014 Blood flow characteristics in the ascending aorta after aortic valve replacement - a pilot study using 4D-flow MRI. *Intl J. Cardiol.* **170** (3), 426–433.
- VORP, D.A., LEE, P.C., WANG, D.H., MAKAROUN, M.S., NEMOTO, E.M., OGAWA, S. & WEBSTER, M.W. 2001 Association of intraluminal thrombus in abdominal aortic aneurysm with local hypoxia and wall weakening. *J. Vasc. Surg.* **34** (2), 291–299.
- VOTTA, E., LE, T.B., STEVANELLA, M., FUSINI, L., CAIANI, E.G., REDAELLI, A. & SOTIROPOULOS, F. 2013 Toward patient-specific simulations of cardiac valves: state-of-the-art and future directions. *J. Biomech.* **46** (2), 217–228.
- WANG, D., SERRACINO-INGLOTT, F. & FENG, J. 2021 Numerical simulations of patient-specific models with multiple plaques in human peripheral artery: a fluid-structure interaction analysis. *Biomech. Model. Mechanobiol.* **20**, 255–265.
- WATSON, C., SAAID, H., VEDULA, V., CARDENAS, J.C., HENKE, P.K., NICLOUD, F., XU, X.Y., HUNT, B.J. & MANNING, K.B. 2024 Venous thromboembolism: review of clinical challenges, biology, assessment, treatment, and modeling. *Ann. Biomed. Engng* **52**, 467–486.
- WELLNHOFER, E., OSMAN, J., KERTZSCHER, U., AFFELD, K., FLECK, E. & GOUBERGRITS, L. 2010 Flow simulation studies in coronary arteries-impact of side-branches. *Atherosclerosis* **213** (2), 475–481.
- WELSH, J.D., *et al.* 2019 Haemodynamic regulation of perivalvular endothelial gene expression prevents deep venous thrombosis. *J. Clin. Invest.* **129** (12), 5489–5500.
- WESTERHOF, N., BOSMAN, F., DE VRIES, C.J. & NOORDERGRAAF, A. 1969 Analog studies of the human systemic arterial tree. *J. Biomech.* **2** (2), 121–143.
- WESTERHOF, N., BOER, C., LAMBERTS, R.R. & SIPKEMA, P. 2006 Cross-talk between cardiac muscle and coronary vasculature. *Physiol. Rev.* **86** (4), 1263–1308.
- WHITEHEAD, K.K., PEKKAN, K., KITAJIMA, H.D., PARIDON, S.M., YOGANATHAN, A.P. & FOGEL, M.A. 2007 Nonlinear power loss during exercise in single-ventricle patients after the Fontan: insights from computational fluid dynamics. *Circulation* **116** (11_supplement), I-165.
- WILSON, R.F., WYCHE, K., CHRISTENSEN, B.V., ZIMMER, S. & LAXSON, D.D. 1990 Effects of adenosine on human coronary arterial circulation. *Circulation* **82** (5), 1595–1606.
- WINDECKER, S., *et al.* 2014 Revascularisation versus medical treatment in patients with stable coronary artery disease: network meta-analysis. *Brit. Med. J.* **348**, g3859.
- WOOD, N.B., ZHAO, S.Z., ZAMBANINI, A., JACKSON, M., GEDROYC, W., THOM, S.A., HUGHES, A.D. & XU, X.Y. 2006 Curvature and tortuosity of the superficial femoral artery: a possible risk factor for peripheral arterial disease. *J. Appl. Physiol. Respir. Environ. Exerc. Physiol.* **101** (5), 1412–1418.
- WU, W., *et al.* 2016 Fluid–structure interaction model of a percutaneous aortic valve: comparison with an in vitro test and feasibility study in a patient-specific case. *Ann. Biomed. Engng* **44** (2), 590–603.
- XIANG, J., NATARAJAN, S.K., TREMMEL, M., MA, D., MOCCO, J., HOPKINS, L.N., SIDDIQUI, A.H., LEVY, E.I. & MENG, H. 2011 Haemodynamic-morphologic discriminants for intracranial aneurysm rupture. *Stroke* **42** (1), 144–152.
- XIANG, J., TUTINO, V.M., SNYDER, K.V. & MENG, H. 2014 CFD: computational fluid dynamics or confounding factor dissemination? The role of haemodynamic in intracranial aneurysm rupture risk assessment. *Am. J. Neuroradiol.* **35** (10), 1849–1857.

- XU, P., LIU, X., SONG, Q., CHEN, G., WANG, D., ZHANG, H., YAN, L., LIU, D. & HUANG, W. 2016 Patient-specific structural effects on haemodynamic in the ischemic lower limb artery. *Sci. Rep.* **6** (1), 39225.
- YANG, W., CHAN, F.P., REDDY, V.M., MARSDEN, A.L. & FEINSTEIN, J.A. 2015 Flow simulations and validation for the first cohort of patients undergoing the Y-graft Fontan procedure. *J. Thorac. Cardiovasc. Surg.* **149** (1), 247–255.
- YANG, W., DONG, M., RABINOVITCH, M., CHAN, F.P., MARSDEN, A.L. & FEINSTEIN, J.A. 2019 Evolution of haemodynamic forces in the pulmonary tree with progressively worsening pulmonary arterial hypertension in pediatric patients. *Biomech. Model. Mechanobiol.* **18** (3), 779–796.
- YANG, W., FEINSTEIN, J.A. & VIGNON-CLEMENTEL, I.E. 2016 Adaptive outflow boundary conditions improve post-operative predictions after repair of peripheral pulmonary artery stenosis. *Biomech. Model. Mechanobiol.* **15** (5), 1345–1353.
- YANG, W., HANLEY, F.L., CHAN, F.P., MARSDEN, A.L., VIGNON-CLEMENTEL, I.E. & FEINSTEIN, J.A. 2018 Computational simulation of postoperative pulmonary flow distribution in Alagille patients with peripheral pulmonary artery stenosis. *Congenit. Heart Dis.* **13** (2), 241–250.
- YANG, W., VIGNON-CLEMENTEL, I.E., TROIANOWSKI, G., REDDY, V.M., FEINSTEIN, J.A. & MARSDEN, A.L. 2012 Hepatic blood flow distribution and performance in conventional and novel Y-graft Fontan geometries: a case series computational fluid dynamics study. *J. Thorac. Cardiovasc. Surg.* **143** (5), 1086–1097.
- YOGANATHAN, A.P., CHANDRAN, K. & SOTIROPOULOS, F. 2005 Flow in prosthetic heart valves: state-of-the-art and future directions. *Ann. Biomed. Engng* **33**, 1689–1694.
- YOGANATHAN, A.P., HE, Z. & JONES, S.C. 2004 Fluid mechanics of heart valves. *Annu. Rev. Biomed. Engng* **6**, 331–362.
- YUSUF, S., *et al.* 1994 Effect of coronary artery bypass graft surgery on survival: overview of 10-year results from randomised trials by the coronary artery bypass graft surgery trialists collaboration. *Lancet* **344** (8922), 563–570.
- ZAJAC, J., ERIKSSON, J., DYVERFELDT, P., BOLGER, A.F., EBBERS, T. & CARLHÄLL, C.-J. 2015 Turbulent kinetic energy in normal and myopathic left ventricles. *J. Magn. Reson. Imag.* **41** (4), 1021–1029.
- ZARINS, C.K., GIDDENS, D.P., BHARADVAJ, B.K., SOTTIURAI, V.S., MABON, R.F. & GLAGOV, S. 1983 Carotid bifurcation atherosclerosis. Quantitative correlation of plaque localization with flow velocity profiles and wall shear stress. *Circ. Res.* **53** (4), 502–514.
- ZHANG, J., BRINDISE, M.C., ROTHENBERGER, S.M., MARKL, M., RAYZ, V.L. & VLACHOS, P.P. 2022a A multi-modality approach for enhancing 4D flow magnetic resonance imaging via sparse representation. *J. R. Soc. Interface* **19**, 20210751.
- ZHANG, J.M., *et al.* 2015 Haemodynamic analysis of patient-specific coronary artery tree. *Intl J. Numer. Meth. Biomed. Engng* **31** (4), e02708.
- ZHANG, J., ROTHENBERGER, S.M., BRINDISE, M.C., MARKL, M., RAYZ, V.L. & VLACHOS, P.P. 2022b Wall shear stress estimation for 4D flow MRI using Navier–Stokes equation correction. *Ann. Biomed. Engng* **50** (12), 1810–1825.
- ZHAO, H., SHAQFEH, E.S. & NARSIMHAN, V. 2012 Shear-induced particle migration and margination in a cellular suspension. *Phys. Fluids* **24** (1), 73602.
- ZHOU, Y., KASSAB, G.S. & MOLLOI, S. 1999 On the design of the coronary arterial tree: a generalization of Murray’s law. *Phys. Med. Biol.* **44** (12), 2929–2945.
- ZHU, C., SEO, J.H. & MITTAL, R. 2018 Computational modelling and analysis of haemodynamics in a simple model of aortic stenosis. *J. Fluid Mech.* **851**, 23–49.
- ZHU, C., SEO, J.H. & MITTAL, R. 2019 Computational modeling and analysis of murmurs generated by modeled aortic stenoses. *J. Biomech. Engng* **141** (4), 041007.
- ZIMMERMANN, J., BÄUMLER, K., LOECHER, M., CORK, T.E., MARSDEN, A.L., ENNIS, D.B. & FLEISCHMANN, D. 2023 Haemodynamic effects of entry and exit tear size in aortic dissection evaluated with in vitro magnetic resonance imaging and fluid–structure interaction simulation. *Sci. Rep.* **13** (1), 1–15.
- ZINGARO, A., DEDE, L., MENGHINI, F., QUARTERONI, A., *et al.* 2021 Haemodynamics of the heart’s left atrium based on a variational multiscale-les numerical method. *Eur. J. Mech. (B/Fluids)* **89**, 380–400.
- ZURITA, P. & HURTADO, D.E. 2022 Computational modeling of capillary perfusion and gas exchange in alveolar tissue. *Comput. Meth. Appl. Mech. Engng* **399**, 115418.